SHEAR WAVE TIME-LAPSE SEISMIC MONITORING OF A TIGHT GAS SANDSTONE RESERVOIR, RULISON FIELD, COLORADO

by

Michael David Rumon

A thesis submitted to the Faculty and the Board of Trustees of the Colorado School of Mines in partial fulfillment of the requirements for the degree of Master of Science (Geophysics).

Golden, Colorado

Date August 31, 2006

Signed: _____
Michael David Rumon

Approved: _____
Dr. Tom Davis
Thesis Advisor

_____
Dr. Terence K. Young
Department Head
Geophysics

ABSTRACT

The Reservoir Characterization Project at the Colorado School of Mines acquired two dedicated nine component (9C) 3D time-lapse surveys over a tight gas sandstone reservoir in western Colorado. The objective of these highly repeatable seismic surveys was to provide the opportunity to monitor reservoir changes resulting from the production of gas. This research focused specifically on the use of time-lapse (4D) poststack migrated shear-wave seismic data as a production monitoring tool in an extensive unconventional reservoir. This is one of the first applications of shear wave data as a tool for monitoring 4D changes.

The basin centered tight gas sandstone reservoir of Rulison Field, located in the Piceance Basin of western Colorado, presents a challenging setting for the application of time-lapse seismic data. The large, approximately 2,500 foot thick, gas producing interval contains discontinuous fluvial and deltaic point bar sandstone reservoir bodies. The limited vertical and horizontal extent, and low porosity and permeability nature of the sandstone packages, limits the understanding of the drainage areas accessed by individual wells. Close well spacing and hydraulic fracturing completion techniques are necessary for economic production rates, and to maximize hydrocarbon recovery. The use of shear-wave time-lapse data enhances the understanding of reservoir connectivity, depleted intervals, and bypassed pay. This provides the ability to avoid depleted intervals in new wells, and identify bypassed pay intervals penetrated by older wells. This type of analysis is essential to enhance drilling and completion efficiency, along with total hydrocarbon recovery in an unconventional tight gas reservoir with currently large reserves, and continually growing potential reserves.

Time-lapse variations were monitored following the cross-equalization of the 2003 and 2004 shear-wave seismic volumes. Cross-equalization was performed to limit random variations resulting from differences in the data not related to production. After this processing step, variations in both the shear-wave splitting coefficient values and

impedance values were observed. The cross-equalization process resulted in highly repeatable fast and slow shear-wave volumes between the two surveys, through both the static interval above the reservoir, and through the reservoir interval. This analysis also provides the first in depth understanding of shear wave time-lapse cross-equalization, and its usefulness.

After the cross-equalization process was applied, changes were observed in the shear-wave splitting coefficients through two intervals of the reservoir. This illustrates the robust nature of using both the slow and fast shear-wave volumes as a measure of change. Strong changes through the reservoir correlate with zones of dense well spacing and high production levels. There is also a strong correlation between expected drainage patterns and zones of change. This indicates the strength of using both fast and slow shear-wave data as a tool for monitoring reservoir changes.

The shear impedance analysis allowed for a high resolution, zone specific understanding of time-lapse changes within the reservoir interval. Changes in the time-lapse data can be associated with perforated and completed sandstone packages in the wells. These changes between highly repeatable surveys, indicates the ability to monitor time-lapse changes associated with gas production. This provides an indication of productive intervals, and the lateral extent of depletion.

The collection of dedicated 4D shear wave information at Rulison Field illustrates the first use of this type of data to monitor production related changes in a tight gas sandstone reservoir. This analysis illustrates the strength of dedicated time-lapse surveys and the thorough cross-equalization scheme. It also shows the potential for increased understanding of reservoir connectivity and productive intervals through a highly discontinuous reservoir interval. The collection and use of shear wave seismic data as a time-lapse monitoring tool is essential in this setting. The increased sensitivity of shear waves to the presence of changing fractures networks is a key component to monitoring reservoir changes in this setting.

TABLE OF CONTENTS

LIST OF FIGURES

LIST OF TABLES

ACKNOWLEDGEMENTS

This research was sponsored by the Reservoir Characterization Project (RCP) at the Colorado School of Mines. I would like to acknowledge the RCP research consortium for collecting and providing the data set that was used, along with the guidance and support in understanding and interpreting the data. I would also like to thank the sponsors of the consortium for their financial support and guidance throughout my research. I would specifically like to thank Williams Production Company (RMT) for providing access to their Rulison Field information, and their guidance along the way.

I would specifically like to thank my thesis committee of Dr. Tom Davis, Dr. Bob Benson, Dr. Mike Batzle, and Dr. Martin Landro. The guidance and experience they provided was essential in expanding my understanding and level of knowledge in numerous disciplines. I would like to personally thank Dr. Tom Davis for his belief in my abilities throughout my thesis work, his continued friendship, and his ability to identify and pursue challenging and important applications for state of the art geophysical technology. The experience that I have gained through my graduate education has provided me with a strong foundation in geophysical techniques, and their application to real world problems.

I would additionally like to acknowledge the rest of the professors and the staff of the geophysics department for their commitment to the success of the students, and dedication to leading the academic world in the understanding and application of geophysical theory and data. Along with the professors I would like to acknowledge and thank my fellow students and friends at the Colorado School of Mines. I greatly appreciate the support and advice that everyone provided and continues to provide.

My final acknowledgement goes to both my family and my fiancée. I greatly appreciate all the support and advice that you have provided throughout my education and life. I could not have done it without you, thank you.

Chapter 1 Introduction

1.1 Introduction

The Rulison Field study is part of Phase X and XI of the industry sponsored Reservoir Characterization Project (RCP) at the Colorado School of Mines. The RCP uses a multi-disciplinary approach to characterize and increase the understanding of complex reservoir scenarios through the integration of petroleum engineering, geological, and geophysical data. This study is focused on the characterization of an unconventional basin centered tight-gas sandstone reservoir located in the Piceance Basin of western Colorado. The overall goal of the RCP is to increase reservoir understanding and production related reservoir changes, through the integration of numerous sources of data. The available data used in the reservoir characterization includes a 3D compressional wave seismic survey collected in 1996, two 3D nine component (9C) dedicated time-lapse (4D) surveys collected in 2003 and 2004, a 3D vertical seismic profile (VSP), core samples collected approximately two miles south of the project area at the Department of Energy's Multiwell Experiment (MWX) (Nelson 2003), micro-seismic data, and an extensive suite of logs from the over 100 wells that have been drilled in the area. The available log data includes image and cross-dipole sonic logs in addition to the traditionally collected log suite. Reservoir characterization has so far included two p-wave time-lapse studies spanning the intervals from 1996 to 2003 (Kusuma 2005) and 2003 to 2004 (Keighley 2006), a geomechanical study of the field (Higgins 2006), pressure related core testing (Rojas 2005), fault mapping through the field (Jansen 2005), along with ongoing studies focused on the geologic framework, micro- and passive seismic data, reservoir modeling, and flow simulation.

The need for understanding and defining production related changes in this type of unconventional reservoir is driven by the significant hydrocarbon reserves that exist

within this field and other tight-gas accumulations worldwide. The current and expected increases in demand for natural gas in both the United States and other countries around the world has led to an increased interest in large, traditionally uneconomic gas accumulations (Law and Curtis 2002). These unconventional tight-gas plays represent a significant resource that is just beginning to be understood. Proved and potential reserves in the Piceance Basin are estimated at between 5 and 10 TCF (Colorado Interstate Gas 2006), and within the United States at over 250 TCF (NaturalGas.org 2004). The research being performed within the RCP is leading to the better understanding of reservoir complexity and production patterns that are essential to the efficient production of tight-gas reservoirs.

The scope of my research is focused on the use of dedicated time-lapse shear-wave seismic surveys to monitor 4D production related reservoir changes. An understanding of production induced changes is essential for increasing gas recovery efficiency, along with increasing the original gas in place that is recoverable. The two main goals of this research include:

- Cross-equalizing the 2003 and 2004 shear-wave seismic surveys to minimize random differences not related to production
- Identify time-lapse changes between the two surveys

The purpose of this information is to provide an increased understanding of depleted zones, drainage patterns, and zones of bypassed pay to increase recovery efficiency and the amount of gas recoverable over the life of the field. With this tight gas reservoir only becoming economic during the early and mid 1990's these types of unconventional reservoirs are still only beginning to be understood. The advent of hydraulic fracturing and completion techniques during the 1980's and 1990's allowed for the establishment of economic gas production rates in the field. These technological advances were essential, but also resulted in the majority of the reservoir understanding coming through the

engineering techniques developed in drilling, completion, and production. While this information and research is vital to development and understanding, the additional insight that can be provided by a geophysical investigation can further aid in the efficient development of these types of reservoirs.

The current drilling plan involves the down spacing of well locations to increase access to virgin reservoir compartments. This decision is based on hydraulic fracture mapping, and information pertaining to expected drainage patterns (Wolhart, Odegard et al. 2005). While this information is important, a better understanding of production patterns can be provided by time-lapse seismic monitoring. Identifying depleted intervals with this type of data can provide insight into the placement of new wells. By monitoring productive intervals and drainage patterns, the placement of new wells can be guided to areas of limited or no depletion. This prevents the drilling of new wells in areas that have already been accessed by surrounding wells. It can also help identify specific intervals of depletion. When this information is combined with drilling plans it can prevent the completion of depleted intervals in newly drilled wells. Both of these types of information provided by the time-lapse seismic data increase the gas recovery efficiency, and the economic viability of these types of reservoirs. The collection and interpretation of this data, at a half or a third the cost of a new well, quickly illustrates the economic benefits it provides in preventing the drilling and completion of new wells in already depleted areas.

The combination of this research with previous work in the areas of fault mapping and the corresponding p-wave time-lapse study illustrates an opportunity for the integration of multiple datasets. This allows for an increased understanding of the reservoir, and production induced changes. Previous fault mapping that was performed on the 2003 RCP p-wave seismic survey provided insight into the distribution of fault trends. It also provided anticipated areas of enhanced natural fracturing, multiple fracture sets, and locally variable and complex stress fields (Jansen 2005). The presence of enhanced natural fracturing within the survey area identifies zones that are expected to

have increased shear wave time-lapse changes. This is due to higher production levels, and the robust response of shear waves to changes in fracture densities. A strong response is also expected to result from artificial fractures created during the hydraulic fracture completions of the wells. This is due to the creation of artificial fracture networks, and a strong initial boost in production early in the life of the wells. The presence of natural and artificial fractures is a key component in this reservoir, providing both increased productivity, and an expected enhancement in the time-lapse signal when monitored with shear wave seismic data. The nature of shear wave data, and its sensitivity to fractures is an important reason for its application in this setting.

A comparison of the time-lapse changes identified in this research with time-lapse changes that were observed in the 2003 and 2004 RCP p-wave surveys, (Keighley 2006) provides an enhanced understanding of productive zones. Larger distributions of changes in the shear wave data illustrates the need for shear wave studies, and their ability to monitor production related changes in this reservoir setting compared to limited changes in the p-wave data. The sensitivity of shear waves to variations in fracture densities and stress fields is an essential component of this type of study. The enhanced sensitivity that shear wave provide over compressional waves is a major reason for the collection and analysis of time-lapse multi-component data at Rulison Field.

1.2 Rulison Field

Rulison Field is located on the eastern edge of the Piceance Basin of western Colorado (Figure 1.1). It is currently being operated by Williams Production RMT. Rulison Field is approximately 100 mi^2, and currently contains over 500 wells that produce from the Williams Fork Formation. Annual gas production has been continually increasing from 31 billion cubic feet (BCF) in 2003 to 41 BCF in 2004, and 55 BCF in 2005 (Colorado Oil and Gas Conservation Commission 2006). The gas produced is a dry gas with minimal oil and water production. Increased gas production is associated with

the continued drilling of new wells, and ongoing improvements in completion techniques. Rulison Field is a small division of the Piceance Basin, which covers over 7110 mi^2 (Topper, Spray et al. 2003), and estimated to contain over 300 trillion cubic feet (TCF) of gas potential. Rulison Field itself is believed to contain an accumulation of several TCF (Kuuskra and Ammer 2004). These numbers are much larger than the proved and potential reserve numbers stated previously, and represent the large amount of potential gas in place.

Rulison Field was deemed uneconomic after its initial discovery in the 1960's. This was a direct result of the low permeability (0.1 to 2.0 microdarcies) nature of the gas producing sandstone packages. Not until advances in completion technology occurred in the middle of the 1980's did the resource become economically viable (Cumella and Ostby 2003). The further development and introduction of hydraulic fracture well completions in the early 1990's drastically increased production and the attraction of this unconventional reservoir. Additional understanding and advances in fracturing techniques through the 1990's, and ongoing advances today have added to the accessibility of the resource at Rulison Field and throughout the Piceance Basin (Wolhart, Odegard et al. 2005).

Along with advances in completion technology, the introduction of decreased well spacing to ten-acres in some areas has also increased the amount of recoverable reserves. Despite tight spacing there is still only minimal communication between wells (Wolhart, Odegard et al. 2005). This indicates that as the field continues to develop advances in reservoir understanding and characterization, and completions practices must continue to allow for the full development this large hydrocarbon resource.

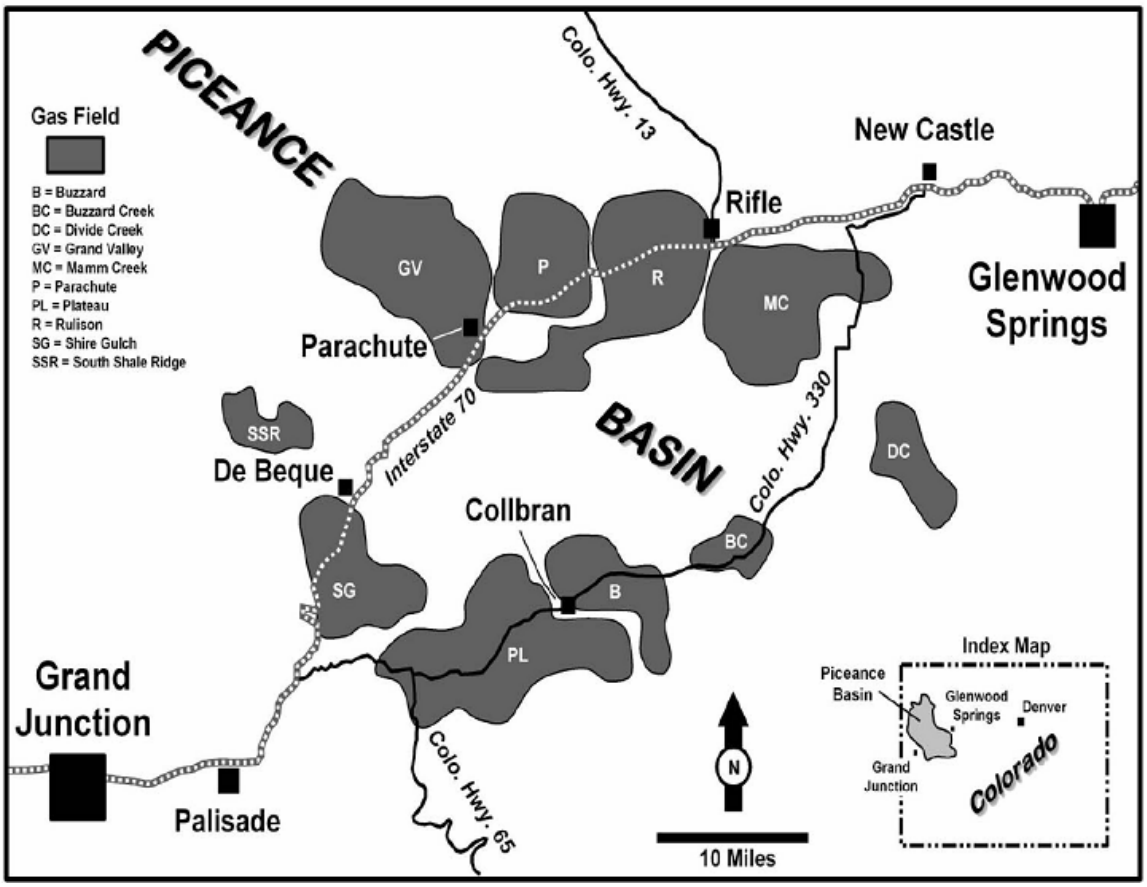

Figure 1.1 - Location of Rulison Field and other surrounding fields in the Piceance Basin of western Colorado. Modified from Cumella and Cole, 2005.

1.3 Geologic Overview

The production at Rulison Field come from a tight basin centered gas accumulation that produces from the Late Cretaceous age Williams Fork Formation of the Mesaverde Group (Figure 1.2) (Johnson 1989). The reservoir produces dry gas from an interval that is approximately 1,700 to 2,400 feet thick in the Rulison Field area (Cumella and Ostby 2003). The Williams Fork Formation can be subdivided into two separate intervals based on the type of depositional environment. The Upper Williams Fork interval (UWF) consists of a coastal plain environment with lenticular fluvial and

floodplain deposits (Cumella and Ostby 2003). Below the UWF interval, the depositional environment transitions into a low-lying deltaic or coastal plain environment. The Lower Williams Fork interval (LWF) contains extensive coal and sandstone deposits. The lower reservoir section is underlain by marine deposits that consist of three widespread regressive sandstone packages separated by intervals of the marine Mancos Shale. The sandstone sequence is underlain by the continuous Mancos Shale interval that was deposited in the Cretaceous Seaway (Cumella and Ostby 2003).

The Lower Williams Fork Formation (LWF) consists of extensive coal and sandstone deposits. This part of the formation is approximately 850 feet thick, and is bounded by the marine Rollins sandstone of the Iles Formation on the bottom, and the beginning of the Cameo coal interval on the top (Figure 1.2) (Cumella and Ostby 2003). The Cameo coal is laterally extensive throughout the field, and can be picked as a strong continuous event in the seismic data. This interval was deposited along a low-lying coastal or delta plain environment that allowed for the deposition of extensive amounts of peat during periods of large accommodation space (Cumella and Ostby 2003). The coal layers are separated by intervals of point bar sandstone deposits that are on average between 30 and 100 feet thick. The point bar deposits were left by meandering streams during times of less accommodation space (Cumella and Ostby 2003).

The Upper Williams Fork Formation (UWF) begins above the Cameo coal interval and continues upward until the Upper Williams Fork shale marker (UMV) is encountered. The approximately 20 foot thick UMV layer is used as the upper limit of the UWF due to its strong and continuous presence in the seismic data (Cumella and Ostby 2003). This is despite the fact that the UWF actually continues upward another 500 feet or so. This shale layer also represents the upper most limit of well completions, with most completions beginning several hundred feet deeper at the beginning of the gas saturated interval. The interval between the UMV marker and Cameo coal interval is associated with a fluvial coastal plain environment. This environment resulted in the

deposition of point bar sandstone packages and more extensive flood plain packages associated with meandering streams (Cumella and Ostby 2003).

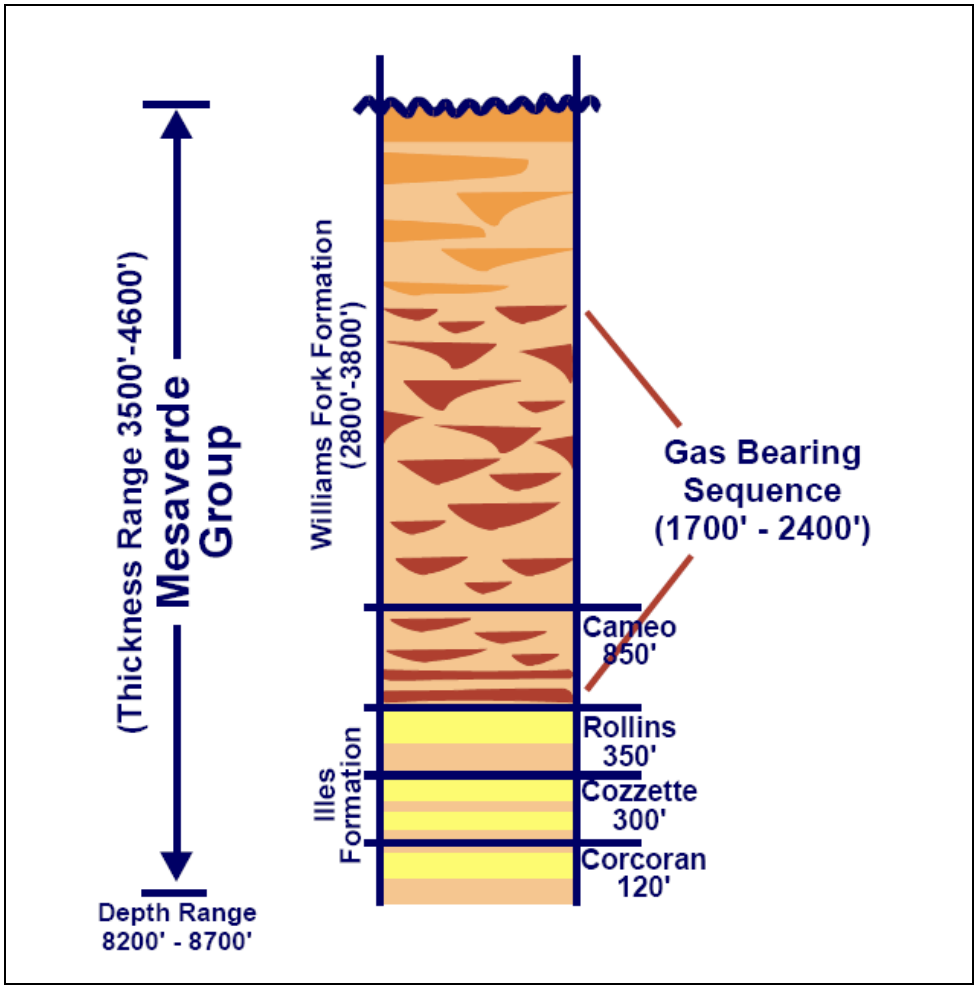

Figure 1.2 - Generalized Mesaverde stratigraphic sequence (Wolhart, Odegard et al. 2005).

There are two major geologic challenges that present themselves in trying to efficiently produce gas from Rulison Field. These challenges include the reservoir properties of the productive sandstone packages, and the packages discontinuous nature. The productive sandstone packages have porosities ranging from 6 to 12 %, and

permeabilities ranging from 0.1 to 5.0 microdarcies (μD). The productive intervals also contain high irreducible water saturations of 50 to 65% that are associated with the presence of authigenic clays (Nelson 2003). The low permeability nature of the matrix component creates a challenge in effectively producing economic quantities of gas. The low permeability of the sandstone reservoir rock is the main reason why this resource is considered a tight gas unconventional play (Law and Curtis 2002). The presence of natural fracturing increases the effective permeability by approximately two orders of magnitude, resulting in values ranging from 10 to 50 μD (Wolhart, Odegard et al. 2005). The intersection of fractured intervals through the reservoir is of key importance in increasing production levels, and increasing the amount of recoverable gas. The use of hydraulic fracturing techniques, beginning in the middle 1980's, also improved production levels (Cumella and Ostby 2003). This effectively increased the presence of fracture pathways to the wellbore, and is also believed to increase the connection with nearby fracture networks. The current fracture technology being utilized at Rulison is resulting in the artificial creation of fractures with half lengths of 300 to 600 feet away from the wellbore (Wolhart, Odegard et al. 2005). Due to the cost associated with fracture treatments, an ability to identify zones of depletion to avoid in new wells is an important aspect of the reservoir characterization. By isolating and completing zones of virgin pressure production costs can be reduced while effectively producing the reservoir. The presence of both natural and artificial fracture networks is also an important reason for utilizing shear wave seismic data as a time-lapse monitoring tool. This is due to its sensitivity to fractures, and thus production related changes in the fracture networks.

The second major challenge in producing this reservoir is the discontinuous nature of the point bar deposits in both the Upper and Lower Williams Fork Formation intervals. These deposits have a lateral extent of 40 to 2,791 feet, with a mean value of 528 feet, and thickness ranges from 0.5 to 29 feet, with a mean value of 9 ft (Cole and Cumella 2005). These values were obtained from outcrop work by Cole and Cumella in 2005 on the exposed Lower Williams Fork interval in Coal Canyon near Palisade,

Colorado (Figure 1.1). While this study is more of a direct description of the LWF, it is also assumed to adequately represent the UWF deposits based on the continued presence of meandering streams depositional environments through both sections.

The challenge with this type of depositional environment is that the productive interval is extremely thick, 1,700 to 2,400 feet, and contains countless numbers of discontinuous lenticular channel deposits. In this scenario there is not a continuous reservoir section, but numerous individual productive reservoir bodies within a large interval penetrated by wells. In many instances these channel deposits are observed to be stacked or amalgamated resulting in higher net to gross sand intervals. While the presence of higher net to gross sandstone intervals might suggest higher well productivity, no strong correlation can be found between expected ultimate recovery (EUR) and net pay (Cumella and Ostby 2003). This indicates that in addition to the challenging low-permeability and discontinuous nature of the sandstone packages a major control on higher well productivity appears to be related to the presence of enhanced natural and artificial fracturing. These fracture networks are associated with the presence of faults running through the reservoir interval (Jansen 2005). Their presence provides expanded drainages areas, both vertically and horizontally that increase production levels in wells. Changes to the fracture densities that result from production also provide an enhanced time-lapse signal when utilizing shear wave seismic data. This is a key reason for the application of shear wave data in this field. The enhanced time-lapse signal over traditional p-wave studies provides an essential reservoir and production understanding that is not possible with traditional data types. The challenge of this reservoir is being able identify drainage areas along with enhanced zones of reservoir connectivity and depletion.

1.4 Time-Lapse Application

The application of dedicated time-lapse shear-wave seismic surveys in this type of reservoir setting is a first in the oil and gas industry. Other shear-wave time-lapse studies have been used to monitor enhanced recovery operations, such as a CO_2 injection at Vacuum Field, New Mexico (Benson and Davis 2000) and (Angerer, Crampin et al. 2000), but have not addressed this type of production scenario. The challenge with this reservoir is that the only cause of production related change results from the depletion of pore pressure. Since dry gas is being produced, little or no fluid substitution is expected, and no enhanced recovery programs are used that could provide an additional time-lapse signal as seen in other time-lapse studies (Greaves and Fulp 1987) and (Eiken, Brevik et al. 2000). Under the current production scenario the primary pressure depletion will only result in a small velocity and little or no density change. This is to be expected due to the already stiff nature of the matrix component of the reservoir rock. This result was evaluated by laboratory work on samples of the Williams Fork Formation taken from the cores collected at the MWX site (Rojas 2005).

Despite the expectation of only small velocity changes resulting from primary pressure depletion, the presence of fractures is anticipated to increase the occurrence of monitorable reservoir changes (MacBeth, Stammeijer et al. 2006). The characteristics and presence of fractures and the dependence on them for strong production is a key reason for evaluating the application of time-lapse shear-wave seismic data in this setting.

1.5 Approach

The approach for evaluating time-lapse changes in the s-wave seismic data involves three main steps. The first step consisted of cross-equalizating the poststack migrated data between the 2003 (base) and the 2004 (monitor) surveys. The goal of this step is to minimize differences in the seismic volumes not related to production, while

preserving and enhancing production related changes. After the equalization process was complete the next step involved the inversion of the volumes to obtain impedance values. This allows for the increased resolution of observable changes. The final step involved the evaluation of time-lapse differences in both traveltimes and impedance values.

Chapter 2 Rulison Field Seismic Data

2.1 Seismic Acquisition Design

The Reservoir Characterizations Project's time-lapse 2003 and 2004 seismic surveys were collected over a heavily drilled and tested portion of Rulison Field which is located in the Piceance Basin of western Colorado (Figure 2.1). The survey is bounded to the south by Interstate 70 and to the north by the topographic feature of the Roan Cliffs. The survey area also includes several additional pieces of seismic and well log information that were vital to earlier studies and understanding of the reservoir. The blue outline defines the extent of the time-lapse RCP surveys in Figure 2.1. The larger green outline in Figure 2.1defines the extent of the 1996 U.S. Department of Energy 3D p-wave seismic survey. The 1996 survey was used in conjunction with the 2003 RCP survey for the first p-wave time-lapse analysis over Rulison Field (Kusuma 2005). The southeast corner of the survey area also contains a 3D walkaway vertical seismic profile (VSP) collected in the RMV 30-21 well during the 2003 survey. The high-resolution seismic information collected around this wellbore provided additional insight into shear wave polarizations and time-delays within the reservoir (Mattocks 2004). Along with additional seismic information the RCP survey area also contains important well log information including; Fullbore Formation MicroImager (FMI) and cross-dipole sonic logs. The image logs provided information concerning horizontal stress alignments, the presence of fractures, and reservoir complexity (Higgins 2006). The cross-dipole sonic logs also provided important information about shear wave velocities, anisotropy, and stress orientations along the wellbore (Burke 2005). The RCP survey area also includes dense well information collected from a 10-acre well spacing pilot area drilled by Williams Production RMT, the operator of the field, along with information from other

wells throughout the field. A previous study by the U.S. Department of Energy, referred to as the Multiwell Experiment (MWX), was completed approximately two miles south of the RCP survey area. This study included three vertical and one horizontal wells. Large sections of core were collected from these wells, along with an extensive suite of logs. Pressure, fracture, hydraulic fracturing, and well communication information were also collected from these wells (Nelson 2003).

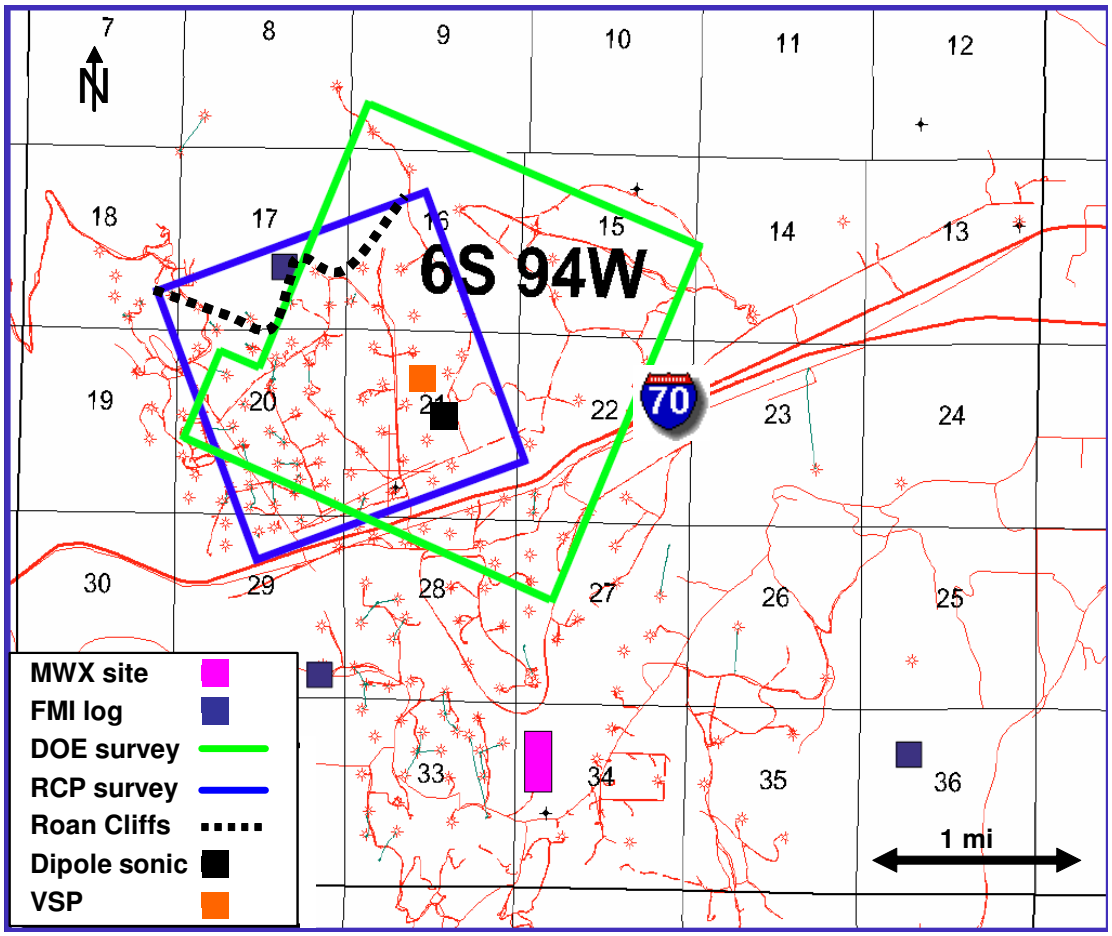

Figure 2.1 - The locations of seismic and well log information collected at Rulison Field (Keighley 2006).

The 2003 and 2004 RCP surveys covered an area of 7260 ft by 8250 ft or 2.15 mi^2 (5.57 km^2). The survey included approximately 1500 receiver and 700 source locations. The receivers were laid on 26 approximately north-south inlines, each containing 66 receiver groups spaced 110 ft apart. The inlines were spaced 330 ft apart in the approximately east-west direction (Figure 2.2). All receivers were active for each source point, with the signals being recorded using radio telemetry. 12 source lines were run perpendicular to the receiver lines in the approximately east-west direction. Each inline contained 75 source locations spaced every 110 ft. Source lines were spaced at 660 ft intervals in the approximately north-south direction (Figure 2.2). The source and receiver locations were surveyed with the use of a global positioning system (GPS). Accurately recording the source and receiver locations during the 2003 survey enabled the acquisition geometry to be closely repeated during the 2004 survey. Due to the repeatability of the survey geometry, the difference between the 2003 and 2004 source and receiver locations were small (Figure 2.3). The standard deviation between the included 2003 and 2004 source and receiver locations were limited to 3.30 ft and 1.98 ft respectively. These values of standard deviation were calculated after excluding source and receiver locations that differed by more than half the source and receiver spacing of 110 feet between the years. The exclusion of source and receiver locations was done during the early stages of processing (Winarsky 2006). This step increased the repeatability of the data by limiting differences in the subsurface volume sampled by corresponding seismic signals recorded during the surveys (Ross and Altan 1997).

As a result of the surveys limited size, the fold quickly decreases from the central region to the edges of the survey (Figure 2.4). The fold decreases from a maximum of nearly 225 to 1 within three-quarters of a mile. The substantial decrease in fold near the edges may result in decreased repeatability, and prevent the interpretation of time-lapse changes near the edges. The presence of low fold data is also apparent on the northern edge of the survey. This area coincides with the rise in topography associated with the Roan Cliffs that prevented full source and receiver coverage (Figure 2.2). The strong

fold coverage through the central part of the survey provides the best opportunity for strong repeatability, and the observation of time-lapse changes. Despite the fact that the fold quickly decreases towards the edges of the survey, the geometry repeatability is still high indicating the potential for observing production induced changes in the lower fold edge regions of the survey.

The sources for both the RCP shear wave surveys were shear vibrators with two orthogonal horizontal sources. The shear sources swept through a range from 5 to 50 Hz. For each source point there were 6 sweeps of 10 seconds each. The shear source vibrated in both the inline and crossline directions at each source location. The signal was recorded using I/O VectorSeis System Four digital single sensor multi-component geophones (Input/Output 2005). A single multi-component geophone was planted at each receiver location (Figure 2.5). The use of a single geophone per receiver location setup enhanced the repeatability between the surveys by allowing for the accurate repeat placement of geophones in the same locations for the second survey. This is in comparison to an array of geophones planted around a single surveyed location. Planting the sensors also increased repeatability by maximizing ground coupling, and limiting the presence of surface noise (Krohn 1984).

An additional important feature of the survey design was the placement of all geophones prior to the initiation of the sources. This allowed for all receiver locations to be active for each source point. Having the entire survey live increased the fold, offset, and azimuthal distribution of the data to maximizing quality in the limited survey area. Constant geophone placement also helped provide consistent ground coupling throughout the shooting of the individual surveys by limiting the interaction between the crew and the sensors. The geophones recorded for 16 seconds at 2 ms sampling for each shear wave source point.

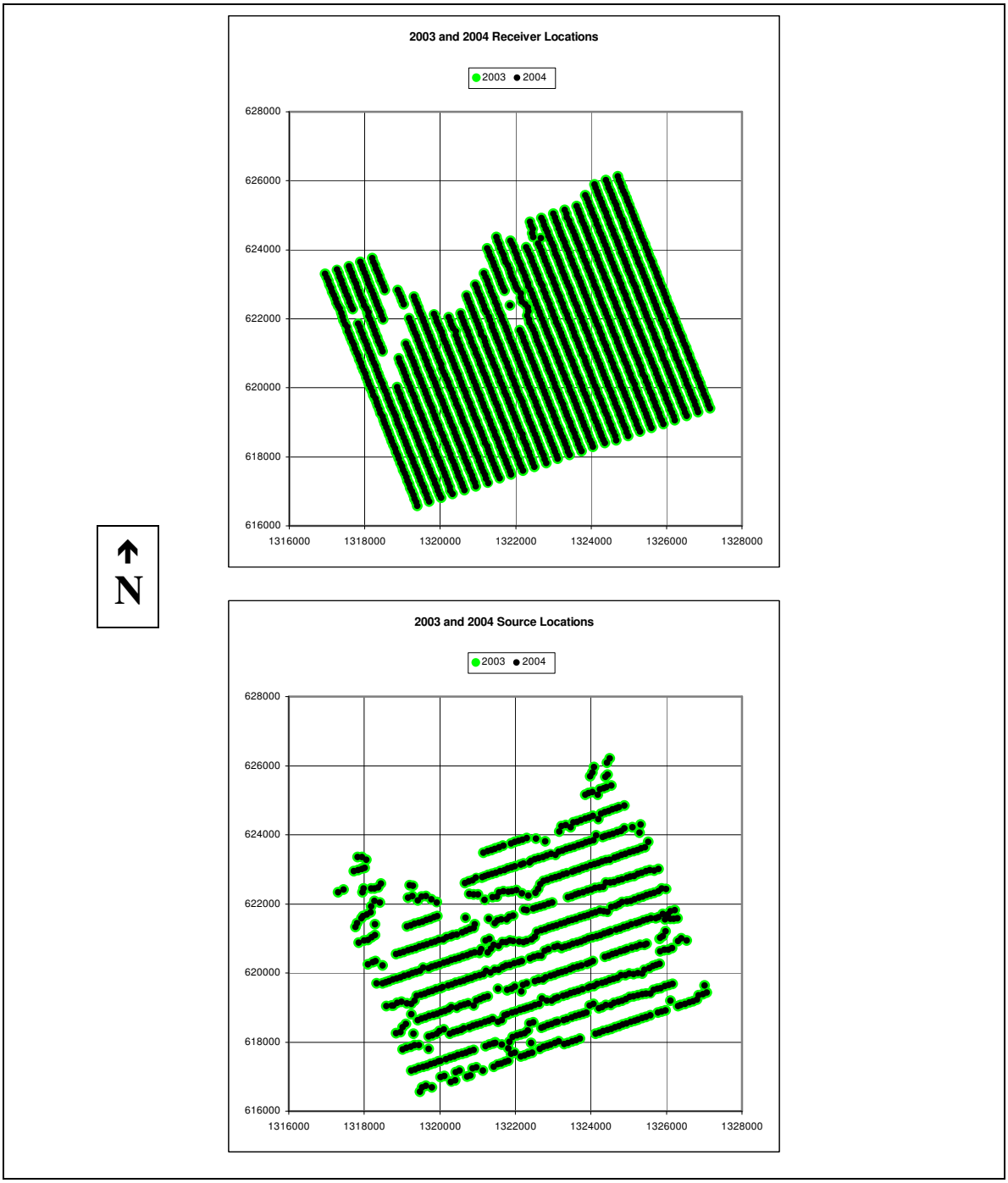

Figure 2.2 - Receiver and source locations for the 2003 and 2004 RCP surveys.

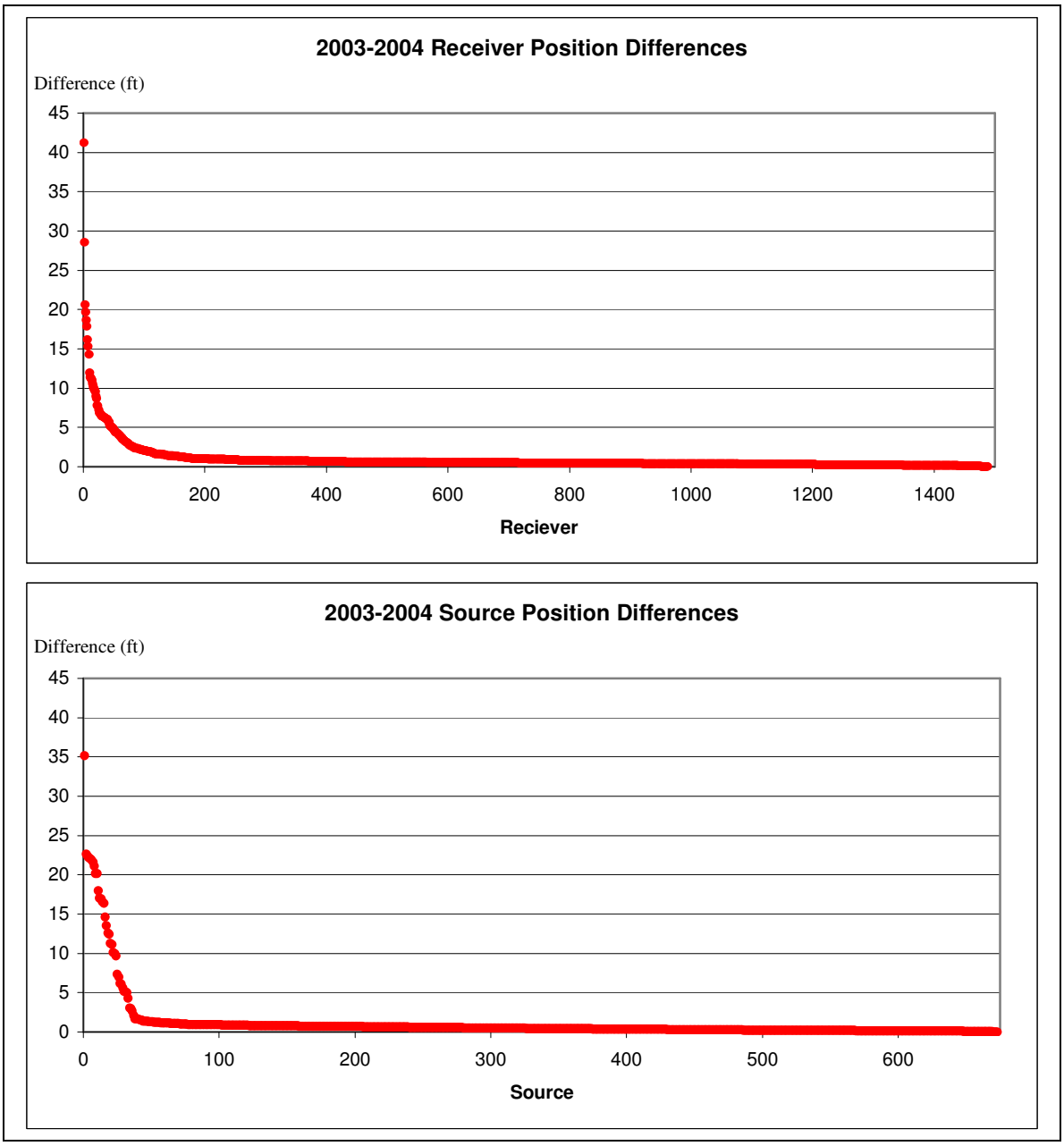

Figure 2.3 - Difference between 2003 and 2004 receiver and source locations for the RCP survey.

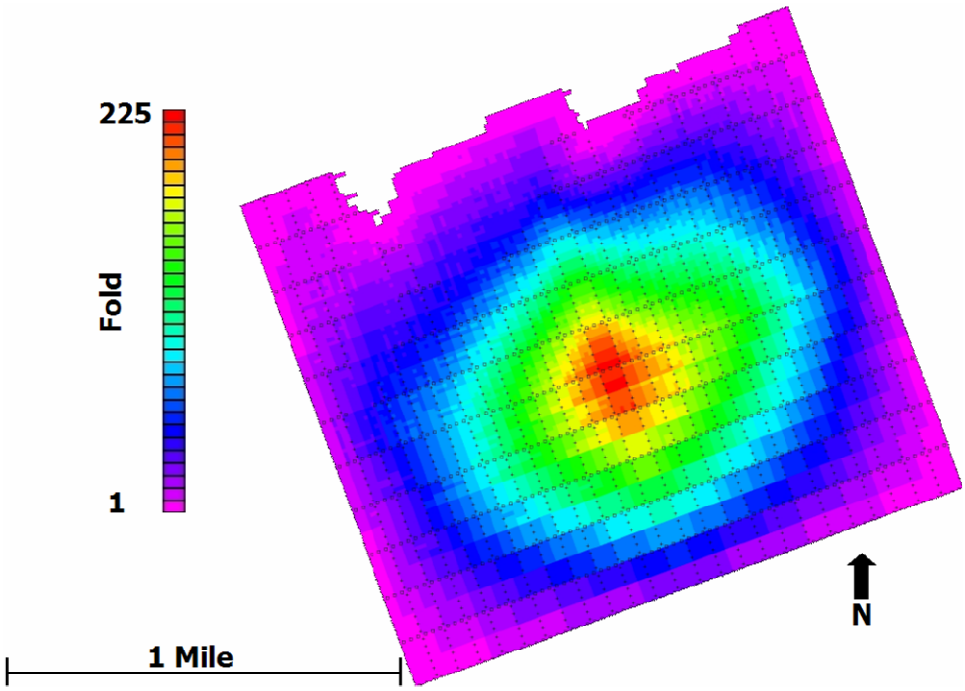

Figure 2.4 - Fold distribution for all offsets.

Figure 2.5 - I/O VectorSeis System Four digital single sensor multi-component geophone. Example of how geophones were buried.

The fact that all the geophones were planted prior to the beginning of the survey could also provide an additional opportunity for the collection of passive seismic data. Depending on noise levels and the presence of tectonic activity, passive seismic data could help to enhance the understanding of possible fault location and production activity, and help to further characterize the reservoir. Permanent receiver locations would even further enhance these aspects by increasing repeatability, decreasing the costs of additional surveys, limiting environmental impact, and allowing for continual or passive seismic monitoring. Passive seismic monitoring can also help to further understand hydraulic fracturing enhancements in the field, and add additional insight into drainage areas and stress patterns.

2.2 Shear Wave Processing

Veritas Geoservices processed the 2003 and 2004 shear wave seismic data collected at Rulison Field. The processing was performed using a time-lapse routine. This implies that the 2003 and 2004 data volumes were processed together with the same routine. Processing the data in this fashion limits differences in the surveys induced by differing processing steps and parameters. This is a major advantage of dedicated time-lapse surveys, where the acquisition and processing routines can be closely matched to maximize repeatability (Ross and Altan 1997). The processing routine for the RCP surveys is provided in Table 2.1, and mimics the type of routine suggested for time-lapse processing (Ross, Cunningham et al. 1996).

Table 2.1 – 2003 and 2004 RCP shear wave processing routine.

Tilt correction applied in field
Demulitplex
Geometry correction
Manual trace edits
Polarity correction – receiver and shot
Spherical divergence correction
Surface consistent amplitude equalization
Alford rotation – N45W
Minimum phase correction
Surface consistent deconvolution
Source/receiver statics – from P-S data
CDP Gather
Velocity analysis (preliminary)
Noise attenuation – Radon Transform
Surface consistent statics (preliminary)
Velocity analysis
First break mutes
Trim statics
Amplitude equalization – mean scaling
Stack
Noise attenuation (Fxy deconvolution)
Migration – Kirchhoff

This sequence of processing steps is consistent with current industry processing practices. The processing routine and parameterization were the same for both surveys. This includes the same normal moveout and migration velocities. One variation that did occur was the independent calculation and application of the static corrections for each year (Winarsky 2006). This was a result of differing ground conditions, dry for the 2003 survey versus wet for the 2004 survey.

The use of shear wave data requires a shear wave specific processing step. This processing step is due to the nature of shear wave propagation. Let us first consider a simple case of vertically propagating waves. As a shear wave is induced by a horizontal source at the surface it will propagate downward with the shear velocity of the medium (Thomsen 2002). Unlike p-waves where the particle motion is in the direction of propagation, or vertical, shear wave particle motion is orthogonal to the direction of propagation. So, for the simple case of a vertically propagating shear wave the particle motion is in the horizontal plane. Assuming the shear wave was excited in an isotropic medium the polarization of the horizontal particle motion would be aligned with the direction of the horizontal source (Thomsen 2002). The wave will continue to propagate with the same particle motion and polarization as long as the medium remains isotropic. In the case that the medium becomes anisotropic, say due to a vertical set of aligned cracks, the single induced shear wave would split into two separate shear waves (Figure 2.6). Splitting of the shear wave will occur if the initial wave's polarization is at any angle other than parallel to the alignment of the crack set. If the polarization angle is parallel to the orientation of the crack set no splitting will be induced (Thomsen 2002). When the wave's polarization is misaligned with the crack set the initial shear wave will split into two orthogonal shear waves, one polarized parallel to the crack set orientation, and one polarized perpendicular to the crack set orientation (Figure 2.6). This process is referred to as shear-wave splitting or birefringence (Crampin 1981). The wave polarized parallel to the crack set is referred to as the fast or S1 shear wave. The wave polarized perpendicular to the crack set is referred to as the slow or S2 shear wave. The terms fast

and slow refer to the propagation velocity of these waves. Since the fast shear wave is polarized parallel to the crack set it only samples the stiff matrix component of the rock, and is unaffected by the crack component. The slow shear wave that is polarized perpendicular to the crack set, however, propagates through a more compliant rock by sampling both the matrix and crack component (Thomsen 2002). Polarization differences result in variations in propagation velocity.

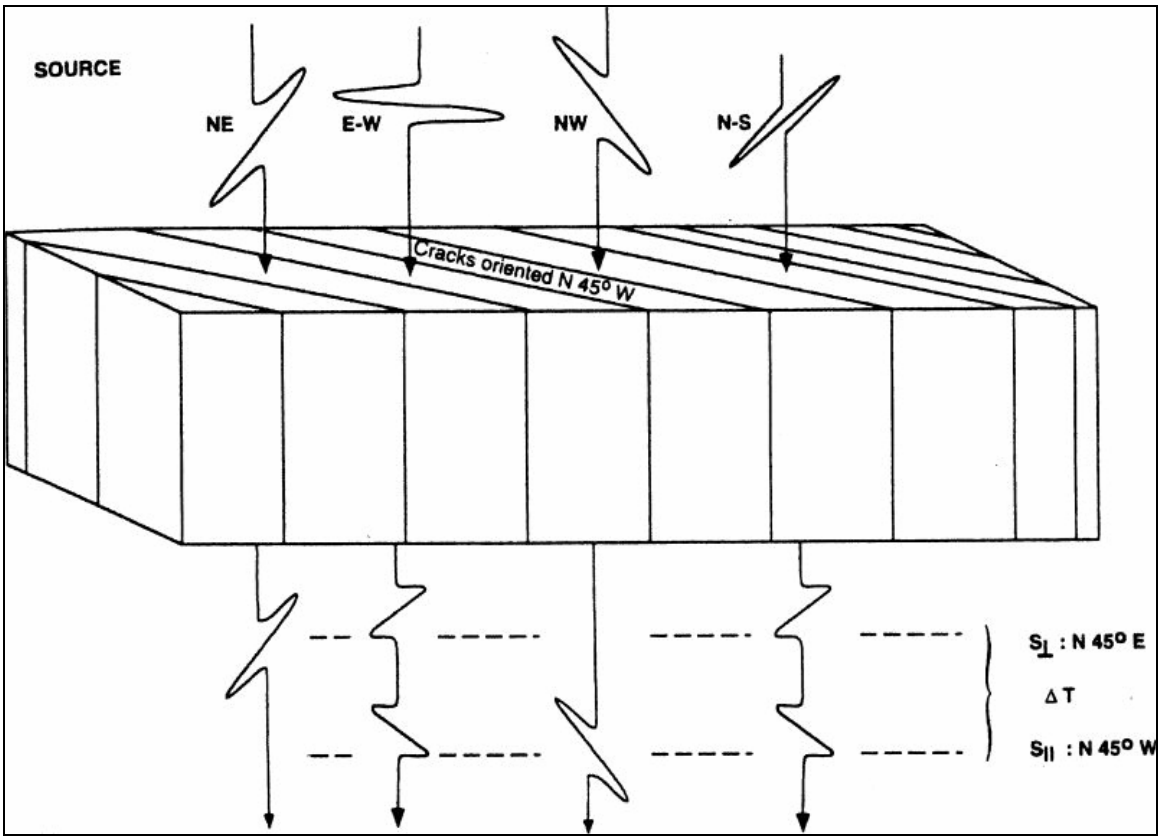

Figure 2.6 - Cartoon of shear-wave splitting phenomenon. Shear waves polarized perpendicular to the crack orientation do not split. Shear waves polarized at an angle to crack set split into fast and slow shear waves polarized parallel and perpendicular to the crack set orientation respectively. (Sheriff and Geldart 1995)

While the separation between the shear wave polarizations induced by velocity variations appears to be a trivial quantity to measure in theory, actual 9C seismic data

often times creates an additional complication. If the crossline and inline sources and receivers are aligned with the natural coordinate system, or crack/fracture/stress orientation, the sources would excite the S1 and S2 polarizations, and the receivers would record the respective S1 and S2 signals. When the survey coordinate system differs from the natural coordinate system both source signals are split. The horizontal receivers then record a fast and slow component from each source. This situation results in a 2 x 2 matrix of crossline and inline sources and receivers with each component containing information or energy from the both polarizations (Figure 2.7). The goal is then to concentrate the energy along the diagonal principle components of the matrix. This is done through a tensor rotation that maximizes the energy on the diagonal, S11 and S22, components while minimizing energy on the off diagonal components (Alford 1986). The angle that allows for the proper energy separations indicates the principal direction of azimuthal anisotropy (Thomsen 2002).

S11 Inline Receivers Inline Sources	S12 Crossline Receivers Inline Sources
S21 Inline Receivers Crossline sources	S22 Crossline Receivers Crossline Sources

Figure 2.7 – 2 x 2 matrix of mixed fast and slow shear wave polarization information due to misalignment of survey and natural coordinate system.

The Alford rotation that was performed on the 2003 and 2004 data volumes consisted of the same single rotation applied to the entire datasets of both surveys. The data was rotated to a direction of N45W. This angle was used because it resulted in the strongest minimization of off diagonal, S12 and S21, energy. The angle is also consistent with the polarization angle calculated from the 2003 VSP data collected in the RMV 30-21 well. The polarization angle collected from the VSP data had an average value of N46W. The similarity in polarization angles derived from the two separate data sets increases the confidence in its application.

In order to apply a single rotation to the data three main assumptions are made. The first assumption is that the subsurface interval above the reservoir is isotropic, so that no shear-wave splitting is induced by this interval. The second assumption is that the orientation of the azimuthal anisotropy is consistent through the reservoir interval. The third assumption is that the necessary rotation angle is consistent between the two surveys. These assumptions imply that there was only a single incidence of shear-wave splitting through the reservoir interval, and that the data was correctly oriented with the natural coordinate system. It also implies that between the 2003 and 2004 surveys the principle direction of anisotropy is consistent, so that a comparison of the fast and slow volumes from the individual surveys is valid. The assumption for change in this reservoir's production scenario is not a change in the orientation of the azimuthal anisotropy, but an observable change in its strength.

The above assumptions were made to simplify and allow the poststack time-lapse analysis of the shear wave data. Additional analysis techniques should also be considered, but do not fall within the scope of this research. These additional tools include a prestack analysis of the s-wave data, further increasing the understanding of lateral variations in anisotropy (Vasconcelos and Grechka 2006). A layer stripping approach could also be applied to allow for an increased understanding of the vertical variation in anisotropy (Thomsen, Tsvankin et al. 1999). The use of these techniques can provide additional insight into production-induced changes in the reservoir, including

both changes in the strength of anisotropy and possible changes in the s-wave polarization directions between the surveys. A more in depth analysis of the VSP data could also provide a higher resolution understanding of vertical variations in anisotropy. The additional collection of a time-lapse VSP survey in the same wellbore could also drastically increase the understanding of production related changes through the high resolution information.

After the time-lapse processing routine a preliminary comparison can be made between the fast and slow shear data volumes of the 2003 (base) and 2004 (monitor) surveys. While the acquisition geometry and processing routine were closely matched between the years to allow for this comparison, additional processing is still required to further increase the repeatability of the surveys. This processing involves zone specific comparisons and cross-equalization process to monitor and further minimize differences in the datasets. The continued presence of differences is a result of slight variations in acquisition geometry, ground conditions, and differing noise sources between the surveys. The cross-equalization routine was used to decrease the presence of random differences between the surveys, and allow for the observation of production-induced changes within the reservoir.

The use of dedicated time-lapse surveys is a key element to the success of monitoring production related changes. This is a result of the challenging and unconventional nature of the reservoir at Rulison Field. Unlike other time-lapse studies that monitored fluid saturation changes, water floods, and other enhanced oil recovery programs, this reservoir presents a new challenge for time-lapse data. Due to the expected small time-lapse changes resulting from gas production, the maximization of repeatability is an essential part to this study. By minimizing differences in acquisition geometry and processing steps the result is an opportunity to observe small production related changes, and increase the reservoir understanding.

Chapter 3 Cross-Equalization

3.1 Introduction

The goal of time-lapse seismic monitoring is to provide the opportunity to monitor subsurface changes through the use of multiple seismic surveys collected at different times (Rickett and Lumley 2001). The subsurface changes of interest can be caused by the production of hydrocarbons or injection scenarios that occur during enhanced oil recovery operations (Lumley 2001). To monitor these changes, differences resulting from acquisition design, noise, weather, and other nonproduction related variations must be minimized between the surveys. The minimization of these variations is achieved through a cross-equalization process. The goal of the cross-equalization process is to increase the repeatability of the surveys and reduce random data variations, while preserving and enhancing the presence of production related changes. Increased repeatability is achieved by minimizing variations and background noise in the data not related to production. The cross-equalization scheme is performed to match a static subsurface interval above the reservoir zone between the two surveys. The idea is that this static subsurface section lies above the productive zone of the reservoir, and is assumed to have not experienced any production related alteration. By matching a zone of the subsurface that has not changed during the interval between the surveys, variations between the surveys not related to production can be minimized.

The three main attribute variations confronted in the data were event arrival times, spectral content, and amplitude content. By matching these three components within the static sections, changes not related to production are minimized through the rest of the data (Rickett and Lumley 2001). The static window used for the matching of the two surveys was a 100 ms time window centered over the Upper Mesa Verde (UMV) seismic

event (Figure 3.1). The window location and size were chosen due to the strength and consistency of the UMV horizon and it's upper and lower bounding events. By basing the cross-equalization window over strong consistent seismic events, there was an increased ability to match the two surveys. For the purpose of this shear wave time-lapse study, the fast (S11) shear wave volumes and the slow (S22) shear wave volumes were matched separately between the base and monitor surveys. The process of cross-equalization was performed using the PRO4D software in the Hampson-Russell software package (Hampson-Russell Software Services 2006).

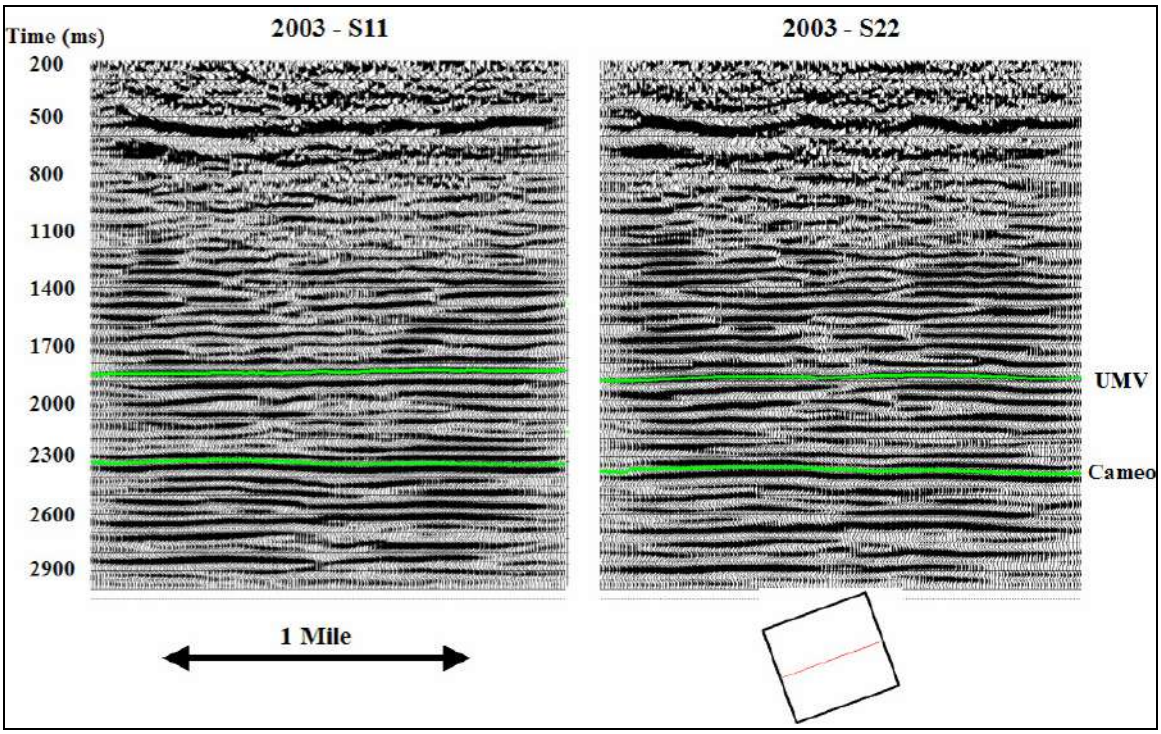

Figure 3.1 - East-west line 72 from the fast (S11) and slow (S22) 2003 data volumes. Upper Mesaverde (UMV) and Cameo events are marked.

In many time-lapse seismic studies acquisition geometries and processing flows must also be matched between the two surveys. The goal of this procedure is to

minimize differences in the data resulting from varying survey design and quality. This additional step is often times performed on seismic surveys that were not shot with a time-lapse analysis in mind, and that may have had significantly varying acquisition geometries and data characteristics (Kusuma 2005). The seismic surveys used in this study, however, were shot as dedicated time-lapse surveys. The term dedicated implies that they were shot with a time-lapse analysis in mind, and that the acquisition geometries and processing were matched as closely as possible from the beginning. The matching of these parameters helps to increase the repeatability between the surveys. Due to the fact that the geometries were matched during the shooting of the surveys no major processing steps were taken to alter the survey designs. The initial time-lapse processing by Veritas Geoservices also helped to minimize slight variations due to differences in acquisition and ground conditions. Since this study is focused on the use of poststack migrated seismic data with similar geometries, the cross-equalization process will focus on event arrival time, spectral content, and seismic amplitude to minimize undesired time-lapse differences.

The seismic data was cross-equalized using four separate steps. Variations in the arrival times for events above the reservoir were minimized using a bulk static time-shift. The purpose of this shift was to align events in the static window between the surveys. The time-shift applied was a trace-by-trace time-invariant bulk shift between the monitor and base surveys. The next step involved matching the spectral content of the two surveys. This was done with the use of a global shaping filter applied to the monitor survey. The filter was derived by a comparison of the seismic information contained in the static windows of the two surveys (Rickett and Lumley 2001). The third step involved trace-by-trace amplitude balancing. The root-mean-square (RMS) gain values applied to the monitor data sets were derived from a trace-by-trace amplitude comparison of the static window intervals for the two surveys. After these first three cross-equalization steps were applied, variations in event arrival times were assessed between the surveys. This provided an indication of variations in seismic velocities with time

(Calvert 2005). A final cross-equalizing step was performed to allow for the comparison of variations in amplitude and impedance values with time. This final step consisted of a time-varying time-shift that aligned corresponding events in time between the monitor and base surveys. This allowed for the comparison of the same subsurface intervals within the seismic data (Johnston 2006).

An additional processing step was also performed prior to beginning of the cross-equalization process. This step involved the application of the trapezoidal band-pass filter, aimed at minimizing the presence of high frequency random noise in the data. The filter ramped up from 0 to 5 Hz, and then ramped back down from 25 to 30 Hz. The result of the band-pass filter was a reduction in the presence of the high frequency noise content (Figure 3.2). Differencing the unfiltered and filtered base S1 volumes illustrates the filters removal of high frequency noise from the data (Figure 3.3). The filter resulted in cleaner difference sections, and an enhanced ability to allow for the observation of time-lapse differences in the strongest frequency range from 10 to 20 Hz. Observable changes are expected to occur through this range; since it is were the majority of the frequency information lies through the reservoir interval. One negative aspect of this filter is the possible loss of seismic information at the UMV (1850 ms) and Cameo coal (2350 ms) events, where more continuous differences occur between the filtered and unfiltered volumes (Figure 3.3). While this presents a possible problem, the reduction in the overall background noise level outweighs the expectation of observing time-lapse changes within the high frequency content of the data. This step was also necessary since the time-lapse analysis was performed on the unfiltered unscaled poststack migrated data. This data was used to limit the number of final processing steps performed by Veritas, and increase the chances of preserving time-lapse changes through a zone specific cross-equalization.

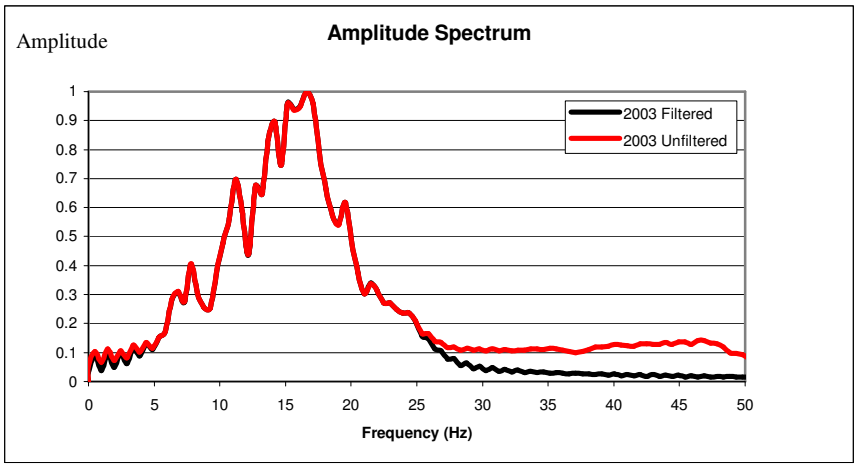

Figure 3.2 - Amplitude spectrum from 1800 to 2800 ms for 2003 S11 data before and after applying 0, 5, 25, 30 Hz bandpass filter.

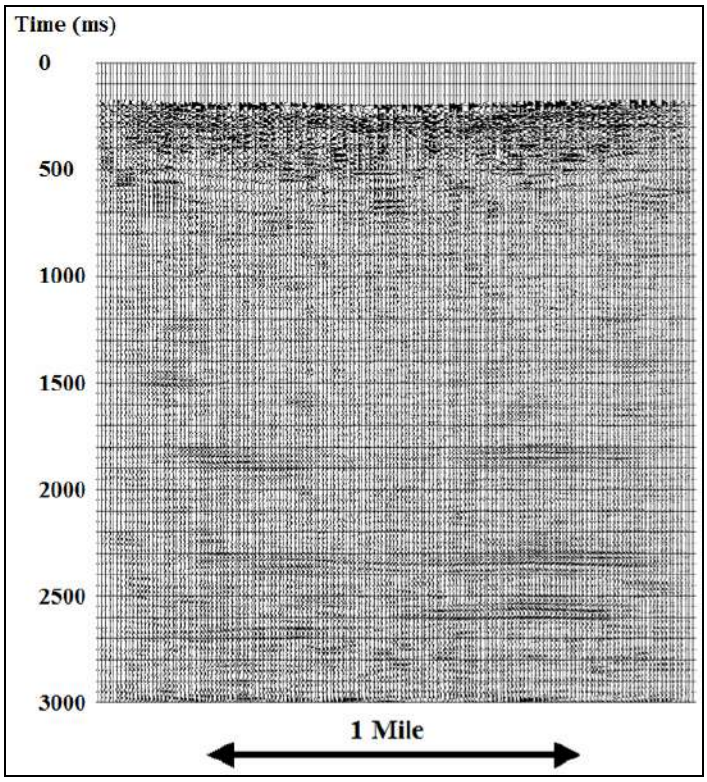

Figure 3.3 - East-west line 72 of the difference between untiltered 2003 S11 and 0, 5, 25, 30 Hz bandpass filtered 2003 S11 volumes.

Similar to the time-lapse processing procedure the goal of each equalization step was to increase the repeatability between the surveys while preserving and enhancing the presence of production-induced changes in the seismic data. Two main techniques were used to monitor this improvement in repeatability. These techniques included monitoring decreases in the normalized root-mean-square difference (NRMS) values, and differences between the amplitude spectrums of the individual surveys. The benchmarks provided by these techniques allowed for an understanding of the improvement in, and strength of the repeatability with each equalization step.

With the conclusion of the cross-equalization process it was possible to observe changes in the subsurface that can be related to the production of gas at Rulison Field. These time-lapse seismic changes through the reservoir were analyzed through the use of velocity and acoustic impedance variations in both the S11 and S22 shear wave volumes.

3.2 Static Time-Shift

The first step in cross-equalizing the base and monitor shear wave seismic surveys was to correct for static time-shifts between them. Static differences were corrected for above the reservoir interval where no production related change was expected. The goal of this step was to align a series of events above the reservoir that correspond between the surveys. This step is similar to the application of static corrections during the primary processing stages, but results in a more refined alignment where no time-shifts are expected. Alignment was achieved by applying a bulk shift to the monitor survey. The bulk shift was a single time-invariant shift applied on a trace-by-trace basis. Time-invariant indicates that a single bulk shift was applied to the entire trace. This step corrects for slight errors in the application of the initial static corrections. As noted in the processing review the initial static corrections were applied independently for both the surveys. This was necessary due to the different ground conditions between the years. The base survey had dry surface conditions compared to the monitor survey, which had

moist surface conditions. Variations in the static corrections are small, but still contribute to slight time-shifts above the reservoir interval (Figure 3.4). Additional errors in the static corrections can be attributed to differing shear wave sources. The 2003 survey used IVI and Mertz 18 shear wave vibrators, while the 2004 survey used an older version of the Mertz 18 vibrator. While the source signatures were matched in the processing routine, slight static variations still existed. The bulk time-shift applied during the first stage of cross-equalization was used to further increase the alignment of the surveys through a more localized static interval, and further increase repeatability between the surveys.

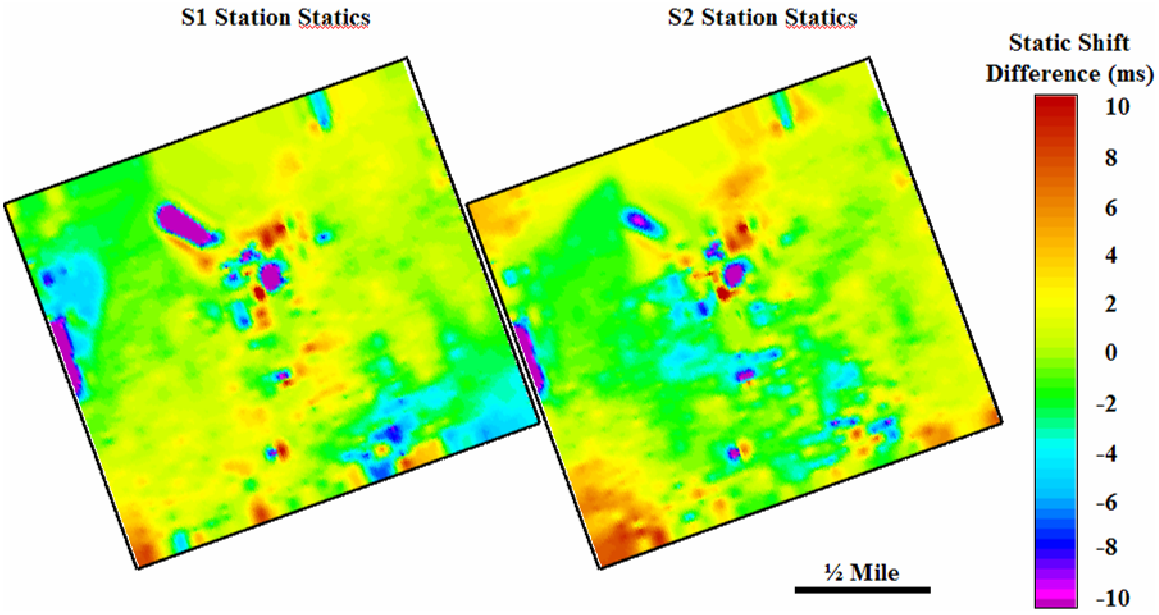

Figure 3.4 - Static station correction differences between the 2004 and 2003 shear wave surveys. Left panel is for S11 data, and right panel is for S22 data.

The value of the time-shift applied was calculated using a cross correlation comparison of a 100 ms window centered over the UMV seismic event. The cross correlation time-shift is calculated as the time-shift necessary to maximize the cross correlation values at corresponding traces between the base and monitor surveys. The

correlation window was the same length for both the S11 and S22 shear volumes, and was chosen to include an entire seismic wavelength. The wavelength for the shear data volumes was calculated using a peak frequency content range from 14 to 17 Hz, and an average velocity of approximately 8000 ft/s (2440 m/s) with a standard deviation of 1100 ft/s (335 m/s). The peak frequency content was calculated from the amplitude spectrum of both the S11 and S22 base data volumes (Figure 3.5). The amplitude spectra were calculated from 1800 to 2800 ms in the seismic data. This interval was chosen as the main zone of interest, since it includes the entire reservoir section. The average velocity was calculated from the cross-dipole sonic log that was run in the RWF 332-21 well located in the southeast corner of the survey (Figure 2.1). The velocity values used were collected from a measured depth of 4040 ft to 7838 ft, spanning the reservoir interval. The frequency range and average velocity gave a range for the wavelength of the seismic data from approximately 471 to 571 ft (144 to 174 m), corresponding to 59 to 71 ms. Based on the calculation for the range of wavelengths the use of a 100 ms cross correlation window is adequate to include an entire wavelength when calculating time-shifts and amplitude comparisons. The UMV horizon used was the UMV event picked in the S11 and S22 shear volumes of the base survey. This positive polarity event occurs at approximately 1850 ms in the S11 volume and 1875 ms in the S22 volume (Figure 3.1). The window over the high amplitude, continuous UMV event was chosen to maximize consistency, and provide a good reference event for the correlation calculation.

Larger correlation windows were also tested, but resulted in large time-shifts and low correlation values. The decreased reliability of the larger window time-shifts was associated with the presence of random variations in event amplitudes above the UMV horizon. The reliability of the time-shifts was measured by the strength of the correlation coefficients, and a comparison of the calculated correlation time-shifts and horizon-based time-shifts.

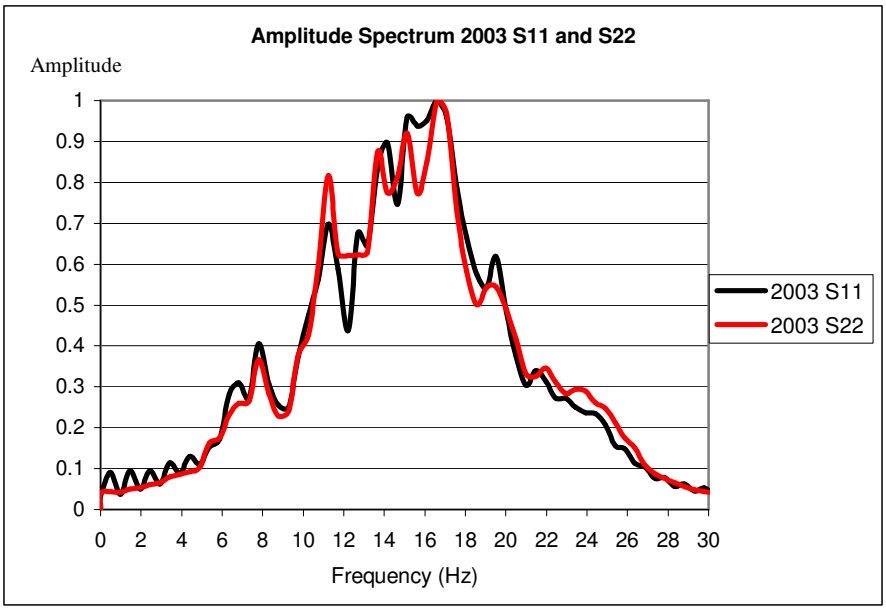

Figure 3.5 - Amplitude spectrum of base (2003) shear wave surveys, for both S11 (fast) and S22 (slow) volumes calculated from 1800 to 2800ms.

Time-shift values between the S11 volumes range from positive values of approximately 3 to 7 ms through the central high fold section of the survey. There is a background time-shift level of between plus and minus 1 ms (Figure 3.6). A mask was applied from +1 to –1 ms to illustrate the background shift. The positive shift values indicate a pull up in the events in the 2004 survey. The positive nature of the time-shifts is a function of using the 2003 survey as the reference volume, while the 2004 survey was used as the input volume. This parameterization fixes the base survey in time, while the monitor survey is shifted to maximize the cross correlation value (Hampson-Russell 2006).

The resulting time-shifts can then be applied to the monitor survey to align corresponding events in time. The time-shift values are relatively small, indicating reliable static corrections and processing to match the surveys. Larger shifts of both positive and negative values are observed along the edges and corners of the survey. These larger shifts are the result of strong variations in the seismic events, and can be

attributed to the presence of edge effects, and increased levels of noise in lower fold areas.

The cross correlation values achieved by the time-shifts are high, most above 0.9 through the central part of the survey (Figure 3.6). This indicates a strong reliability in the calculated time-shifts. The large time-shifts present along the edges of the survey are associated with low correlation values of less than 0.8. Most of these values fall below 0.5 in the low fold edge regions. The presence of low correlation values corresponding to large time-shifts indicates low repeatability, and an unreliable comparison between the two surveys along the edges. These low values forced the focus to be concentrated on the central high fold area of the survey (Figure 2.4).

An additional tool for validating the calculated time-shifts was a comparison between the cross correlation time-shifts, and time-shifts calculated by differencing the time for the picked UMV events in the base and monitor surveys. The values of the correlation time-shifts agree with the horizon based time-shifts from the S11 volumes (Figure 3.7). The horizon based approach exhibits shifts that are slightly higher by approximately a millisecond, but in general there is strong agreement between the magnitude and distribution of time-shifts using both approaches. Crossplotting the time-shifts generated by the two approaches indicates a linear, approximately one-to-one relationship between the two methods (Figure 3.8). The crossplot also indicates a slight positive increase in time-shifts of between 0.5 and 1 ms for the horizon-based shift. The strength of the correlation coefficient, 0.76, indicates that the cross correlation approach is an effective tool for evaluating time-shifts between the two surveys. The strength of this approach was important during the final step of cross-equalization when the time-varying time-shift was performed. It allowed for the calculation of time-shifts when only a few continuous reflectors were present, where horizon-based shifts could not be reliably calculated.

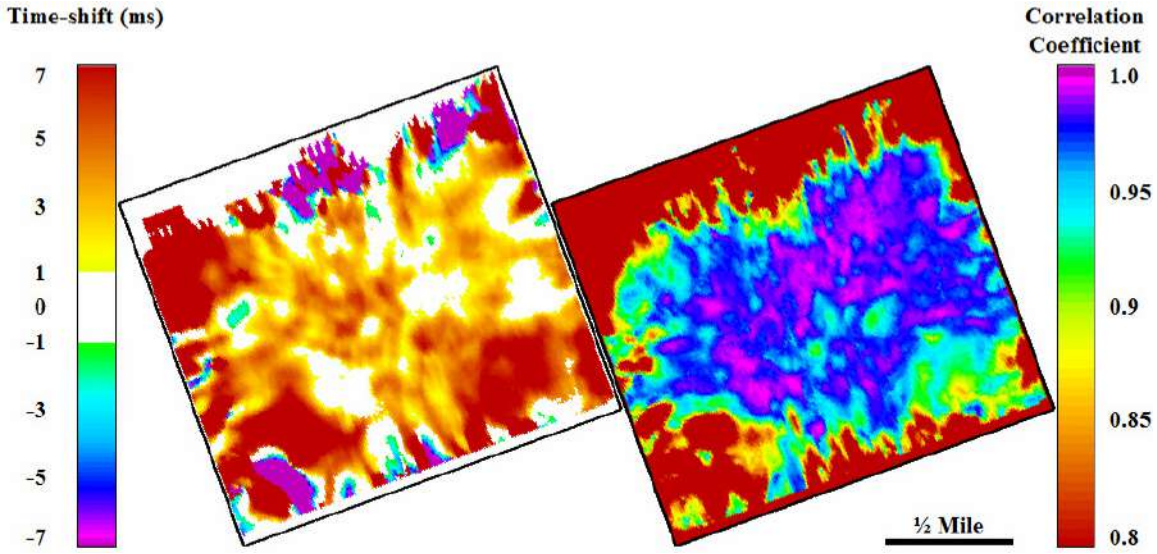

Figure 3.6 - Left panel represents correlation time-shifts calculated at the UMV event between the base (2003) and monitor (2004) S11 surveys. Positive values indicate a pull up of the 2004 UMV event. Right panel indicates correlation strength resulting from the time-shifts.

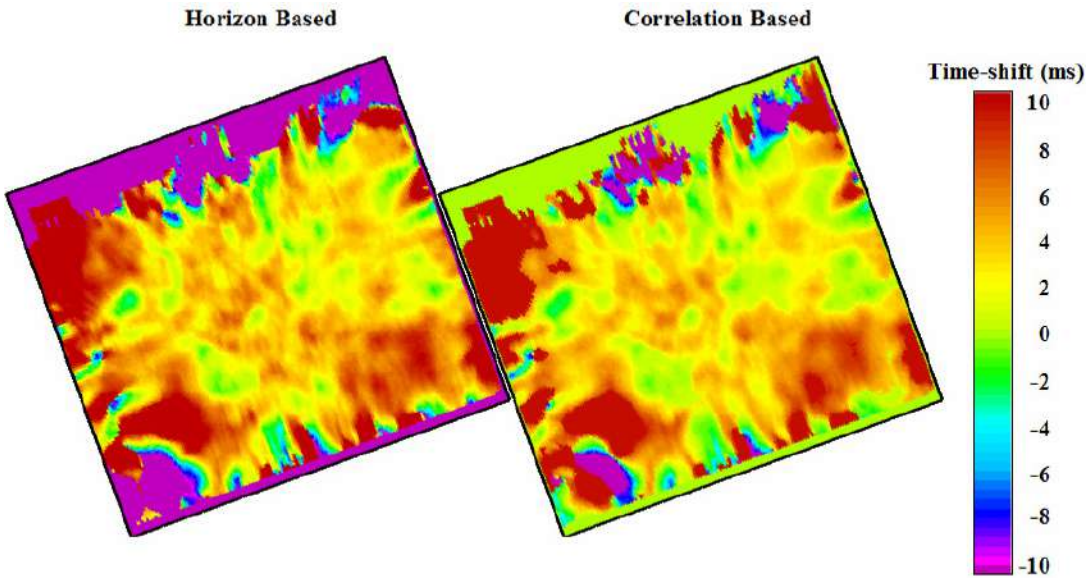

Figure 3.7 - Left panel represents time-shifts between the picked UMV event in the base (2003) and monitor (2004) S11 volumes. Right panel represents the time-shift calculated using the cross correlation approach.

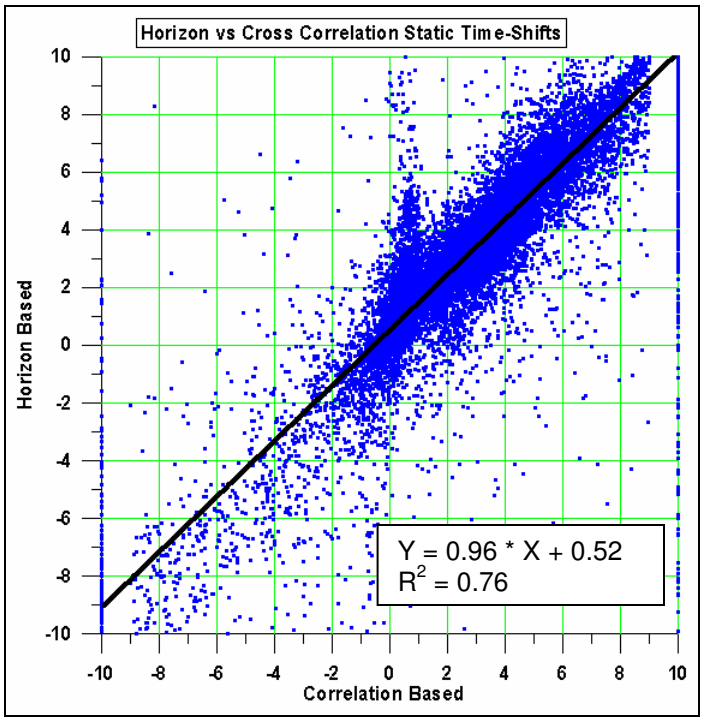

Figure 3.8 - Crossplot of horizon based static time-shift at the UMV, and cross correlation derived time-shifts for the S11 volumes. The units on each axis represent time-shifts in milliseconds.

The static time-shifts applied to the S11 volume of the monitor survey resulted in improvements in the normalized root-mean-square (NRMS) difference at the UMV horizon level. The normalized root-mean-square difference is used as a measure of repeatability between traces over a specified time window in the seismic data. Equation 3.1 expresses how NRMS difference values are calculated (Kragh and Christie 2002).

Equation 3.1

$$NRMS = \frac{2 * RMS(a_t - b_t)}{(RMS(a_t) + RMS(b_t))}$$

Equation 3.2

$$RMS(x_t) = \sqrt{\sum_{t_1}^{t_2} \frac{x_t^{\,2}}{N}}$$

The coefficients a_t and b_t represent the two traces being compared, in this case a corresponding trace from the base and monitor survey. The amplitude comparison is made over the same specified time window in both seismic data sets, represented as t = t_1-t_2 (Kragh and Christie 2002). For this comparison a 100 ms window centered over the UMV event picked in the base survey was used. The values calculated by this equation represent a measure of repeatability between the individual traces, and the surveys as a whole. This measure of repeatability is sensitive to event alignment, shape, and amplitude. Larger values close to one represent low repeatability, while values close to zero represent strong repeatability. When using this measure of repeatability, the goal is to decrease the NRMS difference values with each equalization step, indicating increased repeatability of the surveys. By improving the repeatability of the surveys, the ability to observe production induced subsurface changes increases.

The application of the static time-shift resulted in a significant decrease in the NRMS difference at the UMV level (Figure 3.9). The UMV level was used as a benchmark for understanding the increased repeatability resulting from the equalization process within the static interval. The decrease in difference is most notable through the central high fold area of the survey. After the static shift, the histogram of the normalized difference map improves from a peak at approximately 35%, to one that has been shifted to approximately 15%. Along with being shifted, the peak is also strengthened. Figure 3.9 uses fractional differences, which have been changed to percent differences within the text. The large decrease in the normalized difference indicates an increased event alignment and repeatability after the application of the first equalization step.

The normalized root-mean-square difference was also monitored at the Cameo coal level in the reservoir. This secondary measure was performed to gauge improvements through a section of the reservoir where production related change is expected. After the application of the bulk static shift to the S11 monitor volume there was also a decrease in the NRMS difference at this level. The normalized difference was calculated for a 100 ms window centered over the Cameo horizon of the base S11 survey. The peak of the histogram of the difference map decreased from slightly over 20% to around 18% (Figure 3.10). Along with the peak of the histogram shifting to lower values, there was also an increase in the strength of the peak, indicating a larger presence of low NRMS difference values. The improvement in the NRMS difference through an interval within the reservoir illustrates an overall increase in repeatability of the volumes.

A similar cross correlation derived static shift was also calculated and applied to the monitor S22 volume. This cross correlation shift was also calculated using the base survey as the reference and the monitor survey as the input volume. A 100 ms interval centered over the UMV event of the base survey was used as the correlation window. Time-shift values for the S22 volumes were slightly larger than those derived for the S11 volumes. Larger time-shift values could be the result of slighter higher noise levels in the S22 data compared to the S11 data. The time-shifts reached a maximum value of approximately 10 ms through the central part of the survey (Figure 3.11). The S22 time-shifts also exhibit the presence of strong edge effects. This can be seen as increased time-shifts, both positive and negative, and decreased correlation coefficient values. The central high fold area of the survey exhibits the dominance of positive time-shifts. This indicates a pull up at the UMV level from the base to monitor survey. The correlation coefficient is also high, above 0.9 for most of the central survey area. Lower values do exist through the central part of the survey, but are still strong and reliable with the lowest value dropping to only 0.75. The low correlation coefficient values appear to be caused by the presence of slight variations in amplitudes along the UMV event. Strong positive and negative time-shifts also appear near the edges of the survey. While

this may be the result of edge effects in the data, the presence of strong correlation values along the east and west side of the survey indicate reliability in these time-shifts at this level.

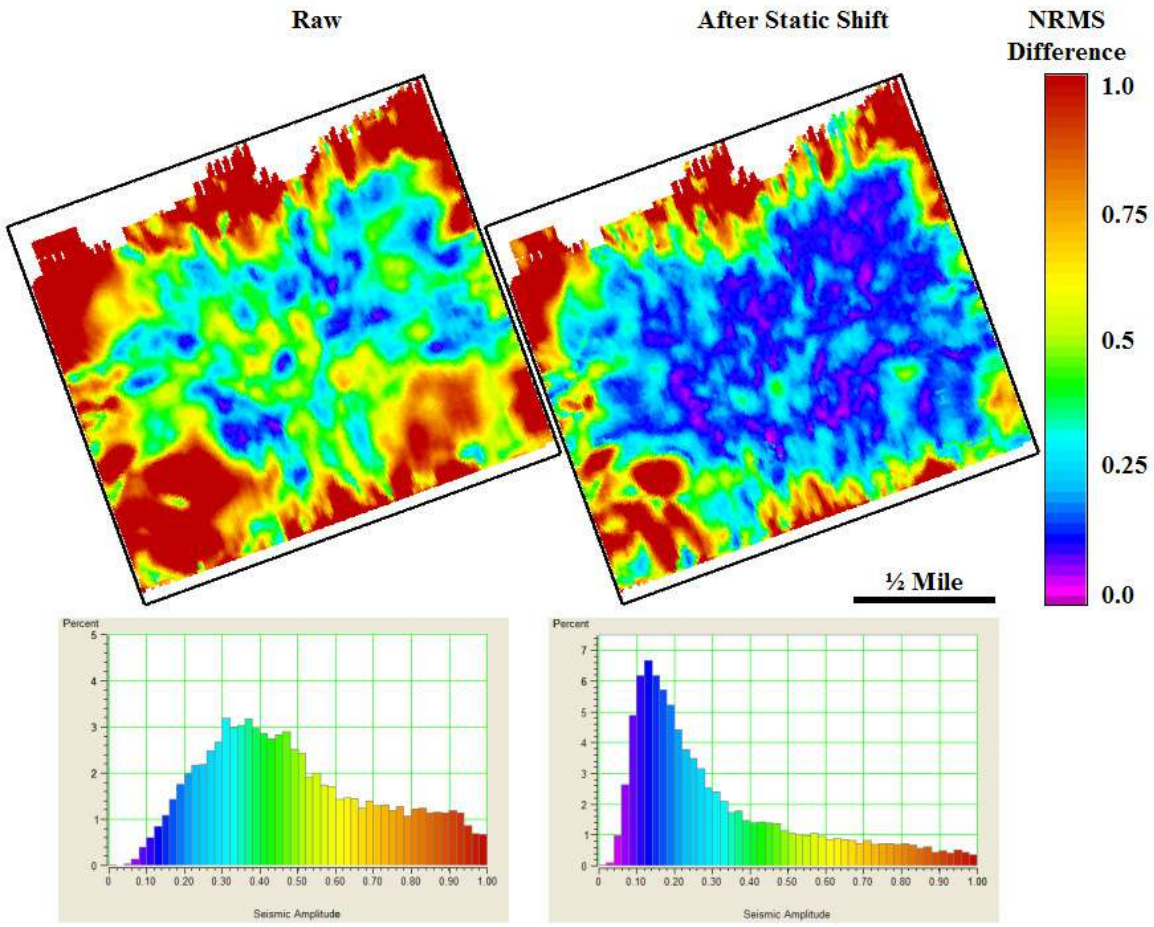

Figure 3.9 - Normalized root-mean-square difference between the base and monitor S11 surveys for a 100 ms window centered over the S11 UMV event. Left panel is prior to any equalization. Right panel is after the application of the static shift. Histograms of maps are also plotted.

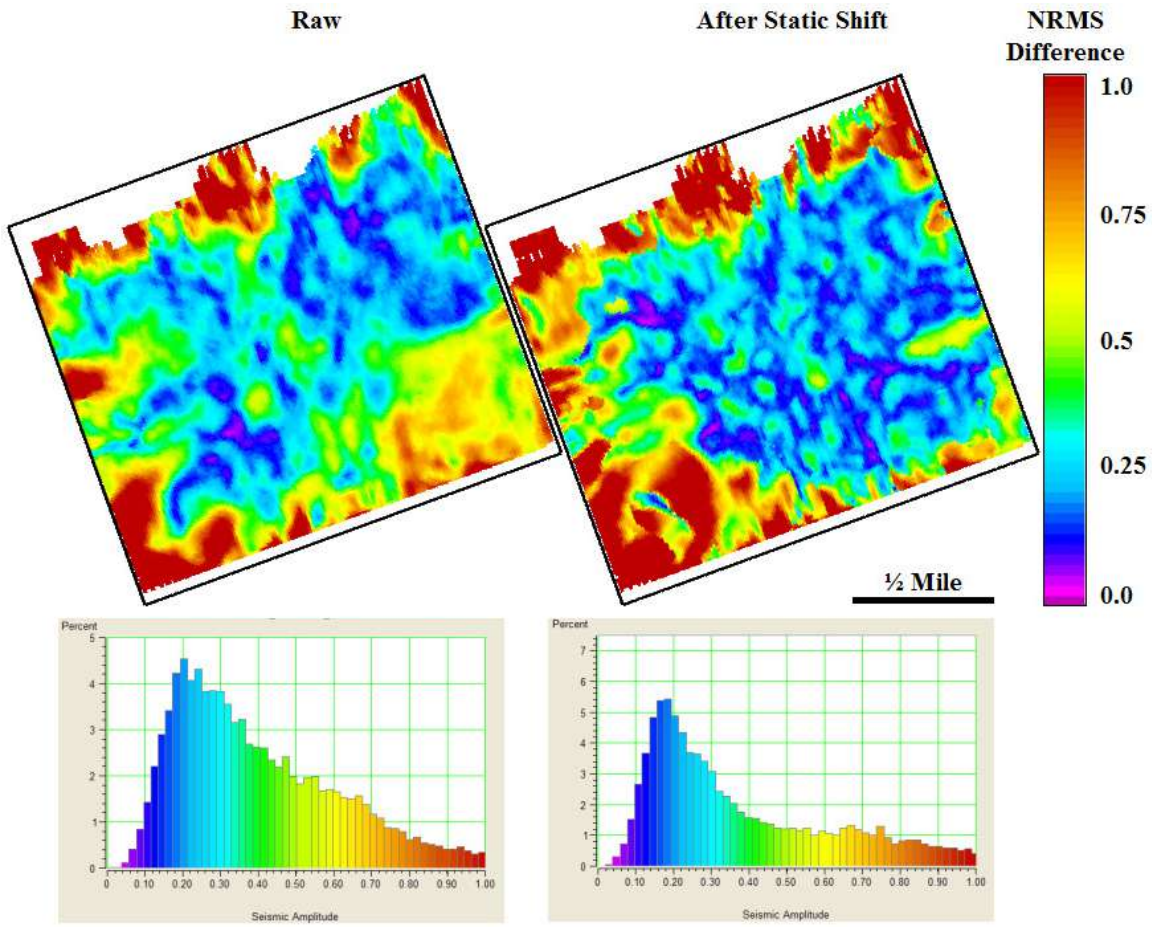

Figure 3.10 - Normalized root-mean-square difference between the base and monitor S11 surveys for a 100 ms window centered over the S11 Cameo event. Left panel is prior to any equalization. Right panel is after the application of the static shift. Histograms of maps are also plotted.

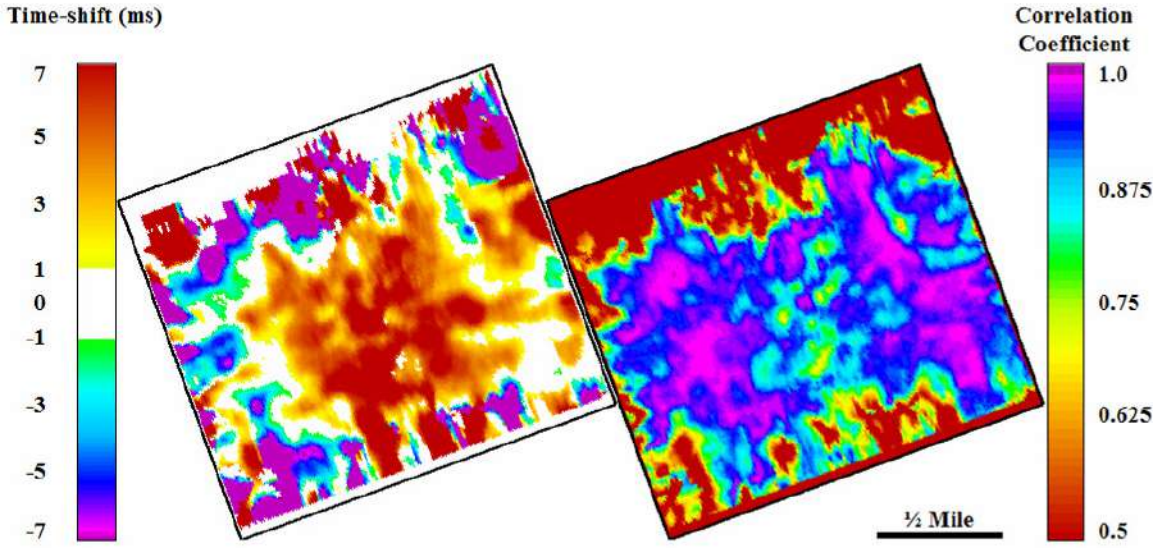

Figure 3.11 - Left panel represents correlation time-shifts calculated at the UMV event between the base (2003) and monitor (2004) S22 surveys. Positive values indicate a pull up of the 2004 UMV event. Right panel indicates correlation strength resulting from the time-shifts.

Horizon based time-shifts calculated from the UMV event also correspond to correlation based time-shift values in the S22 data (Figure 3.12). The horizon based shifts are slightly higher than the correlation based shifts by approximately 0.5 to 1 ms. Despite the slight positive shift the time-shifts have corresponding ranges and distribution of values. The horizon-based shifts also show the presence of negative time-shifts along the western edge of the survey, increasing their reliability. Crossplotting the horizon based time-shifts and the cross correlation time-shifts reveals a strong one-to-one correlation of 0.71 (Figure 3.13). The presence of strong correlation coefficients derived from the cross correlation method, and similarities in time-shifts calculated with both methods indicates the strength of using a cross correlation window approach for calculating both static time-shifts and time-varying time-shifts.

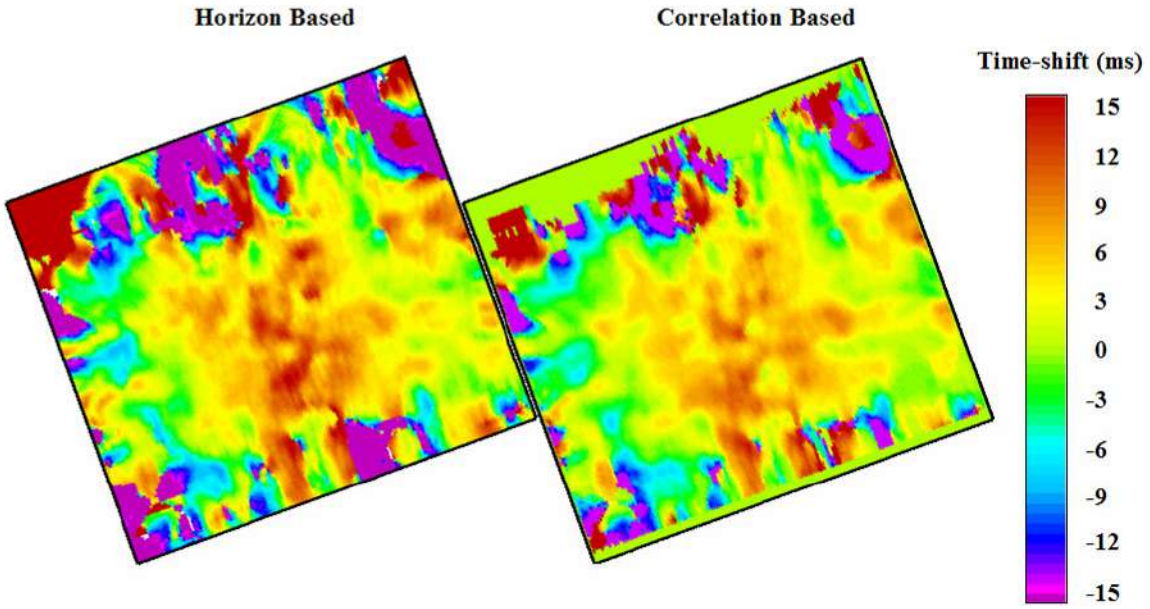

Figure 3.12 - Left panel represents time-shifts between the picked UMV events in the base (2003) and monitor (2004) S22 volumes. Right panel represents time-shifts calculated using the cross correlation approach.

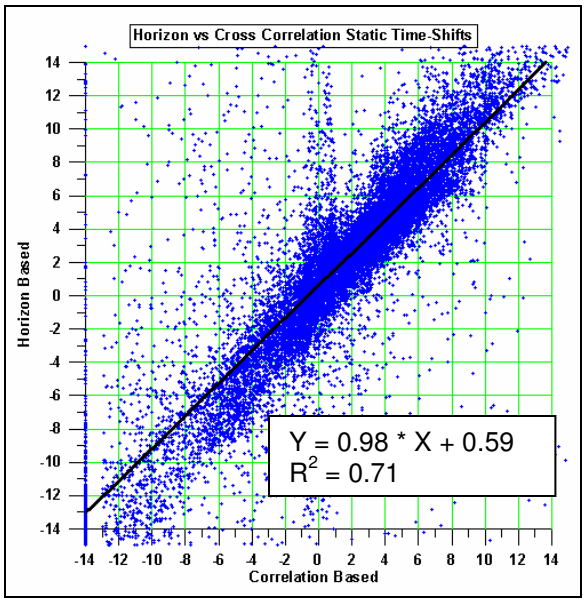

Figure 3.13 - Crossplot of horizon based static time-shift and cross correlation derived time-shifts at the UMV level for the S22 volumes. The units on each axis represent time-shifts in milliseconds.

The result of applying the static time-shifts to the monitor S22 volume was a strong decrease in the normalized root-mean-square difference at the UMV level (Figure 3.14). The histogram of the NRMS difference decreased from a broad peak centered at approximately 50% difference, to a narrower peak centered at approximately 25% difference. The decrease in the NRMS difference indicates an increase in the repeatability between the monitor and base surveys after the initial equalization step. It also shows the importance of such an alignment to minimizing survey differences.

The Cameo coal level exhibited a similar decrease in the NRMS difference after the application of the static shift. The histogram of the NRMS difference decreased from a broad peak centered at approximately 40% difference, to a strengthened peak centered between 20 and 25% difference (Figure 3.15). The decrease in the NRMS difference through this subsection of the reservoir zone indicates the effectiveness of increasing the surveys repeatability through the first stage of equalization. It also provides a benchmark for understanding repeatability through the rest of the reservoir interval.

An additional tool for understanding improvements in repeatability is a comparison of the amplitude spectrum of the seismic volumes at each stage of the equalization. A goal of the cross-equalization routine is to increase the match between the frequency contents of the surveys. Monitoring this information can also illustrate the affect that the equalization steps have on the frequency content of the data. The first step of the equalization process resulted in insignificant changes in the amplitude spectra. This is to be expected due to the fact that a bulk shift should not be affecting the frequency content of the data, and because the preliminary match of the spectral content of the surveys was performed during the initial processing performed by Veritas. Also, significant variations in the frequency content of the two data sets are not expected to result from the production of gas at Rulison Field. This is due to the fact that the sources had the same frequency content, along with no significant fluid substitutions or saturation changes occurring during production. Throughout the equalization processing, the

frequency content of the data volumes is expected to remain relatively constant with only slight improvements in matching expected.

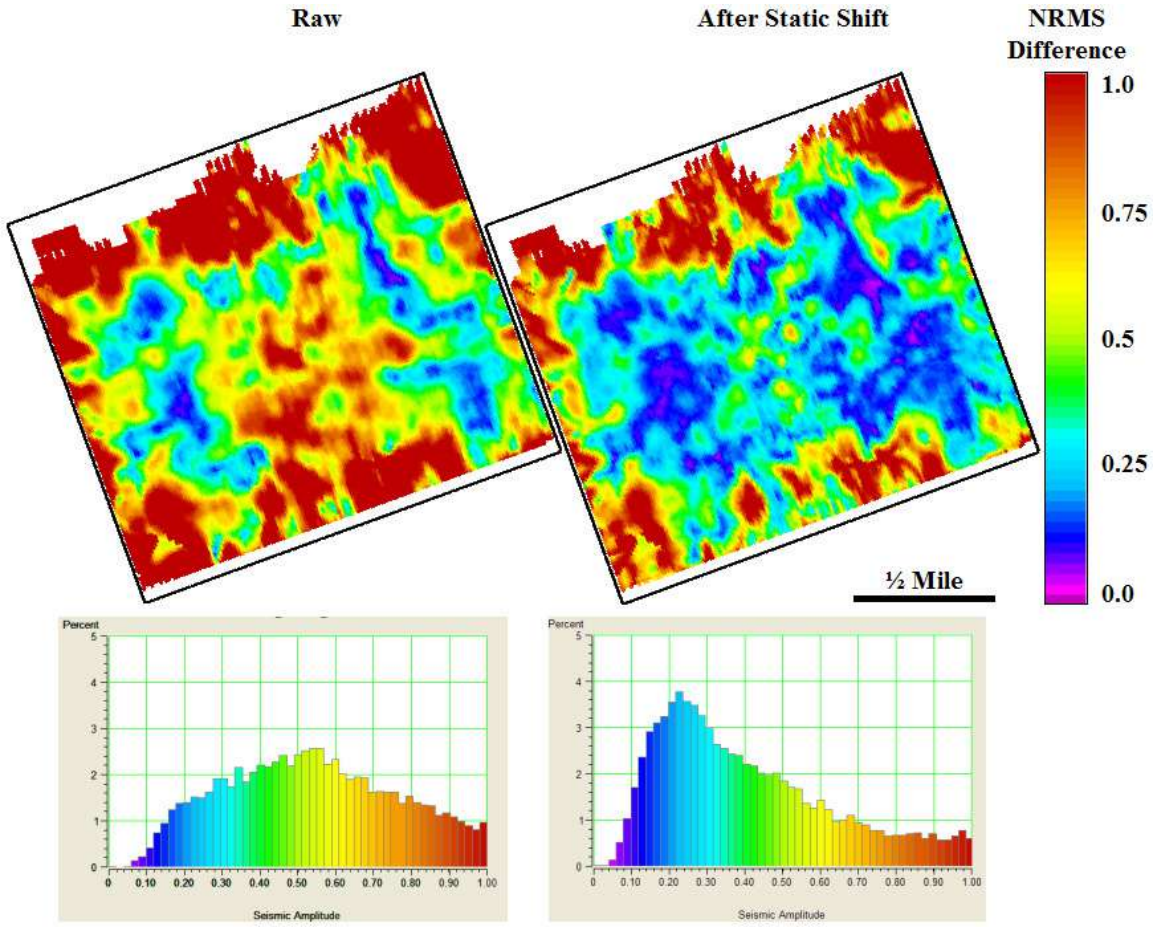

Figure 3.14 - Normalized root-mean-square difference for a 100 ms window centered over the S22 UMV event. Left panel is prior to equalization. Right panel is after the application of the static shift. The histograms of the maps are also plotted.

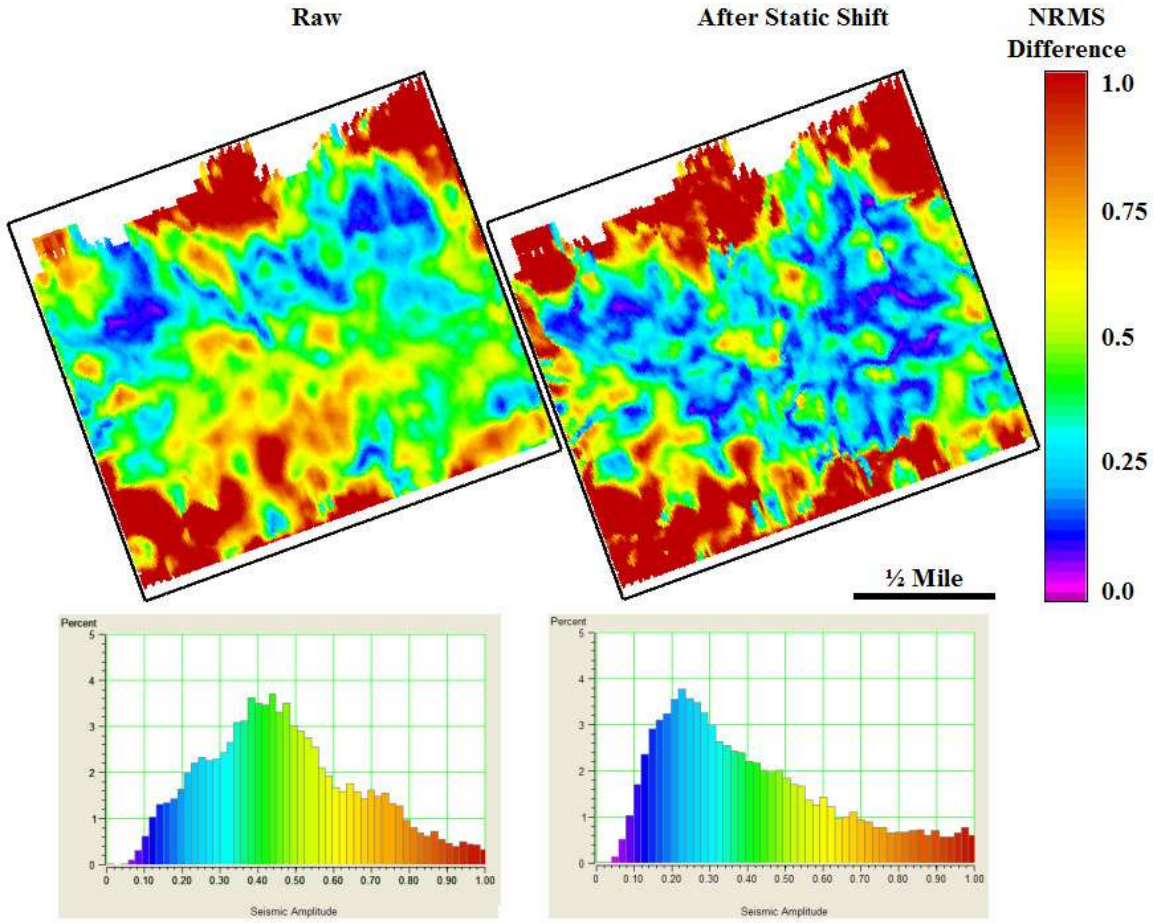

Figure 3.15 - Normalized root-mean-square difference for a 100 ms window centered over the S22 Cameo event. Left panel is prior to equalization. Right panel is after the application of the static shift. The histograms of the maps are also plotted.

3.3 Frequency Balancing

The second stage in the cross-equalization process involved matching the frequency content of the time-lapse surveys. Similar to the static time-shift, this process was performed separately on the S11 and S22 data volumes. The goal of this equalization step is to match the shape of the traces from one survey to the next using a Wiener-Levinson approach (Hampson-Russell 2006). The monitor survey was matched to the base survey with the application of a global shaping filter. This filter was derived

from a 100 ms window centered over the UMV horizon. The global filter was chosen so that a single shaping filter would be created and applied to the entire monitor data volume. This approach was chosen after also testing a trace-by-trace method. The trace-by-trace method introduced significant differences in the data volumes, resulting from noticeable striping induced by the creation of localized time-shifts between the surveys. The global filter was 81 samples long, and had a correlation threshold of 0.8 for both the S11 and S22 data sets. The length of the global filter was chosen to be approximately twice the length of the average seismic wavelength. With 2 ms sampling the filter had a length of 164 ms, while the wavelength of the data ranged from approximately 59 to 71 ms. By holding the filter length to approximately two wavelengths it allows for the correct amount of matching between the surveys. A longer filter may cause overwhelming amounts of matching that could eliminate production-induced differences (Rickett and Lumley 2001).

The correlation threshold provided a lower limit for traces to be included in calculating the average filter. Traces between the surveys with a cross correlation coefficient of less than 0.8 were excluded from the filter calculation (Hampson-Russell 2006). The correlation threshold eliminated the inclusion of largely varying traces between the surveys in calculating the filter. Large variations in corresponding traces mainly occur along the edges of the surveys, and were associated with low fold areas and edge effects.

The application of the global shaping filter to the monitor data volume resulted in the increased repeatability of the monitor and base S11 data volumes at the UMV level. The normalized root-mean-square difference at the UMV level was decreased with this step (Figure 3.16). The decrease in the NRMS difference was not as significant as with the application of the static shift, but did allow for the peak of the difference histogram to drop a couple of percentage points. After this step the peak of the histogram rests near a difference of 10-12% at the UMV level. The limited degree of improvement in repeatability at this stage is due to the fact that the surveys were also matched during the

initial processing performed by Veritas. High acquisition and processing repeatability also plays a major role in matching the frequency content of the surveys. The frequency matching of the surveys during the initial processing and cross-equalization was necessary due to the fact that three different shear vibrators were used during the acquisition. The application of a shaping filter at this stage in the cross-equalization process is to further enhance the repeatability of the surveys through the matching of a localized static interval. This process helps to eliminate frequency variations not related to production so that production induced changes could be observed.

While noticeable decreases in the histogram of the NRMS difference occurred at the UMV level (Figure 3.16), a slight broadening of the histogram's peak of the NRMS difference occurred at the Cameo event level (Figure 3.17). The peak of the difference histogram still occurs at approximately 18 to 20%, but has a decrease in strength of approximately 0.5 to 1%. The decreased strength of the histogram's peak is a function of a general increase in the NRMS difference at the Cameo level. The change in the NRMS difference at this level between the static shift and frequency matching steps of the equalization process is on the order of +/- 5% (Figure 3.18). There is a slight bias towards a negative change in the NRMS difference, indicating an increase in the NRMS difference through this interval. There are also positive shifts indicative of improvements in repeatability through this interval. Both increases and decreases in the NRMS difference are expected in the reservoir interval with this cross-equalization step. Compared to the static UMV interval, the Cameo reservoir interval is expected to experience production related changes that result in enhanced NRMS differences.

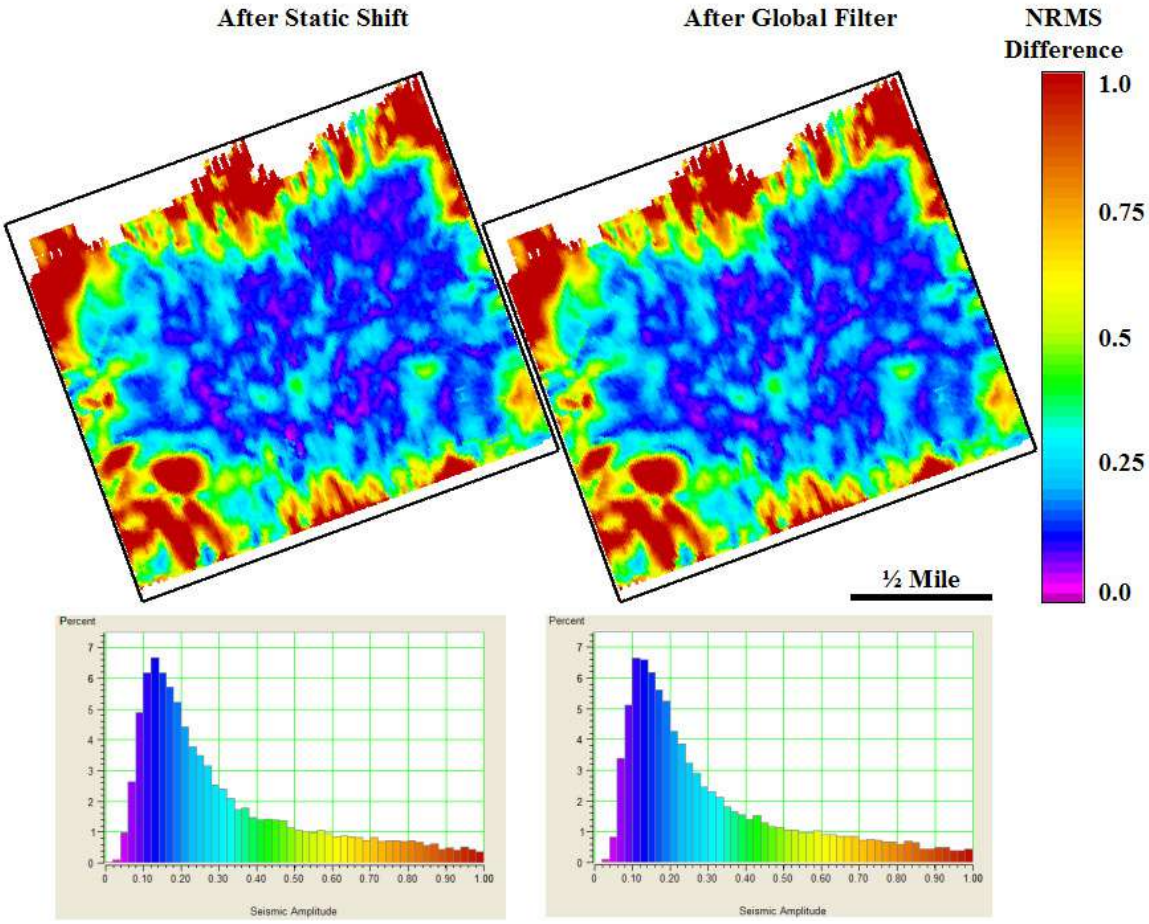

Figure 3.16 - Normalized root-mean-square difference for a 100 ms window centered over the S11 UMV event. Left panel is after the application of the static shift. Right panel is after the application of the global shaping filter. The histograms of the maps are also plotted.

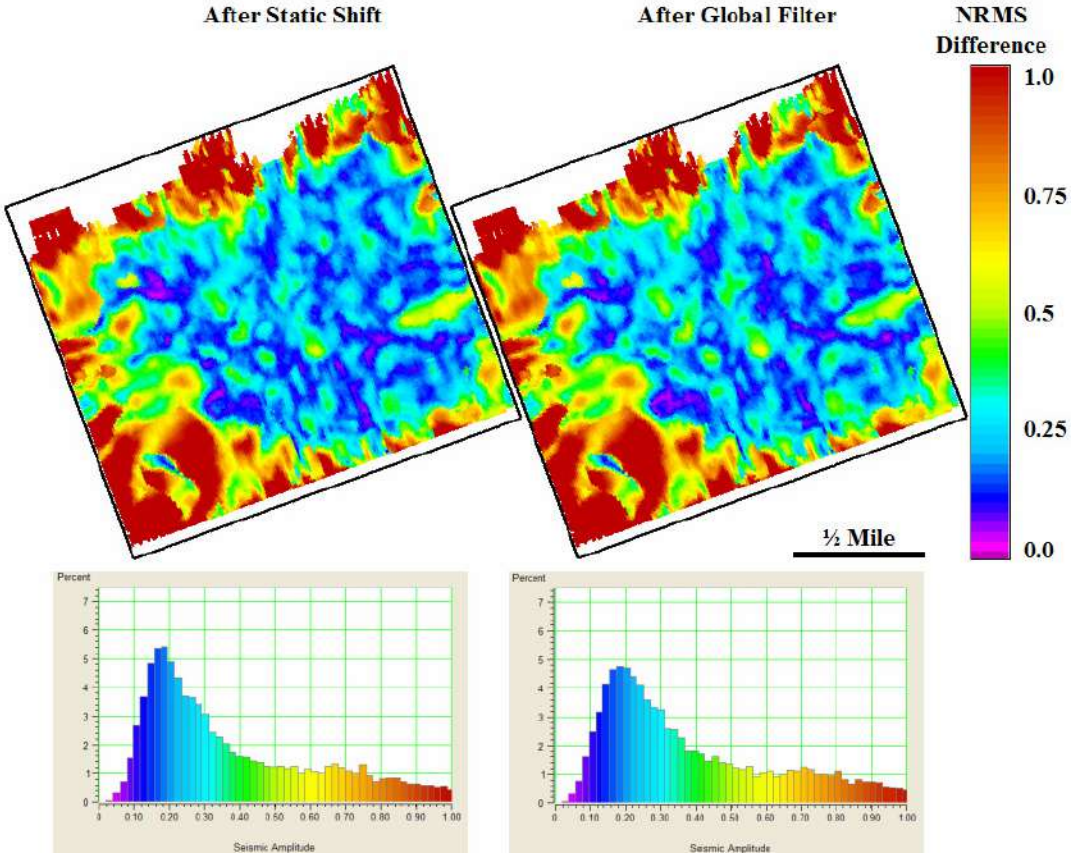

Figure 3.17 - NRMS difference for a 100 ms window centered over the S11 Cameo event. Left panel is after the application of the static shift. Right panel is after the application of the global shaping filter. The histograms of the maps are also plotted.

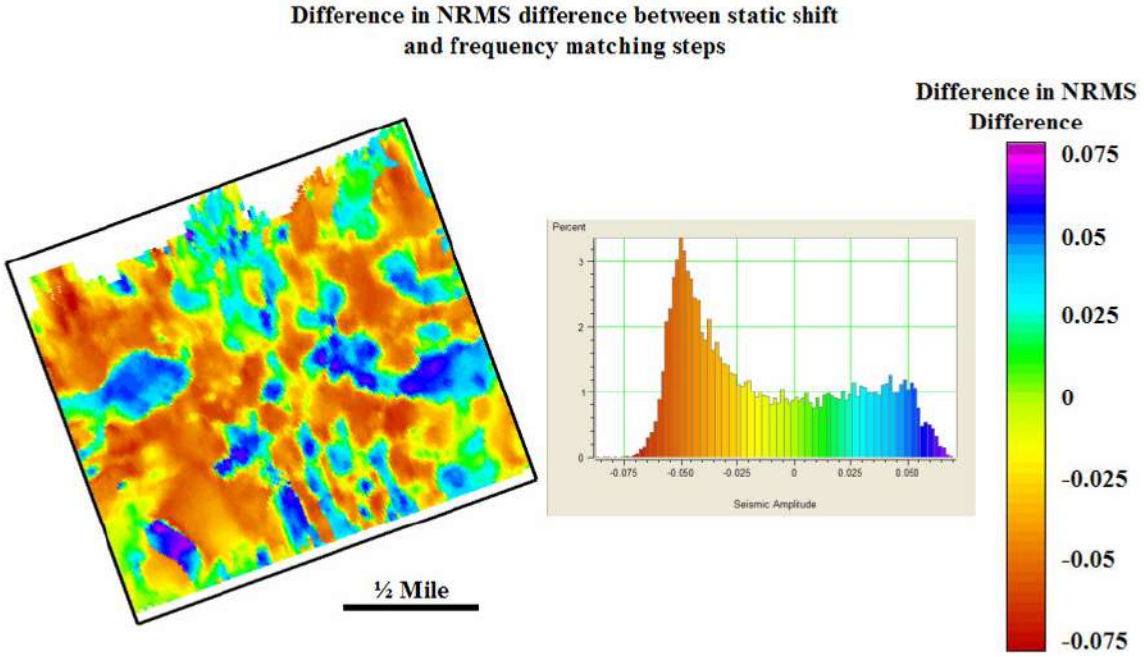

Figure 3.18 - Difference in the S11 NRMS difference at the Cameo level between the static shift and frequency matching steps of the cross-equalization process. Positive difference values indicate decreased NRMS difference values with the application of the frequency matching. Negative difference values indicate increases in the NRMS difference, or decreased repeatability.

Monitoring improvements in survey repeatability was also performed using a comparison of the frequency content of the base and monitor surveys. For this procedure differences between the amplitude spectra of the surveys are expected to decrease after each equalization step. The application of the shaping filter resulted in both decreases and increases in the difference between the amplitude spectrum of the base and monitor surveys compared to the original survey spectra (Figure 3.19). At low frequencies of less than approximately 13 Hz, the shaping filter decreases the difference in the frequency content. Through the range of approximately 13 to 21 Hz there are minimal variations in the frequency content. Above 21 Hz there are slight increases in the separation of the frequency content. Since the majority of the frequency information falls between 10 and 21 Hz, the shaping filter has resulted in improved frequency content matching.

The initial differences in the frequency content from 0 to 30 Hz between the surveys averaged –0.027, with a standard deviation of 0.039, was improved to –0.011 and 0.044 respectively, after the application of the shaping filter. The range from 0 to 30 Hz was chosen, since that is where the majority of the frequency content falls. The improvement is an indication of increased alignment of the frequency content of the data volumes. While improvements and differences are expected, the low average values also indicate a strong consistency between the surveys. This consistency is the result of high repeatability in both the acquisition and processing of the two surveys. The application of the shaping filter provides enhanced frequency matching guided by a static subsurface interval, and the increased ability to monitor time-lapse changes through the reservoir.

Further matching of the frequency contents would require the application of a stronger shaping filter. This filter would result in the overmatching of the surveys, and the reduction of observable time-lapse differences (Rickett and Lumley 2001). The goal here was to increase the match between the surveys, while also preserving or enhancing the presence of production related changes. This is why complete matching of the frequency content is not desired or expected. The optimal balance with this step, along with the rest of the cross-equalization steps is to maximize repeatability, while also preserving production related changes (Calvert 2005). The improvement in the match between the frequency content of the data volumes, the improvement in the NRMS difference at the UMV level, along with the presence of improvements in the NRMS difference at the Cameo level support the parameterization and application of the shaping filter to the S11 volumes.

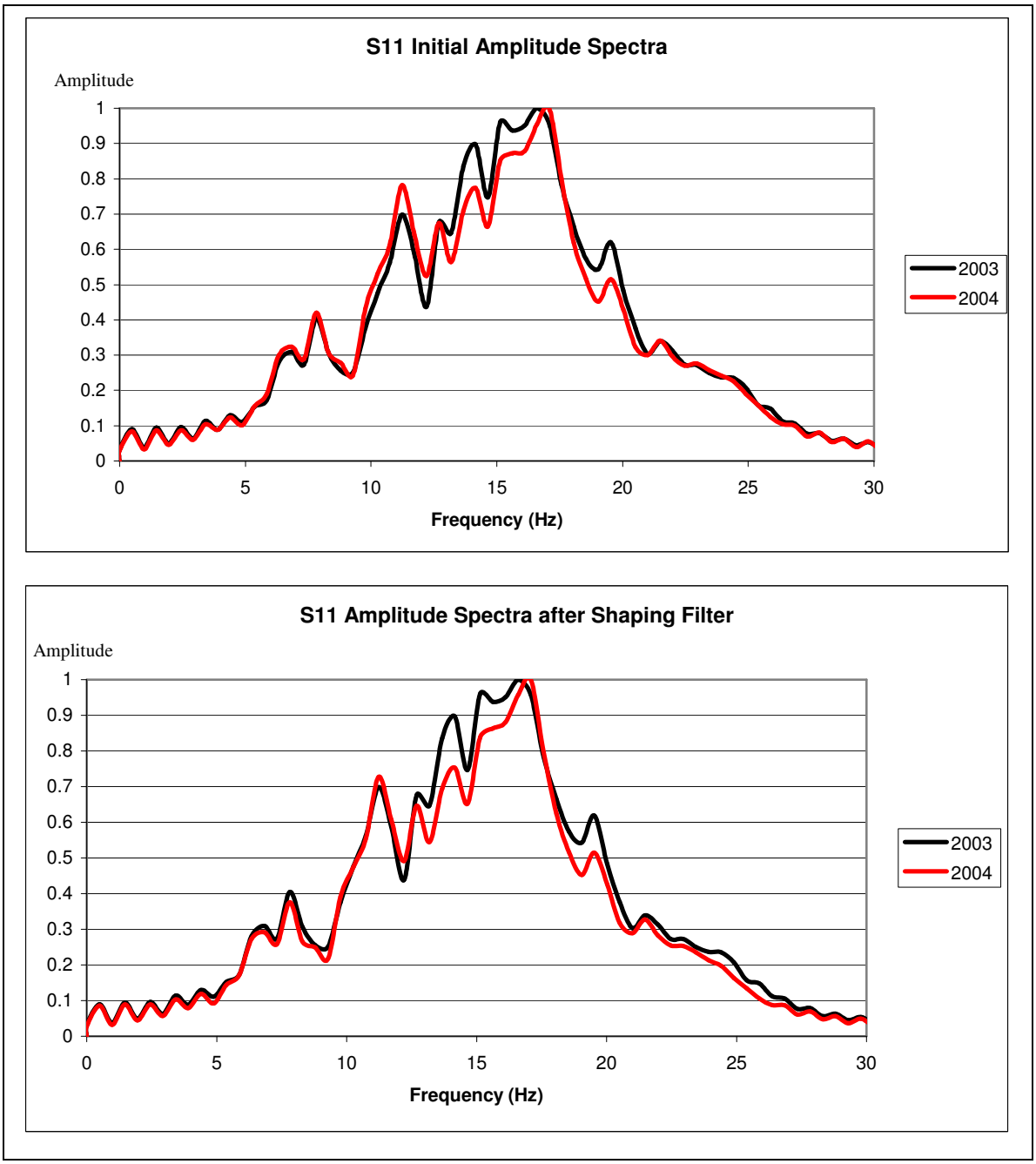

Figure 3.19 - Amplitude spectrum of 2003 and 2004 S11 data volumes calculated from 1800 to 2800 ms. Top is prior to the application of any cross-equalization steps, bottom is after the application of the shaping filter to the 2004 volume.

A similar shaping filter procedure was developed for the S22 volumes. The filter was created using the 2003 as the reference and the 2004 as the input volume. The filter was applied to the 2004 survey. The filter was also 81 samples long, and had a correlation threshold of 0.8. As with the S11 data, the length of this filter includes just over two wavelengths of seismic information. The application of the shaping filter resulted in a decrease in the NRMS difference at the UMV level (Figure 3.20). Differences within the maps are difficult to locate, but are evident in the histogram displays. The histograms indicate a shift of the NRMS difference peak to lower values. The peak of the histogram now occurs at approximately 18% difference, compared to 23% difference after the application of the static shift. This is a good indication that the shaping filter at the UMV level has increased repeatability of the surveys. Similar to the S11 data, the increase in repeatability after this step was not as significant as with the first step of equalization. This is related to the fact that preliminary matching of the data was performed during the initial processing, along with the high repeatability between the data acquisition and processing of the two surveys.

Decreases in the NRMS difference at the Cameo level also occurred at this stage (Figure 3.21). While it is difficult to observe specific areas of change in the map views, a strengthening of the histogram's peak at low NRMS difference values is observable. The strengthening of the peak indicates a trend toward decreased values of NRMS difference. Only slight changes were observed due to the surveys already strong repeatability.

Comparing the amplitude spectra before and after the application of the shaping filter provides additional insight into survey repeatability. A comparison between the spectrum of the base and monitor data volumes illustrates slight increases in the separation of their frequency content after the application of the shaping filter (Figure 3.22). The average difference in the frequency content of the original S22 data volumes from a range of 0 to 30 Hz is –0.052, with a standard deviation of 0.043. This increased slightly to an average value of –0.063, with a standard deviation of 0.047 after the shaping filter was applied.

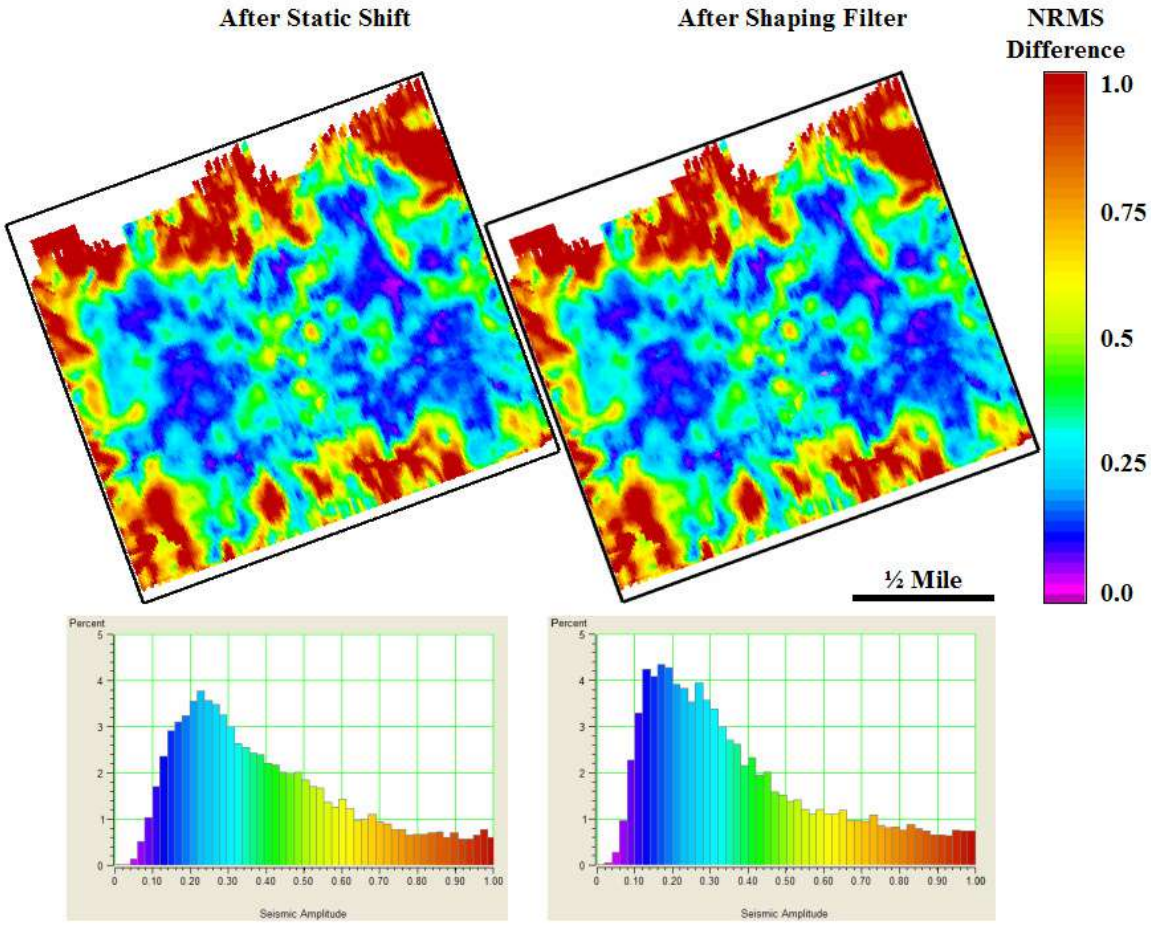

Figure 3.20 - NRMS difference for a 100 ms window centered over the S22 UMV event. Left panel is after the application of the static shift. Right panel is after the application of the global shaping filter. The histograms of the maps are also plotted.

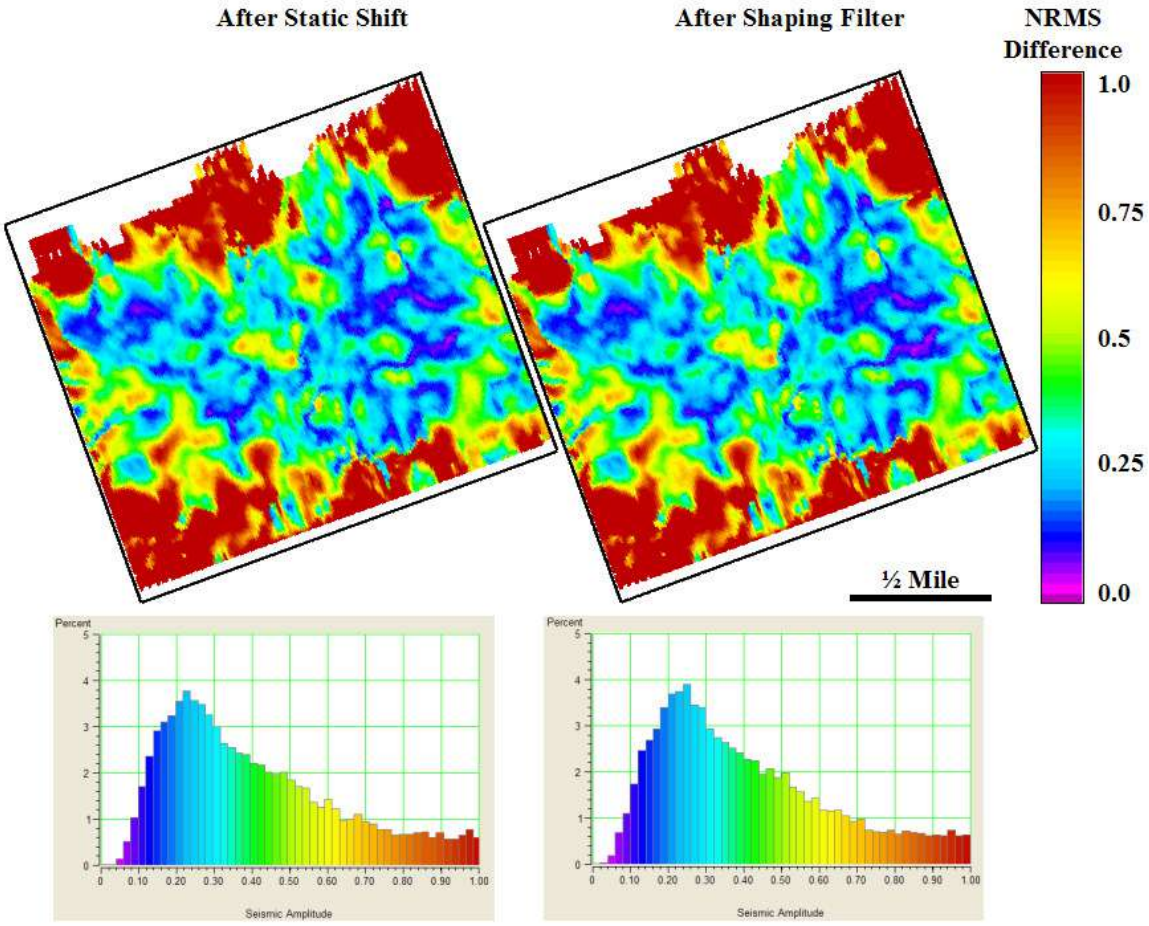

Figure 3.21 - NRMS difference for a 100 ms window centered over the S22 Cameo event. Left panel is after the application of the static shift. Right panel is after the application of the global shaping filter. The histograms of the maps are also plotted.

While the shaping filter did not improve the match of the surveys overall frequency content, the increased variations were small. As with the S11 data, these small values illustrate the consistency that is expected with dedicated time-lapse surveys. Slight difference increases may have resulted from the application of the shaping filter to the 2004 volume. Due to the fact that the base survey has a slightly higher content of frequencies over the range of interest from 0 to 30 Hz, a better parameterization may have been the application of the shaping filter to the base volume. This would have allowed for a reduction in its frequency content, compared to attempting to boost the monitor survey's. Another suggestion is that due to the frequency contents being initially closely matched, frequency matching may not have been a necessary step in the cross-equalization routine. Despite small variations in the amplitude spectra, the decreased NRMS differences at both the UMV and Cameo level indicate improved repeatability between the surveys, and the need for this cross-equalization step.

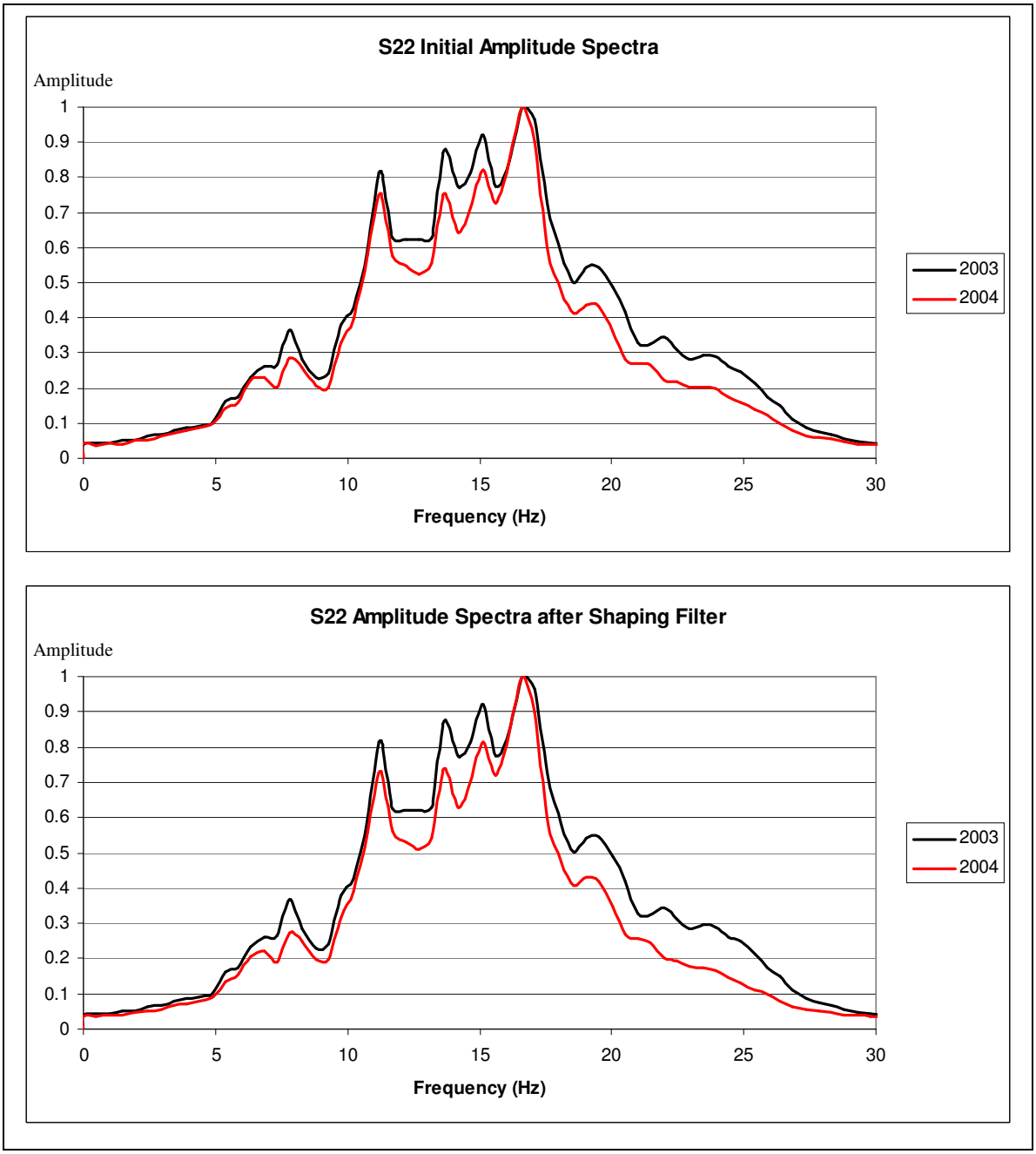

Figure 3.22 - Amplitude spectrum of 2003 and 2004 S22 data volumes calculated from 1800 to 2800 ms. Top is prior to the application of any cross-equalization steps, bottom is after the application of the shaping filter to the 2004 volume.

3.4 Amplitude Matching

The third step in the cross-equalization process involves the matching of event amplitudes between the base and monitor surveys. The amplitude matching is done through a comparison of root-mean-square amplitude values of the two surveys. A 100 ms window centered over the UMV event was used to calculate the root-mean-square factor that was applied to the monitor volumes (Rickett and Lumley 2001). The same window was used for both the S11 and S22 volumes. The calculation of this factor was performed on a trace-by-trace basis. Under the assumption that the UMV level has not experienced any production related change, the goal of this step is to achieve optimal amplitude balancing anchored on a strong, continuous event that is highly consistent between the surveys. Increased amplitude balancing allows for further comparisons of seismic attributes to be made with increased confidence.

After the application of amplitude matching, improvements in the NRMS difference at the UMV level were observed (Figure 3.23). Improvements can be seen as a slight strengthening of the peak of the maps histogram, along with a slight shift to lower difference values of approximately 12%. Only small improvements are observed at this point due to amplitude equalization also having been performed during the initial processing. At the Cameo level, the peak of the maps histogram occurs at the same difference values before and after the application of amplitude matching (Figure 3.24). The strength of the peak, however, is decreased slightly after amplitude matching. The cause for the decreased strength of the peak is a result of increased NRMS differences along the edges of the survey (Figure 3.25). The increased difference through low fold, low repeatability areas, decreases the presence of low NRMS differences, and broadens the histograms peak. The general trend of changes in the NRMS difference through the central portion of the survey is approximately +/- 2.5% (Figure 3.25). Improvements in repeatability would be expected through zones associated with no production related change. The areas of increased NRMS difference, or positive difference values, may

provide insight into areas of production related change as differences are enhanced by the cross-equalization procedure.

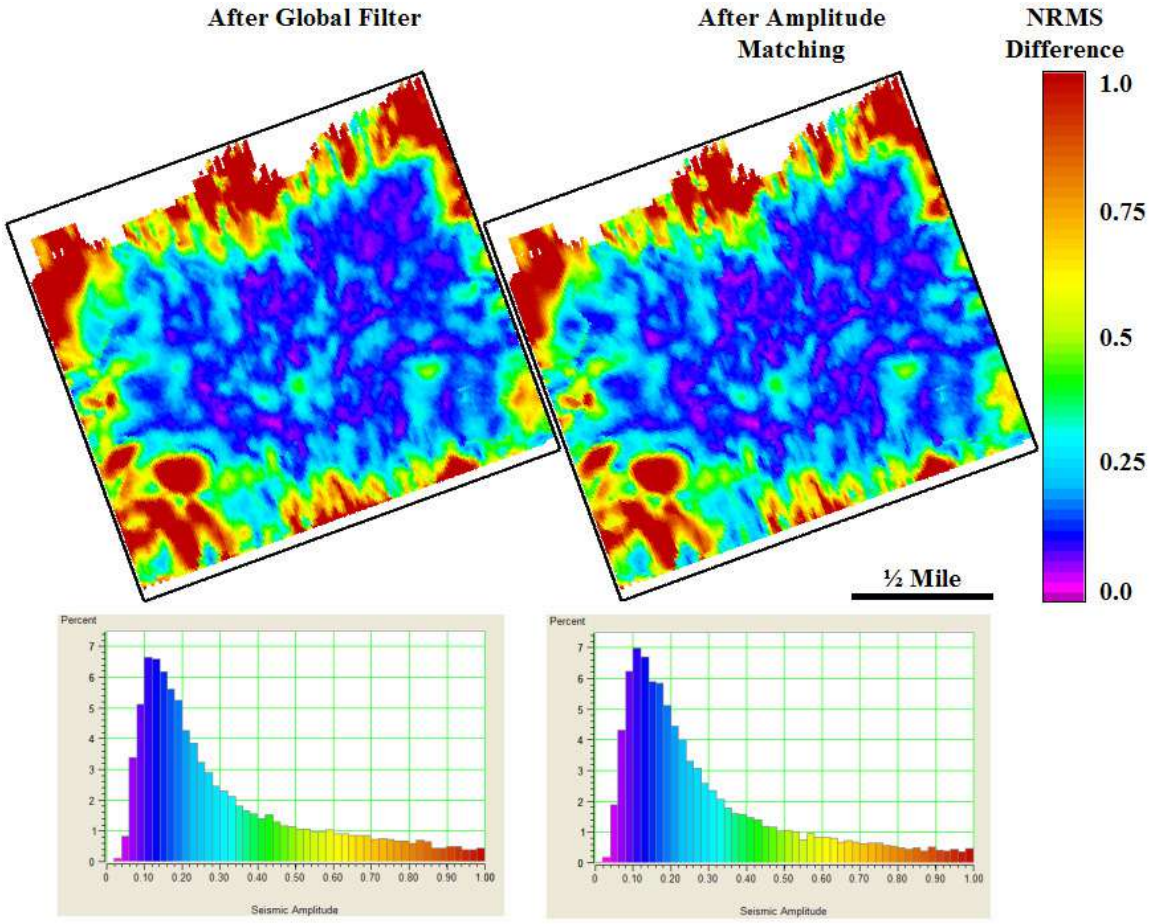

Figure 3.23 - NRMS difference for a 100 ms window centered over the S11 UMV event. Left panel is after the application of the global shaping filter. Right panel is after the application of the amplitude gain factor. The histograms of the maps are also plotted.

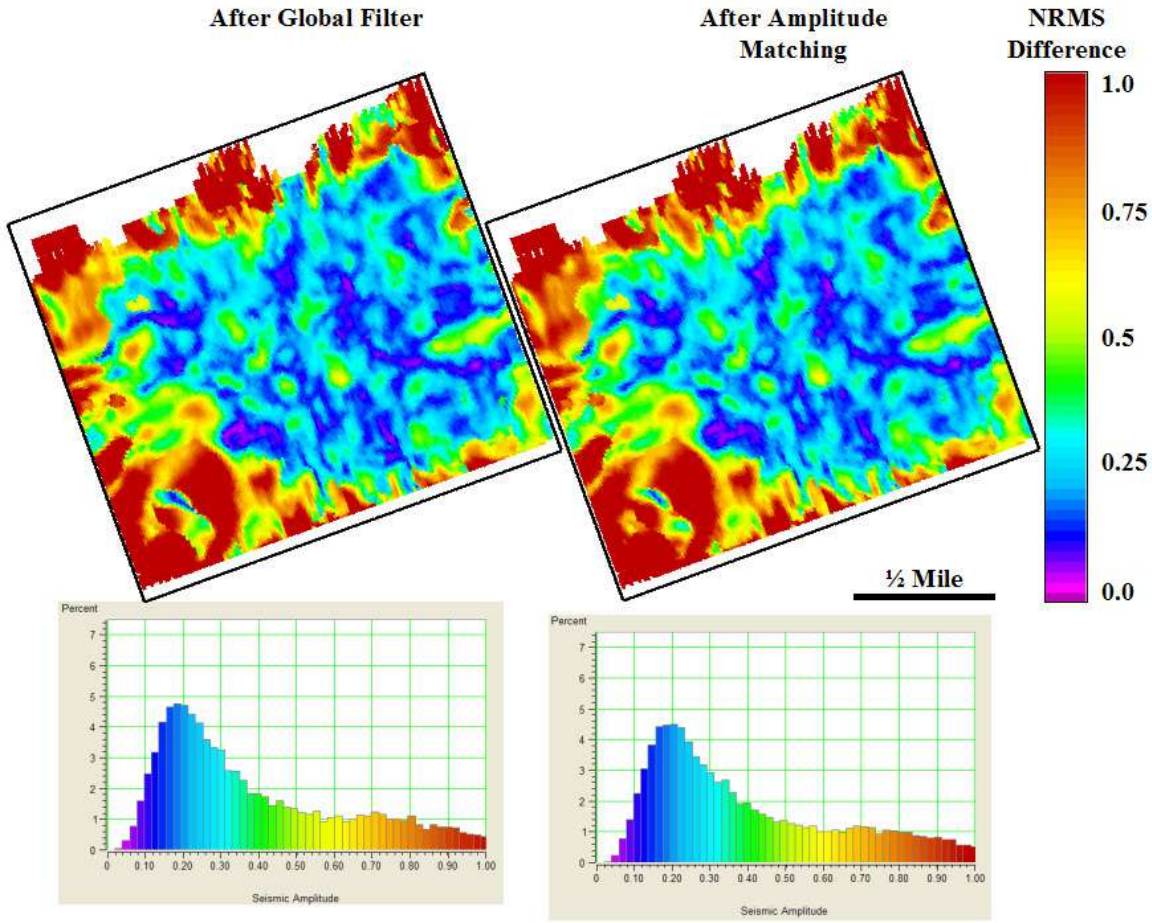

Figure 3.24 - NRMS difference for a 100 ms window centered over the S11 Cameo event. Left panel is after the application of the global shaping filter. Right panel is after the application of the amplitude gain factor. The histograms of the maps are also plotted.

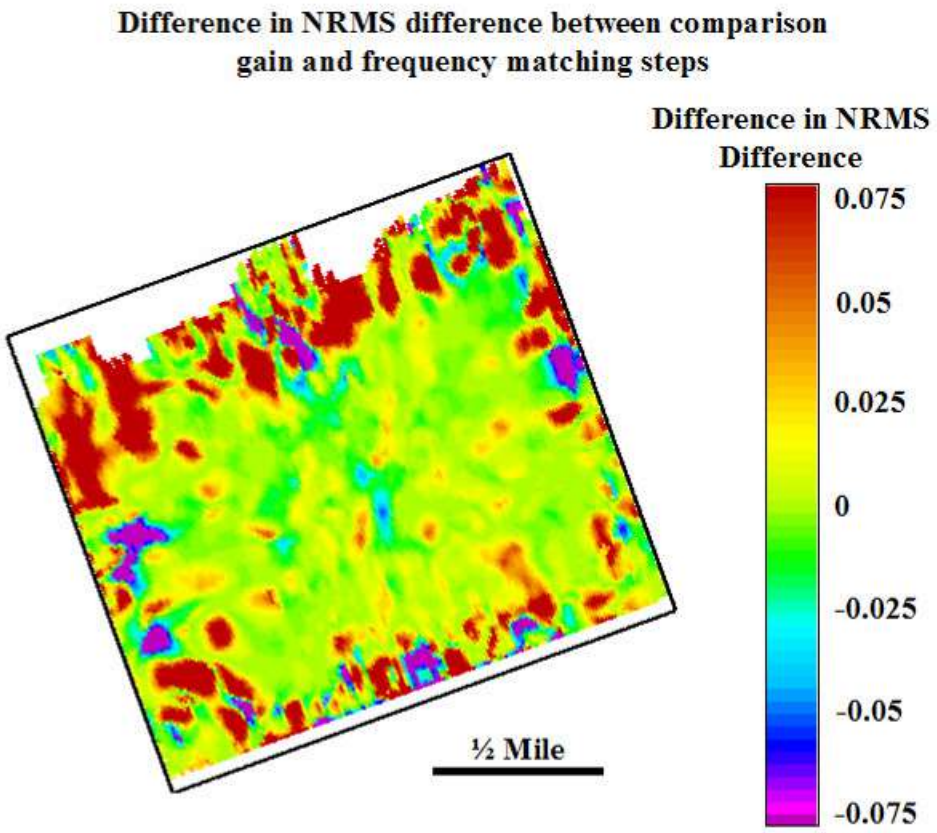

Figure 3.25 - Difference in the S11 NRMS difference at the Cameo level after the application of the amplitude equalization and the shaping filter. Positive values indicate increased NRMS difference after the application of the amplitude equalization, or decreased repeatability.

Amplitude matching was also performed on the S22 data volumes. The same 100 ms window centered over the S22 UMV event was used to calculate the root-mean-square gain factor. This gain factor was then applied to the monitor data volume. Improvements in the NRMS difference at the UMV level resulted from the amplitude equalization (Figure 3.26). While the location of the histograms peak remained at approximately 18% difference, the strength of the peak increased by approximately half a percent. The increase in the strength of the peak indicates increased repeatability at the UMV level resulting from a general decrease in NRMS difference values. As with the S11 data the improvement in repeatability is not as significant as with the first

equalization step. This is again the result of preliminary amplitude equalization during the initial processing of the data.

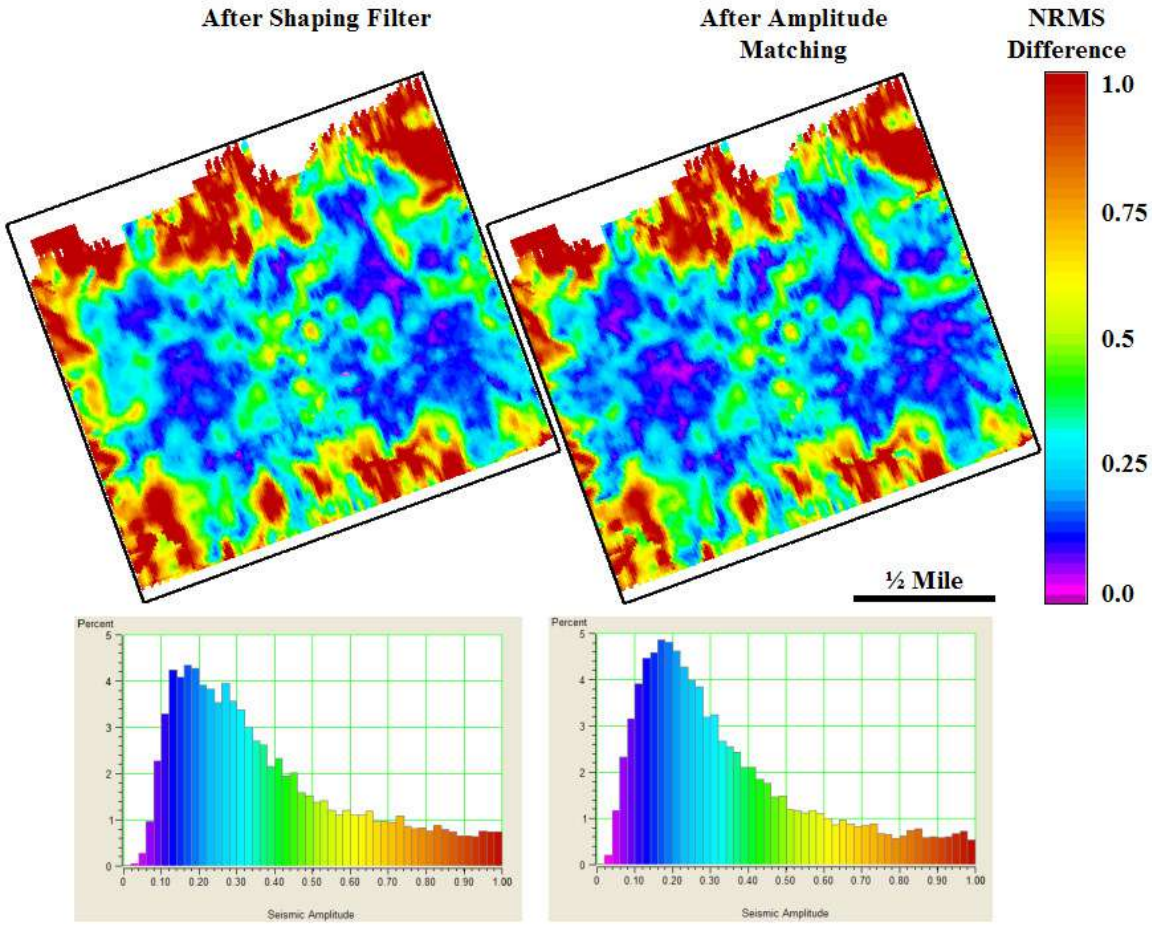

Figure 3.26 - NRMS difference for a 100 ms window centered over the S22 UMV event. Left panel is after the application of the global shaping filter. Right panel is after the application of the amplitude gain factor. The histograms of the maps are also plotted.

NRMS differences at the Cameo level were also affected by the amplitude matching (Figure 3.27). The location of the histograms peak still occurs at approximately the same value of 25% difference. Change in the histogram peak appears as the decreased presence of low difference values to the left of the peak, while the presence of higher difference values to the right of the peak increase. Similar to the Cameo level in

the S11 data after this equalization step, the main cause of the peaks broadening is due to the increased difference along the low fold, low repeatability edges of the survey (Figure 3.28). In this case, however, there is also increased change through the central part of the survey that contributes to the broadening of the peak. Zones of increased NRMS difference through the central portion of the survey may result from the enhancement of production related time-lapse changes as the cross-equalization continues, revealing potential areas of interest.

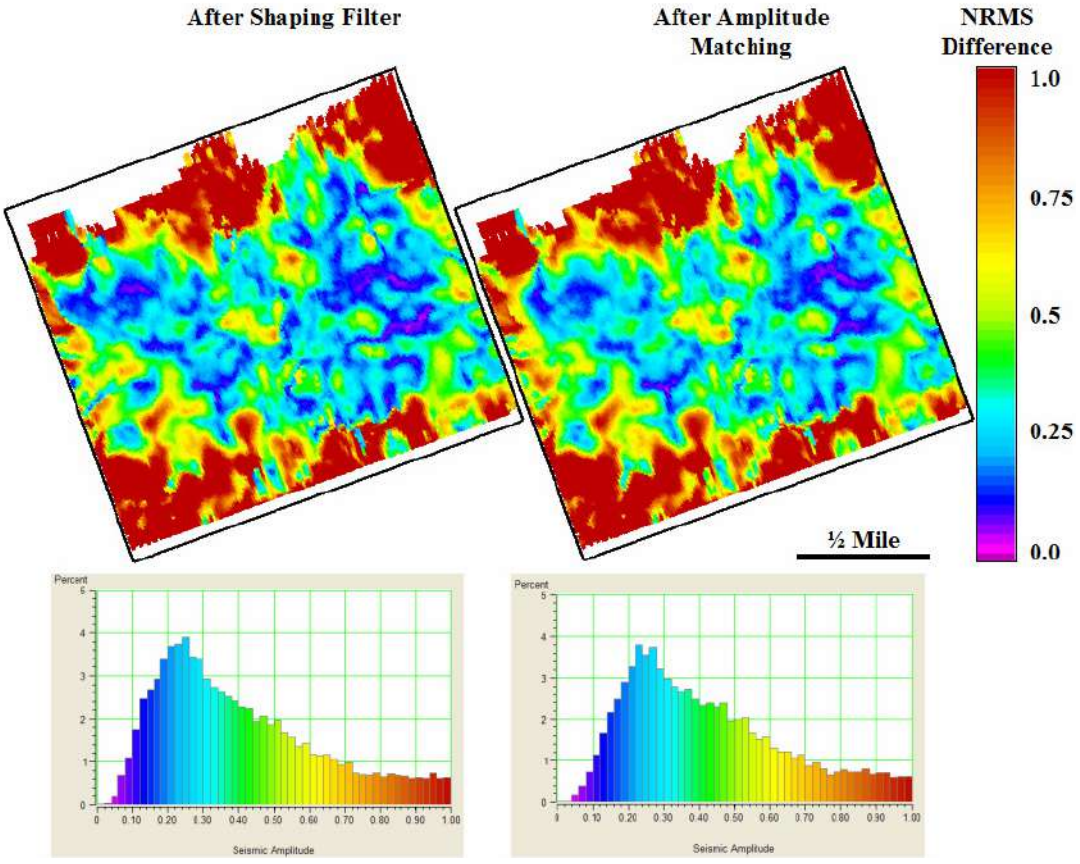

Figure 3.27 - NRMS difference for a 100 ms window centered over the S22 Cameo event. Left panel is after the application of the global shaping filter. Right panel is after the application of the amplitude gain factor. The histograms of the maps are also plotted.

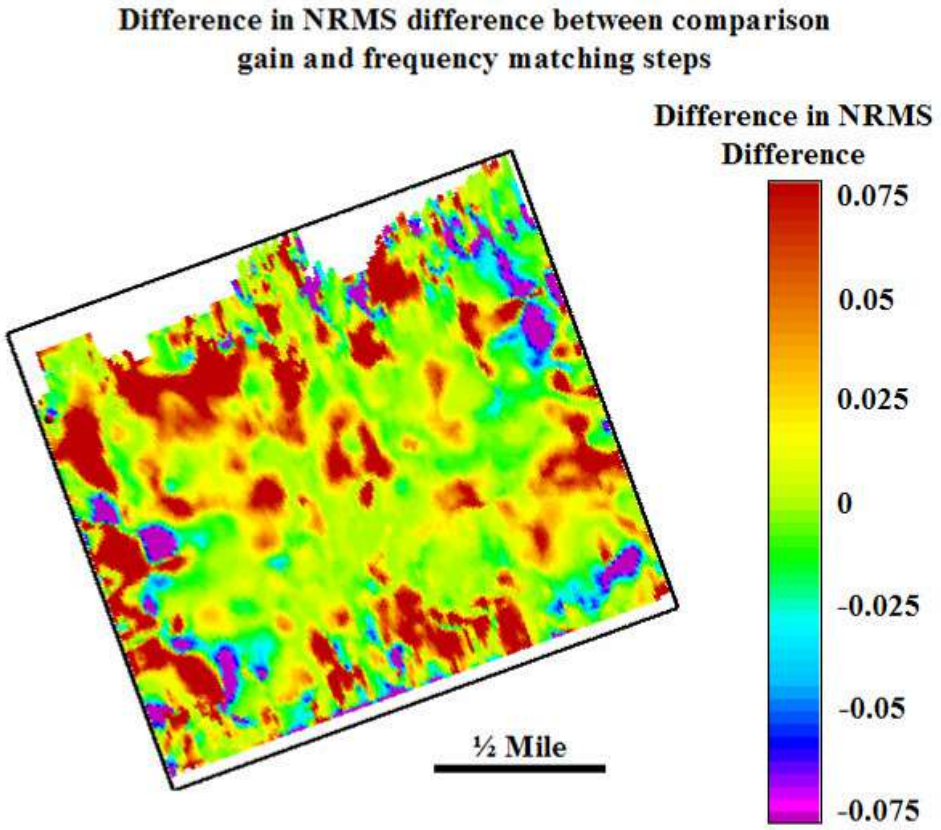

Figure 3.28 - Difference in the S22 NRMS difference at the Cameo level after the application of the amplitude equalization and the shaping filter. Positive values indicate increased NRMS difference after the application of the amplitude equalization, or decreased repeatability.

The application of the amplitude equalization between the base and monitor volumes only resulted in slight improvements between the amplitude spectra of the two surveys. Only minimal changes are expected due to the fact that the frequency content of the volumes is not being directly altered. Due to this consistency, the amplitude spectra were not used as a measure of increased repeatability for this stage of the equalization process.

After the third stage of cross-equalization traveltime changes between corresponding events in the base and monitor surveys can be evaluated. The alignment of event arrival times above the reservoir, and the balancing of the frequency and amplitude contents, allows for the comparison of event arrival time variations through the

reservoir section. With this information it is possible to understand velocity changes between the base and monitor surveys. These changes will provide information on changes in shear-wave splitting that are anticipated to result from changes in stress magnitudes and/or fracture densities with production. Several examples of changes in shear-wave splitting coefficients resulting from stress variations have been observed in earthquake zones (Crampin and Gau 2005).

The first three stages of cross-equalization have resulted in significant improvements in the repeatability between the base and monitor surveys. The NRMS difference for the S11 data volumes improved from a peak at approximately 35% to 12% at the UMV level, and approximately 22% to 20% at the Cameo level. For the S22 volumes the difference improved from a peak at approximately 55% to 18% at the UMV level, and approximately 40% to 25% at the Cameo level. As expected, the strongest improvements occurred at the UMV level. This is a result of the cross-equalization processes deriving the correction factors from this interval, thus maximizing data matching in this interval compared to the rest of the survey. Due to this, larger survey variations were expected through the reservoir section. Also, because the static shift correction only aligned the events in the 100 ms window centered over the UMV event, time-shifts between corresponding events through the reservoir are still present. This prevented a complete comparison of the same subsurface interval at the Cameo level, resulting in larger NRMS difference values. The preservation of time-shifts with time, however, allows for the comparison of traveltime variations between the surveys.

3.5 Time-Varying Time-Shift

The final cross-equalization step involved the application of a time-varying time-shift. The purpose of this step was to correct for traveltime variations within the reservoir. This was achieved by aligning corresponding seismic events between the surveys. The alignment of seismic events in time allows for a direct comparison of the

same sampled subsurface intervals between the surveys through the use of event amplitudes and impedance values. The time-varying time-shift was performed using a 100 ms sliding cross correlation window. This window size was chosen to correspond to the correlation window used in the calculation of the static time-shift, and to include at least one wavelength of seismic information. Beginning at zero time the 100 ms correlation window calculated the time-shift necessary to maximize the cross correlation coefficient on a trace-by-trace basis. This is the same approach that was used to calculate the static time-shift in the first step of the cross-equalization. After calculating a time-shift and correlation coefficient for the first sample, the correlation window steps down a sample and calculates a new time-shift and correlation coefficient. This process is repeated through the entire data set for each sample. Similar to the static time-shift calculation, the base survey was used as the reference survey, while the monitor survey was used as the input volume. Using this setup the calculated time-shifts are associated with shifting the monitor survey to align with the base. Positive time-shifts indicate a pull-up or velocity increase from the base to monitor survey. Negative time-shifts indicate a pull-down or velocity decrease from the base to monitor surveys. The S11 and S22 data volumes were correlated separately between the surveys.

The time-varying time-shift process results in the creation of two data volumes. The first data volume contains the sample-by-sample time-shifts that were calculated for the data sets. The second data volume contains the values of the correlation coefficients maximized by the application of the time-shifts. To align the base and monitor surveys the sample-by-sample time-shift volumes were applied to the monitor seismic volumes. The application of the time-shifts was limited to those that corresponded to correlation coefficient values of greater than 0.8. The threshold helped prevent the introduction of erroneous time-shifts in the monitor surveys resulting from variations in amplitude and seismic signature that adversely affected the calculation of the correlation time-shift. Low correlation coefficient values and large time-shifts dominantly occurred near the surface, along the low fold edges of the survey, and through the low energy zone between

the UMV and Cameo events. Large time-shifts and low correlation values indicate that the time-shifts are unreliable, and occur as a result of amplitude and seismic character variations between the surveys. Weak and discontinuous events can limit the ability of the correlation window to develop a strong correlation from one survey to the next, and may also result in the mismatch of events. After the application of the sample-by-sample time-shifts, comparisons can be made regarding time-lapse amplitude and impedance variations. The assumption is that the surveys have been correctly aligned to allow for a comparison of the same subsurface interval between the years, and the observation of time-lapse changes.

Following the application of the time-varying time-shifts, the NRMS difference at the UMV and Cameo levels between the S11 volumes decreased further. At the UMV level the peak of the NRMS difference histogram strengthened and shifted to a lower value of 10% difference (Figure 3.29). This improvement indicates that after the final stage of equalization the static section above the reservoir is highly repeatable. The map views of the NRMS distribution at the UMV level also indicate improvement in repeatability through the central high fold area of the survey. The NRMS difference at the Cameo level also decreased after time-varying time-shift (Figure 3.30). The peak of the NRMS difference histogram was strengthened considerable, along with being shifted from a peak difference at approximately 20% to a peak difference of approximately 15%. The improvement in the repeatability at this level illustrates the importance of aligning corresponding events in time, so that comparisons of the same subsurface intervals and seismic events can be made between the surveys.

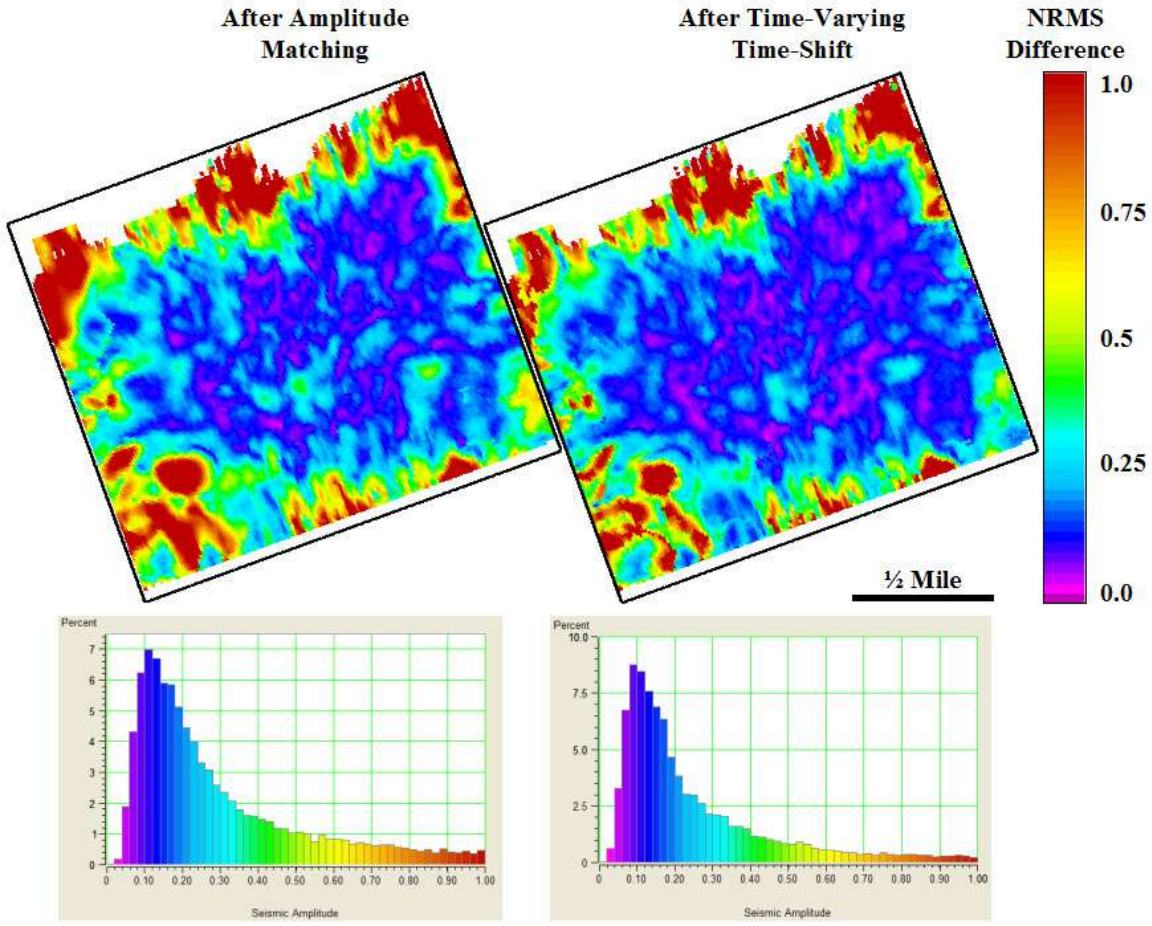

Figure 3.29 - NRMS difference for a 100 ms window centered over the S11 UMV event. Left panel is after the application of amplitude matching. Right panel is after the application of the time-varying time-shift. The histograms of the maps are also plotted.

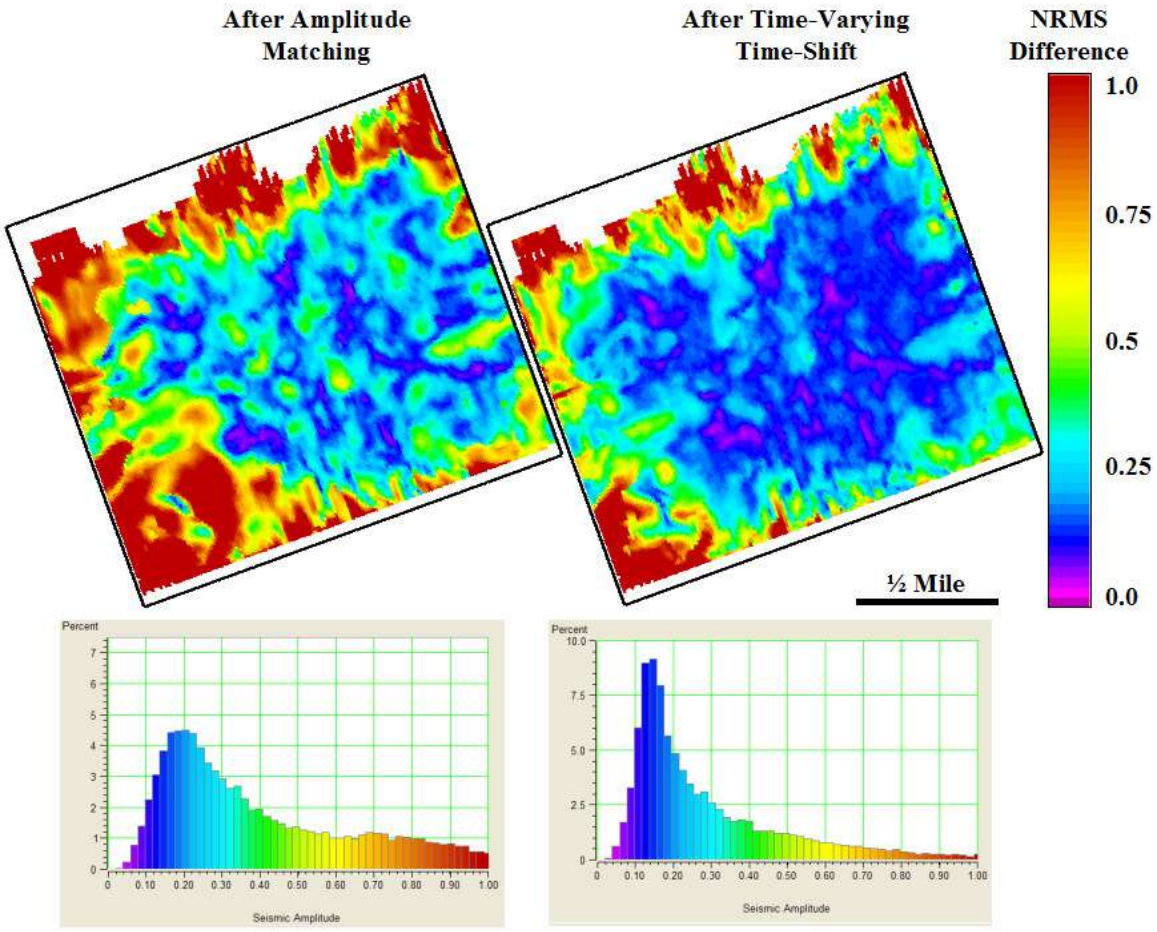

Figure 3.30 - NRMS difference for a 100 ms window centered over the S11 Cameo event. Left panel is after the application of amplitude matching. Right panel is after the application of the time-varying time-shift. The histograms of the maps are also plotted.

Along with a decrease in the NRMS difference at both the UMV and Cameo levels there was also an improvement in the alignment of the amplitude spectrum between the base and equalized monitor surveys. The difference in the frequency content extracted from 1800 to 2800 ms for the two data sets was reduced through most of the frequency range, except from approximately 22 to 25 Hz (Figure 3.31). The overall improvement in the match of the frequency content of the data indicates increased matching of the surveys. While increased alignment of the frequency content is

expected, the imperfect nature of the cross-equalization process is not capable of fully eliminating differences in the data. Increases in the difference of the frequency content from 22 to 25 Hz may be the result of errors in the correlation time-shifts, or may indicate the enhancement of production related differences resulting from the cross-equalization process. The low difference in the frequency contents reinforces the consistent nature of the data volumes between the surveys that allow for a time-lapse analysis.

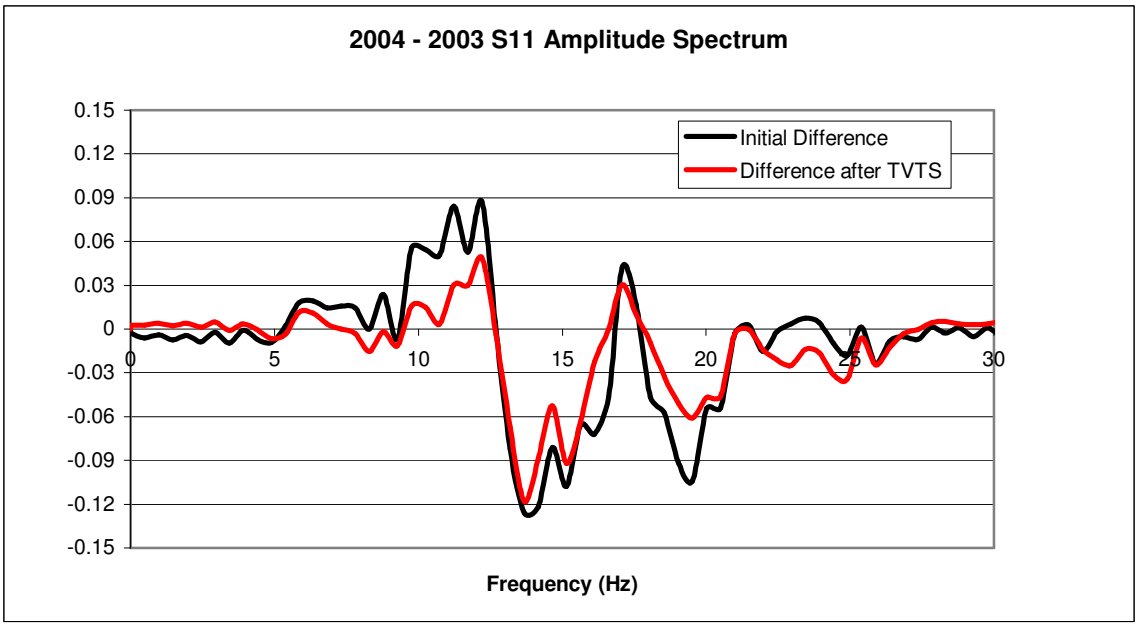

Figure 3.31 - Difference in amplitude spectrum between the 2004 and 2003 S11 volumes. Black line represents the initial difference before equalization. The red line represents the difference after the cross-equalization process.

The goal of the cross-equalization process is to reduce differences between the base and monitor seismic surveys while preserving and enhancing production related seismic variations in the data. After the application of the four main equalization steps, the difference between the S11 data volumes is reduced (Figure 3.32). The main reduction in the difference of the surveys occurs along the strong continuous reflectors near the UMV event. The reduction is a result of using this interval as the static section

used to match the surveys. Strong difference reductions also occur through the rest of the survey indicating a strong match and high repeatability between the surveys.

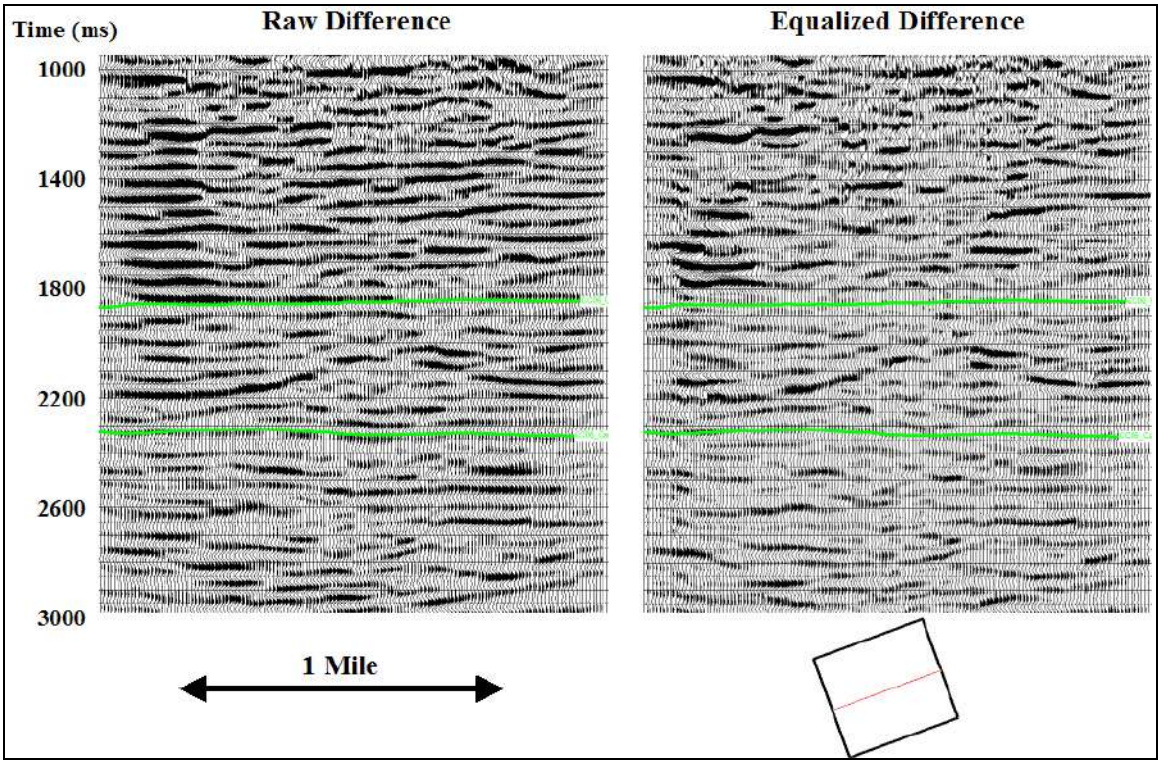

Figure 3.32 – Approximately east-west running crossline 72 of the difference between the S11 monitor and base volumes. Left is the initial difference, right is the difference after the equalization of the monitor survey. Top green horizon marks the UMV event, and the second green horizon marks the Cameo event.

Similar to the S11 data the application of the time-varying time-shifts to the monitor S22 survey reduced the NRMS differences at both the UMV and Cameo levels. The NRMS difference at the UMV level was reduced through the central high fold portion of the survey (Figure 3.33). A comparison of the histograms of the difference maps show that the dominant difference value was reduced from about 18% to approximately 15%. Accompanying the shift is a strengthening of the histogram's peak.

The strengthening indicates an overall reduction in the difference between the surveys at this level.

The Cameo level also experienced a reduction in the NRMS difference values between the surveys. The reduction in the difference at this level is also concentrated through the central portion of the survey (Figure 3.34). The peak of the histogram also experienced a shift from approximately 25% to 20%, with a strong increase in the concentration of low difference values. This indicates an overall improvement in the S22 base and monitor survey repeatability.

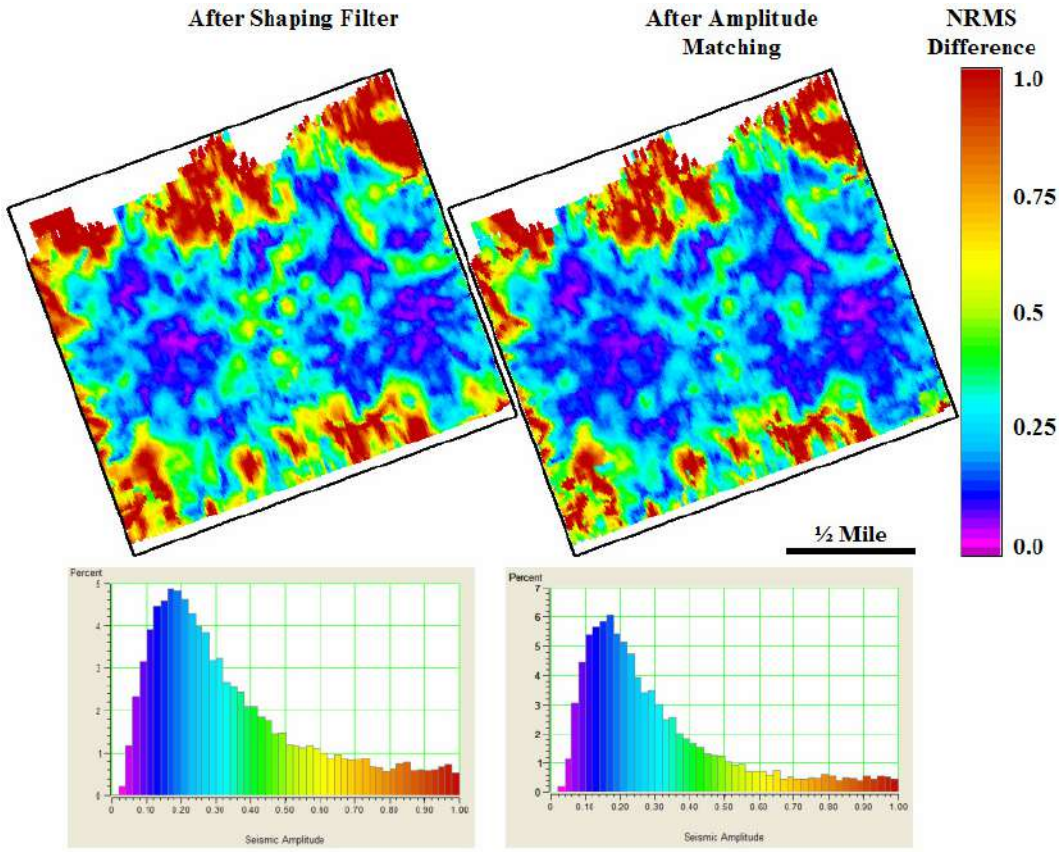

Figure 3.33 - NRMS difference for a 100 ms window centered over the S22 UMV event. Left panel is after the application of amplitude matching. Right panel is after the application of the time-varying time-shift. The histograms of the maps are also plotted

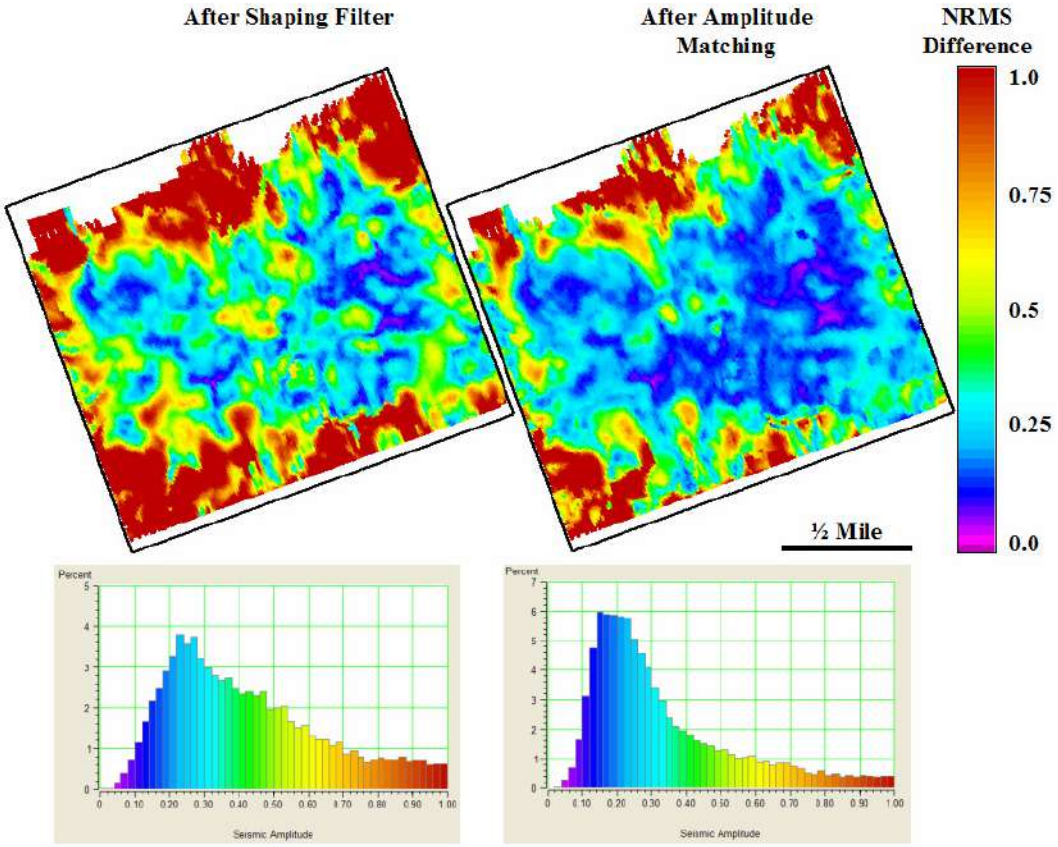

Figure 3.34 - NRMS difference for a 100 ms window centered over the S22 Cameo event. Left panel is after the application of amplitude matching. Right panel is after the application of the time-varying time-shift. The histograms of the maps are also plotted.

The application of the time-varying time-shift to the S22 monitor volume also increased the match between the frequency content of the two surveys. The match was increased through most of the frequency range from 0 to 30 Hz, except from approximately 22 to 26 Hz (Figure 3.35). The increased difference at these frequencies matches a similar observation in the S11 data. The difference through this range of frequencies is attributed to the imperfect nature of the cross-equalization process, and/or the enhancement of production related differences within the reservoir section.

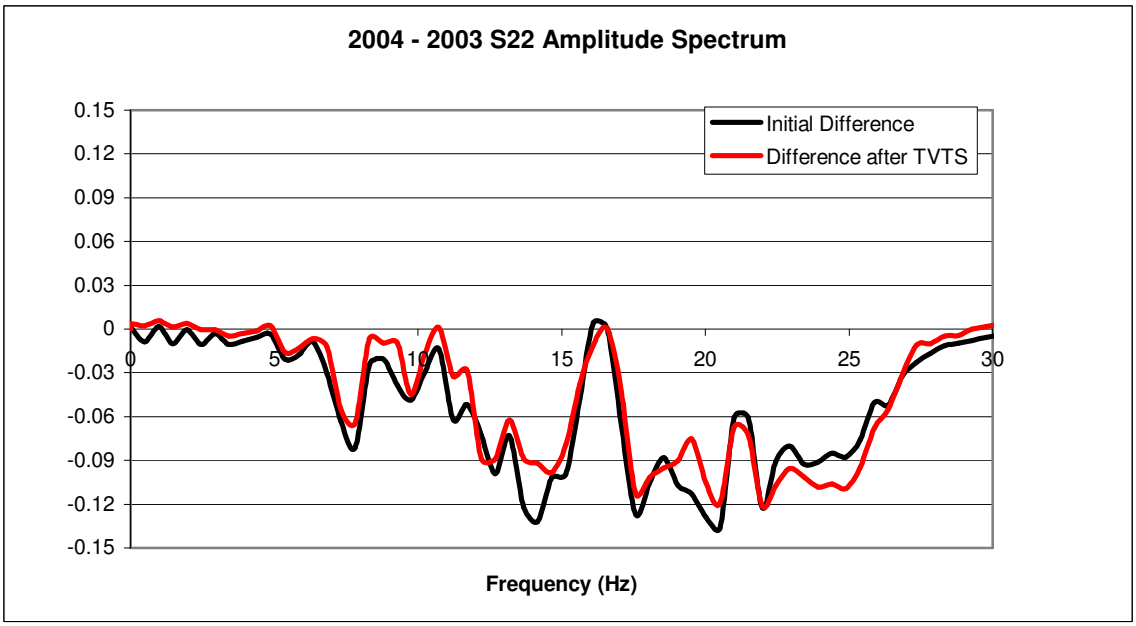

Figure 3.35 - Difference in amplitude spectrum between 2004 and 2003 S22 volumes calculated from 1800 to 2800 ms. The black line represents the initial difference before any equalization. The red line represents the difference after the application of the time-varying time-shift.

The cross-equalization process resulted in an overall reduction in the differences between the monitor and base S22 volurmes (Figure 3.36). The reduction is most notable through the static interval around the UMV horizon. The strong reduction through this interval is a result of specifically matching this static section between the surveys. Reductions in differences between the UMV and Cameo, and below the Cameo horizon indicate a strong match after the application of the cross-equalization routine.

The cross-equalization procedure resulted in high repeatability between the fast and slow shear wave volumes collected during the 2003 and 2004 seismic surveys conducted at Rulison Field. The initially high repeatability was a result of the dedicated time-lapse style of the surveys. Strong matching of the acquisition and processing provided initially strong repeatability prior to the implementation of the cross-equalization procedure. The cross-equalization procedure further increased the repeatability of the surveys. After the third stage of cross-equalization the normalized

root-mean square differences in the S11 data volumes were reduced to 12% at the UMV level and 20% at the Cameo level. The S22 data volumes also experienced strong reduction in the NRMS differences resulting in values of 18 % difference at the UMV level and 25% at the Cameo. These measures of strong repeatability allow for a confident interpretation of traveltime variations between the surveys, and between the fast and slow volumes for both surveys. The low values also illustrate the power of dedicated time-lapse seismic surveys in reducing survey differences.

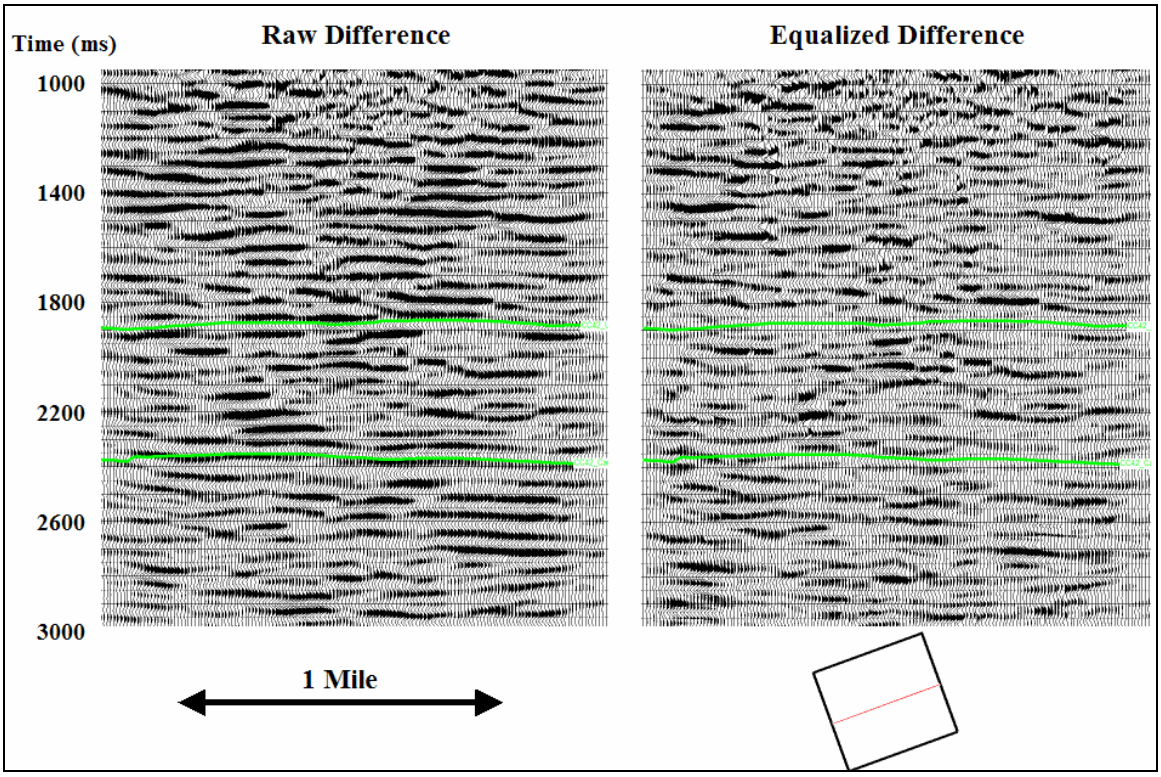

Figure 3.36 - Crossline 72 of the difference between the S22 monitor and base surveys. Left is the initial difference, right is the difference after the cross-equalization of the monitor survey. Top green horizon marks the UMV event, while the second green horizon marks the Cameo event.

Following the fourth stage of cross-equalization the normalized differences were reduced to 10% at the UMV level and 15% at the Cameo level for the S11 data. Similar

reductions occurred in the S22 data with normalized differences of 15% at the UMV level and 20% at the Cameo level. The small noise levels in the data after the cross-equalization procedure represents exceptional data repeatability. Previous time-lapse surveys have noise levels ranging from approximately 25 to 40% for dedicated surveys, and 60% and higher for legacy and repeat surveys (MacBeth, Stammeijer et al. 2006). Increased repeatability is possible, but would require permanent source and receivers (Meunier, Huguet et al. 2000). The strong survey repeatability at this stage allows for a comparison of impedance values between the surveys, and further illustrates the strength of dedicated time-lapse surveys and processing. This high repeatability is essential in this study due to the expected small time-lapse change resulting from gas production and pressure depletion.

With the conclusion of the cross-equalization process the shear wave time-lapse surveys are now comparable. By minimizing differences not related to production in the surveys, an analysis of production-induced variations can be made. This analysis included monitoring time-shift, amplitude, and impedance variations between the surveys. Evaluating time-lapse changes in this geologic setting provides the opportunity to increase the understanding of reservoir complexity, and the strong potential for the application of shear-wave time-lapse seismic monitoring in tight-gas sandstone reservoirs along with other unconventional reservoirs.

Chapter 4 Time-Lapse Changes

4.1 Introduction

Following the cross-equalization of the 2003 and 2004 fast and slow shear-wave seismic volumes, a comparison was made of their data content. This enabled an evaluation of time-lapse changes. Variations in the seismic surveys can be attributed to two main causes. The first of these causes is the presence of slight differences in the acquisition and processing of the two surveys. As noted earlier these variations can be caused by slight differences in acquisition geometries, source signatures, and the presence of noise. Due to the time-lapse acquisition, processing, and cross-equalization procedure these changes not related to production have been reduced. These type of changes were also assumed to be random, so as to not appear as continuous events in the data, but as low-level background noise. The second cause of time-lapse changes was attributed to the production of gas from the reservoir.

Gas production was expected to induce changes in the subsurface resulting from the depletion of pore pressure. Pore pressure reduction results in an increase in the effective pressure as the overburden or confining pressure is held constant.

Equation 4.1

$$P_e = P_c - nP_p$$

Equation 4.1 describes the relationship between effective pressure (P_e), confining pressure (P_c), and pore pressure (P_p). The effective pressure coefficient, *n*, accounts for the degree that changes in pore pressure attribute to changes in effective pressure, and is

heavily influenced by rock properties (Hoffman, Xu et al. 2005). The expectation is that as pore pressure is reduced, observable changes in the shear wave propagation velocities as noted by (Eberhart-Phillips, Han et al. 1989) will occur. Velocity changes between the fast and slow shear-waves can reveal pressure-related changes in shear-wave splitting and anisotropy, and provide an enhanced ability to observe time-lapse changes (Talley, Davis et al. 1998).

Velocity variations are interpreted through traveltime differences or time-shifts between corresponding events in the base and monitor surveys. Time-shifts were calculated using a cross correlation window technique. This technique is the same that was used to calculate the sample-by-sample time-shifts that were applied in the fourth step of cross-equalization. Changes in traveltime can indicate velocity changes in the S11 and S22 volumes separately, or can be calculated between the S11 and S22 to provide an understanding of changes in the shear-wave splitting coefficients.

Additionally, time-lapse changes in the amplitude and impedance values between the surveys can also provide insight into production induced rock property changes. This technique is dependent on proper alignment and balance of the surveys, so that the same subsurface intervals are being compared between the surveys. This technique is based off the assumption that these attributes contain information that is associated with the presence of localized changes in the subsurface (Thomsen 2002).

Proper balance and alignment between the surveys was essential for the application of these comparative procedures. Unlike many previous time-lapse studies focused on pore pressure increases, (Eiken, Brevik et al. 2000) and (Davis, Terrell et al. 2003), and fluid saturation changes, (Gouveia, Johnston et al. 2004) and (Boyd-Gorst, Fail et al. 2001), decreases in pore pressure in low porosity, tight sandstone reservoirs are expected to produce relatively small changes (MacBeth, Stammeijer et al. 2006). Due to the expected small time-lapse changes, strong repeatability and survey matching is essential for their identification. The use of dedicated time-lapse seismic surveys,

parallel processing, and cross-equalization provided highly repeatable data that allowed for the time-lapse analysis in the challenging setting of the reservoir at Rulison Field.

The presence of fractures in the reservoir is anticipated to enhance production related changes (MacBeth, Stammeijer et al. 2006). The fractured nature of the reservoir plays a major role in increasing permeability and production levels, and is also a key component to increasing the understanding of reservoir complexity and changes. As pressure is depleted and subsurface stresses are altered, the fractured rock component is expected to be more sensitive than the matrix component of the rock. This results in the enhanced ability to identify changes within these fractured intervals, due to their more compliant nature. Fractured intervals are also likely to experience larger production related changes under the assumption that high productivity wells have intersected fracture networks, resulting in zones of increased gas production and broader pressure depletion. The understanding of fracture network connectivity and their drainage patterns are two key components of this study. Their understanding can increase production and drilling efficiency, and the ultimate amount of produced gas. An additional expectation is a strong response of the deeper coal intervals to production and stress changes. The observation of changes through the coal intervals can provide additional information on the production of gas from the less understood coastal and marine reservoir intervals. Understanding changes in the coals can help identify the extent of coal production and reservoir connectivity within them, and the potential for gas sourcing from the coals into faults and fracture networks. The investigation of these aspects can provide a deeper understanding of the reservoir, and provide the opportunity for investigating additional bypassed high productivity intervals.

4.2 Time-Shifts

The time-shift analysis was performed after the third stage of equalization. At this stage in the equalization the static shift above the reservoir was corrected, and the

frequency and amplitude contents were balanced between the surveys. These processes removed any static differences that occurred above the reservoir, while preserving time-shifts through the reservoir interval. This allowed for cross correlation time-shifts to be computed through the reservoir interval, and an understanding of velocity variations and shear-wave splitting coefficient changes between the surveys to be observed.

Time-shifts were calculated using a sliding 100 ms cross correlation window. This is the same technique that calculated the time-varying time-shifts that were applied in the fourth step of the cross-equalization. The size for the window was chosen to include just over a wavelength of information, so as to provide enough data to properly align individual seismic events. For this calculation the base survey was held as the reference, while the monitor survey was shifted as the input volume. Under this parameterization positive time-shifts indicate a velocity increase, or event pull up from the base to monitor surveys. A negative time-shift indicates a velocity decrease, or event pull down from the base to monitor surveys. Time-shifts are calculated as the shift necessary to maximize the correlation coefficient for the windowed interval being compared between the surveys. The time-shifts were calculated on a trace-by-trace basis, so as to increase individual matching of the traces, and preserve lateral variations in time-shifts. The first correlation window began at the first data sample equal to time zero in the data volumes. After the calculation of the first time-shift, the window stepped down a sample, and the time-shift calculation was repeated. This was continued through the entire data set resulting in a sample-by-sample time-shift volume. The resulting time-shift volume contains the same values that were applied to the monitor survey during the fourth step of the cross-equalization. A correlation coefficient volume was also created to provide a measure of data repeatability, and time-shift reliability.

The time-shift volumes provide an understanding of the distribution and value of time-shifts with depth (Figure 4.1). Along the UMV horizon there are minimal time-shifts present. Time-shifts through this zone are expected to be small, +/- 0.5 to 1 ms, due to the previous static alignment of this interval, and the fact that no production

related change is expected to have occurred. The interval along the UMV horizon is also associated with high correlation coefficient values (Figure 4.1). These strong values are a result of strong continuous reflectors, and indicate high confidence in the time-shift values and repeatability through this interval. Moving deeper into the fluvial point bar interval of the upper reservoir between the UMV and Cameo horizons, zones of increased time-shifts (greater than +/- 9 ms) and decreased correlation coefficient values (less than 0.6) are present. These values result in the time-shifts having low reliability, and are associated with discontinuous low energy events through this interval. Once the Cameo horizon is reached the time-shifts and correlation coefficients stabilize. This is a function of stronger more continuous events that are associated with the coastal and marine environments of the lower reservoir section. The correlation coefficient strength through this interval increases the time-shifts reliability, and overall interval repeatability. Reliable time-shifts and strong correlation values continue to approximately 2900 ms in both the S11 and S22 data sets. This zone includes the entire lower reservoir interval that has been perforated, and that is believed to be productive. The deepest perforation occurred at 8683 feet measured depth, with an average maximum perforation depth of 7540 feet measured depth within the survey area.

Calculating a volume of sample-by-sample time-shifts and the corresponding correlation coefficients provides two main benefits. These benefits are the ability to monitor time-shift values both through vertical and horizontal slices. The vertical slice view, as seen in Figure 4.1, provides an understanding of the origin and reliability of time-shifts. The horizontal view can then provide an understanding of the lateral distribution of time-shifts. Horizontal slices can be extracted along picked horizons, or at a single time slice (Figure 4.2). Figure 4.2 illustrates the lateral distribution of time-shifts at the UMV level for both the S11 and S22 data sets. As expected, the central high fold portion of the survey exhibits low-level background time-shifts of +/- 0.5 ms. These shifts jump slightly to near +/- 1 ms, but only in isolated areas. From this information the minimum level of noise is approximately +/- 0.5 ms. Vertical and horizontal slices can

also be extracted from the correlation coefficient volumes providing a measure for the reliability of interpreted time-shifts (Figure 4.2).

The small values of time-shifts at the UMV level are mainly confined to the central part of the surveys (Figure 4.2). This area corresponds to the high fold, high repeatability area where strong alignment and equalization occurred. Strong correlation values are also present through this region, with most values approaching 1. There is, however, a presence of lower correlation values in the central portion of the S22 slice. Even though these values are slightly lower, they are still considered reliable with values of greater than 0.8, and low-level time-shifts close to 1 ms. The presence of small time-shifts and strong correlation values at the UMV level indicates the correct application of the bulk shift in the first equalization step to remove static differences between the surveys.

Larger negative and positive time-shift values occur along the edges of the surveys. These large shifts can be attributed to the presence of edge effects, and higher levels of noise through the low fold portions of the survey. The large time-shift areas also correspond to low correlation values that limit reliability. Due to the expectation of small background shifts at the UMV level, the search for interpretable time-lapse changes will be focused on the central portion of the survey. While acquisition geometry and processing repeatability are high for these edge regions, the low fold nature of the data was unable to adequately limit the presence of noise. This resulted in larger variations in event amplitude, seismic character, and event arrival times that cannot be interpreted as valid production related time-lapse changes.

Extracting time-shift and cross correlation slices at the Cameo level reveals larger time-shifts in the S11 and S22 data volumes at this level compared to the UMV level (Figure 4.3). It must be noted that the time-shifts observed here are a result of accumulating shifts through the entire interval between the UMV and Cameo events. This limits the vertical resolution of the information, but provides an overall look at time-shifts in the upper reservoir.

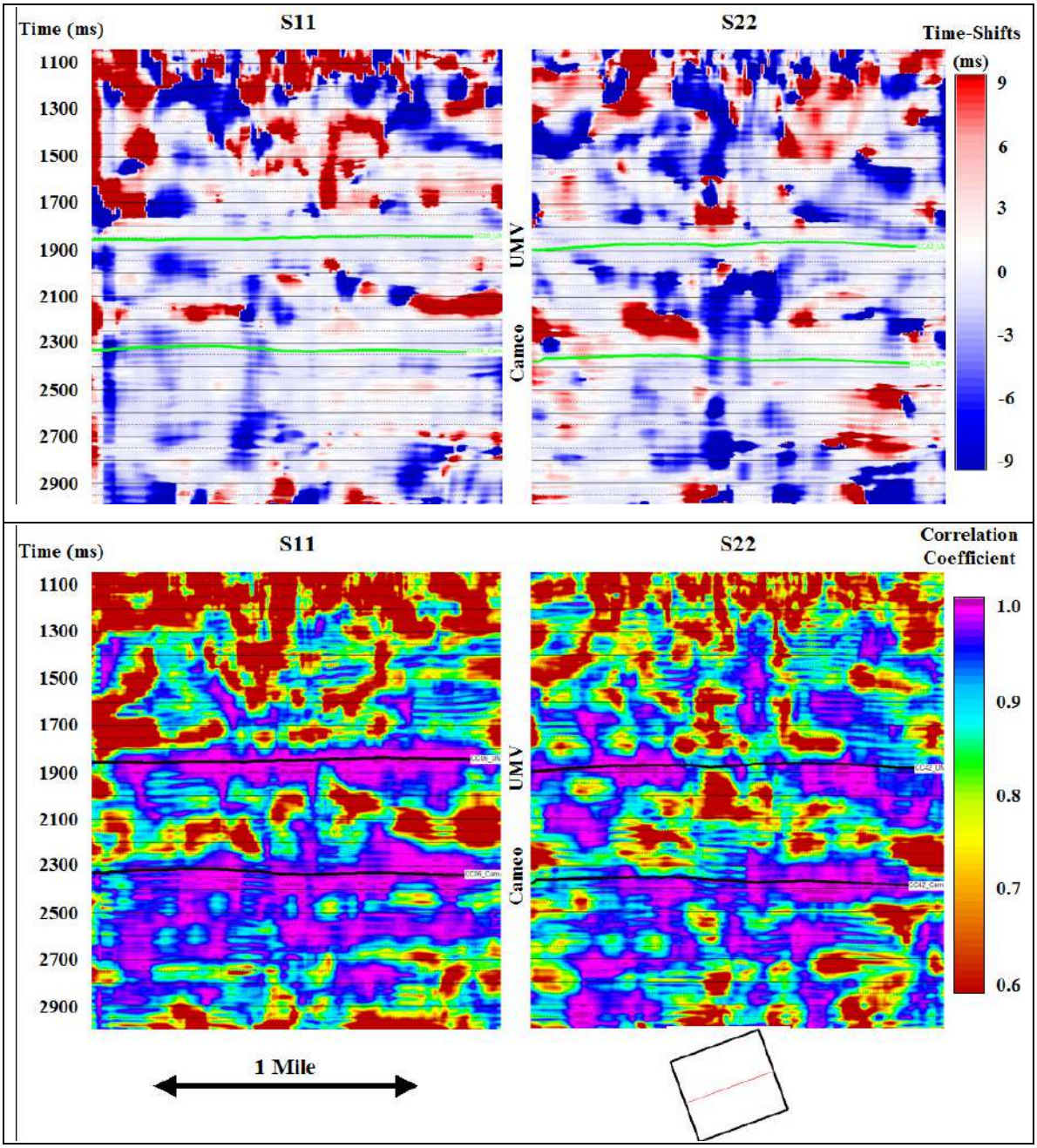

Figure 4.1 - Top panels are the cross correlation time-shifts for the S11 and S22 volumes between the monitor and base surveys. Positive values indicate a pull up or velocity increase from the base to monitor survey. Bottom panels are the correlation coefficients for the S11 and S22 volumes resulting from the application of the calculated time-shifts. East-west crossline 72 is displayed.

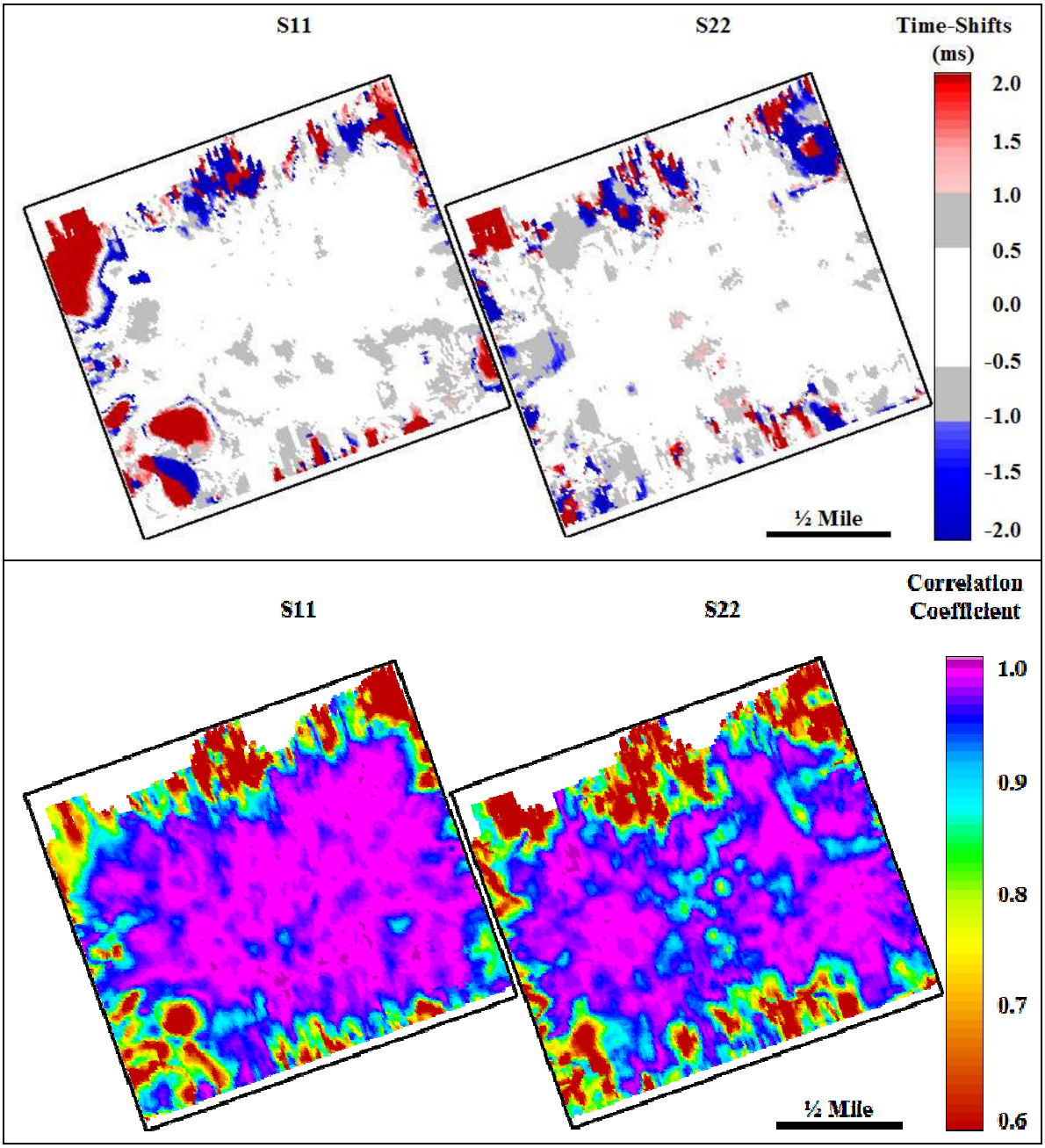

Figure 4.2 - Top panels are the cross correlation time-shift values extracted from the S11 and S22 sample-by-sample time-shift volumes at the UMV horizon level. Bottom panels are the corresponding correlation coefficients at the UMV level resulting from the time-shifts.

The Cameo level of the S11 volume has a background time-shift level of +/- 2ms through the central region of the survey. This area also contains a dominant distribution of negative time-shifts that reach values close to –7 ms. Negative time-shifts for this comparison correspond to the pull down of the seismic event from 2003 to 2004. This would imply a velocity decrease over the time-lapse interval. The central area also contains strong correlation values approaching values of 1, implying strong reliability in the time-shifts. There is also a presence of positive time-shifts at this level, but they are of weaker value than the negative shifts. The positive time-shifts reach a maximum value of approximately 4 ms through the central portion of the survey, and would result from a pull up in the seismic event caused by a velocity increase. The central area of focus can also be extended at this level due to the strong correlation values of greater than 0.8 extending to the edges of the survey. By extending the area of reliability toward the western side of the survey, a zone of strong positive shifts (5+ ms) in the northwest quadrant, and a zone of strong negative shifts (5- ms) in the southwest quadrant can be included in the analysis.

The Cameo level slices extracted from the S22 volumes have similar characteristics as the slices extracted from the S11 volumes (Figure 4.3). The central north-south running section of the time-shift slice is dominated by the presence of negative time-shifts. These time-shifts reach a maximum value of approximately –7 ms, and correspond to strong correlation coefficient values approaching 1. Moving east and west from the central third of the survey results in an increased presence of positive time-shifts. These values reach a maximum of approximately 7 ms, but on average range from 3 to 5 ms. Similar to the S11 slices the area of focus can be extended close to the eastern and western edges of the survey due to strong correlation values.

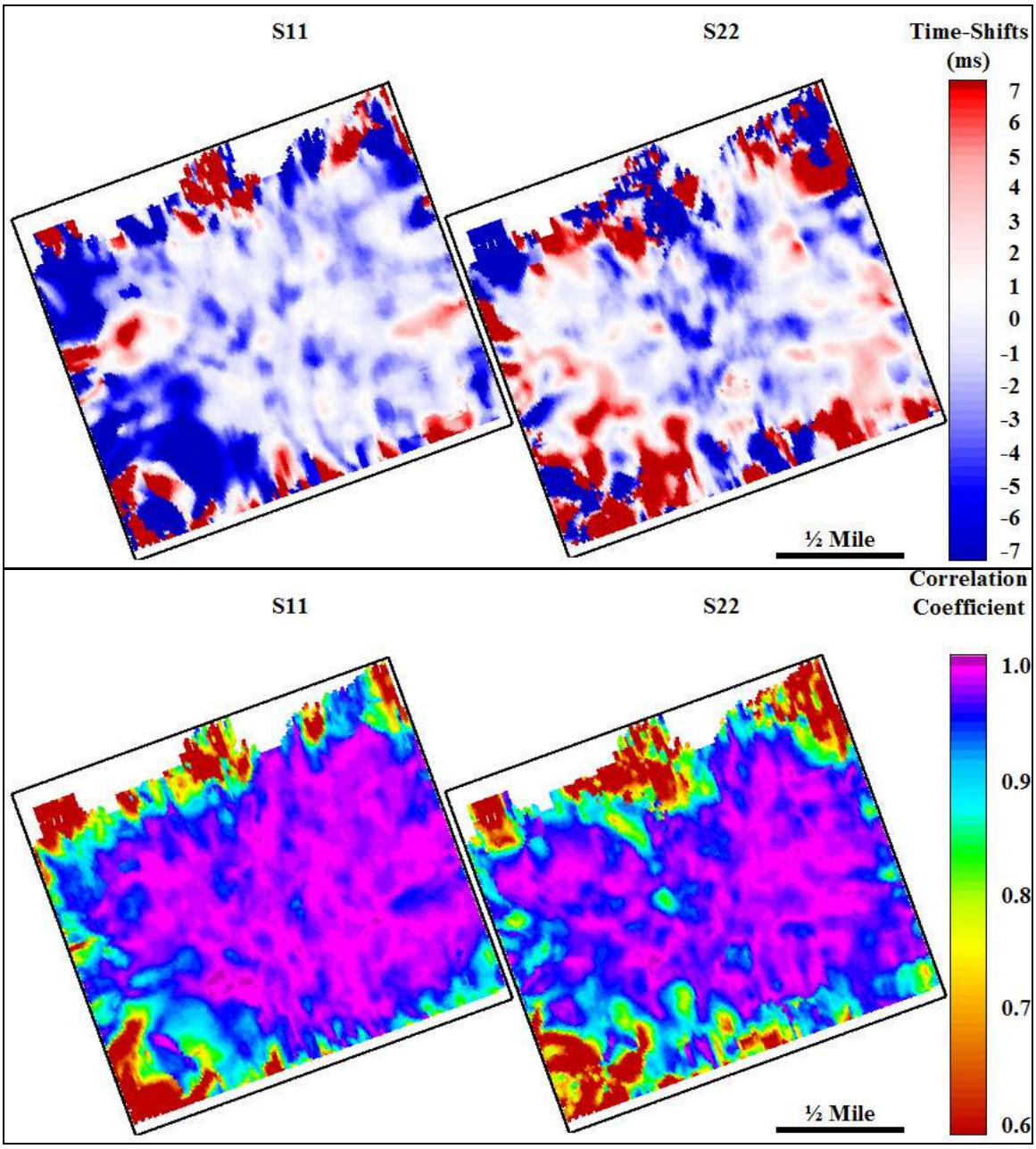

Figure 4.3 - Top panels are cross correlation time-shift values extracted from the S11 and S22 sample-by-sample time-shift volumes at the Cameo horizon level. Bottom panels are the corresponding correlation coefficients at the Cameo level resulting from the time-shifts.

4.3 Shear-Wave Splitting

While time-shifts calculated by comparing the fast shear volumes between the surveys, and the slow shear volumes between the surveys provides information concerning velocity variations in similarly polarized waves, the use of time-shifts between the fast and slow shear-wave volumes within the individual surveys can enhance the understanding of subsurface changes. Comparisons of the fast and slow shear-wave event arrival times provide information about shear-wave splitting, and changes in the anisotropic nature of the reservoir. Shear-wave splitting coefficients measure the variation in velocity between the fast shear-wave polarized parallel to fracture or crack orientation, and the slow shear-wave polarized perpendicular to the fracture or crack orientation. The polarizations could also be a result of variable stress magnitudes in the subsurface, or a combination of stress and fractures. An assumption that is made in order to calculate these values is that orthorhombic symmetry is present in the subsurface, and that the wave polarizations are consistent both vertically and laterally through the seismically sampled subsurface interval (Thomsen 2002). As noted earlier, the interval above the UMV horizon is considered to be negligibly anisotropic, so as to not induce a separate instance of shear-wave splitting. It is also considered to be static, so that no time-shifts at this level are expected to result from production. This assumption is needed to validate the static alignment of the UMV event in the first stage of equalization.

Traveltimes between high amplitude, continuous subsurface events were used to calculate variations in the fast and slow shear-wave velocities. Strong continuous events are necessary to provide high confidence in the horizon picks, and a laterally extensive surface through the survey. Differences in event arrival times were compared between the fast and slow volumes independently for each survey. The shear-splitting coefficients were calculated using Equation 4.2 (Lynn and Thomsen 1986).

Equation 4.2

$$\frac{(\Delta T_{S22} - \Delta T_{S11})}{\Delta T_{S11}} * 100 = \gamma$$

ΔT_{S22} represents the traveltime between two bounding events in the slow shear volume, and ΔT_{S11} represents the traveltime between the same bounding events in the fast shear volume. Taking the ratio of these two numbers provides a normalized dimensionless value of the shear-wave splitting coefficient. The coefficient was multiplied by 100 to provide a percent value.

This calculation was limited to large intervals bounded by strong continuous reflectors. Large interval comparisons are necessary to prevent the dominance of error in the calculations (Thomsen 2002). These stipulations limited the use of this technique to intervals between the UMV and Cameo horizons, and between the Cameo horizon and a horizon picked at approximately 2700 ms (Figure 4.4). The UMV to Cameo interval has a time thickness of approximately 500 ms, or approximately 2000 feet thick. The Cameo to 2700 ms interval has a time thickness of approximately 350 to 375 ms, or approximately 1400 feet thick. The 2700 ms horizon is below the maximum level of drilling and completions for the reservoir. Other continuous reflectors are present in the data, but occur near the UMV and Cameo events, preventing the calculation of splitting coefficients over a large interval.

Positive shear-wave coefficients indicate that the slow shear-wave has a slower velocity, or larger traveltime than the fast shear-wave. This is expected assuming the rotation of the data was correct, and the polarizations are consistent throughout and between the surveys. A negative value would indicate the flipping of the fast and slow polarizations, where the fast shear-wave actually propagates at a slower velocity than the slow shear-wave.

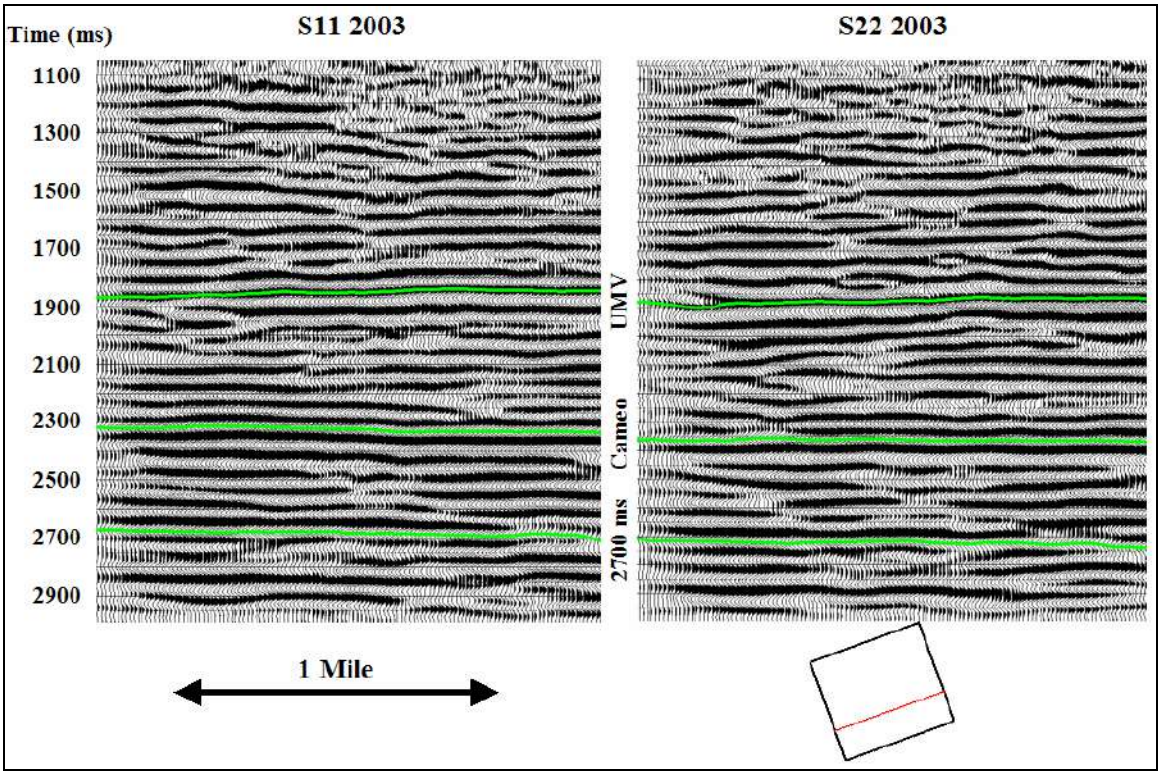

Figure 4.4 - 2003 S11 and S22 crossline 98 seismic sections with UMV, Cameo, and 2700 ms horizons marked.

4.3.1 Upper Reservoir

The calculation of shear-wave splitting coefficients between the UMV and Cameo horizons was performed using the horizons picked prior to the equalization process. Since a comparison of the interval time thickness is being made the cross-equalization process is unnecessary due to it not altering this relationship. For both the 2003 and 2004 surveys the values of the splitting coefficients for the UMV to Cameo interval fall between 0 and +10% (Figure 4.5). The dominant presence of positive values increases the confidence in the rotation, and resulting separation of the fast and slow shear-wave information during the initial processing. There is a small presence of negative splitting

coefficients that occur along the edges of the surveys. The negative values are attributed to the presence of edge effects and increased noise levels in low fold areas.

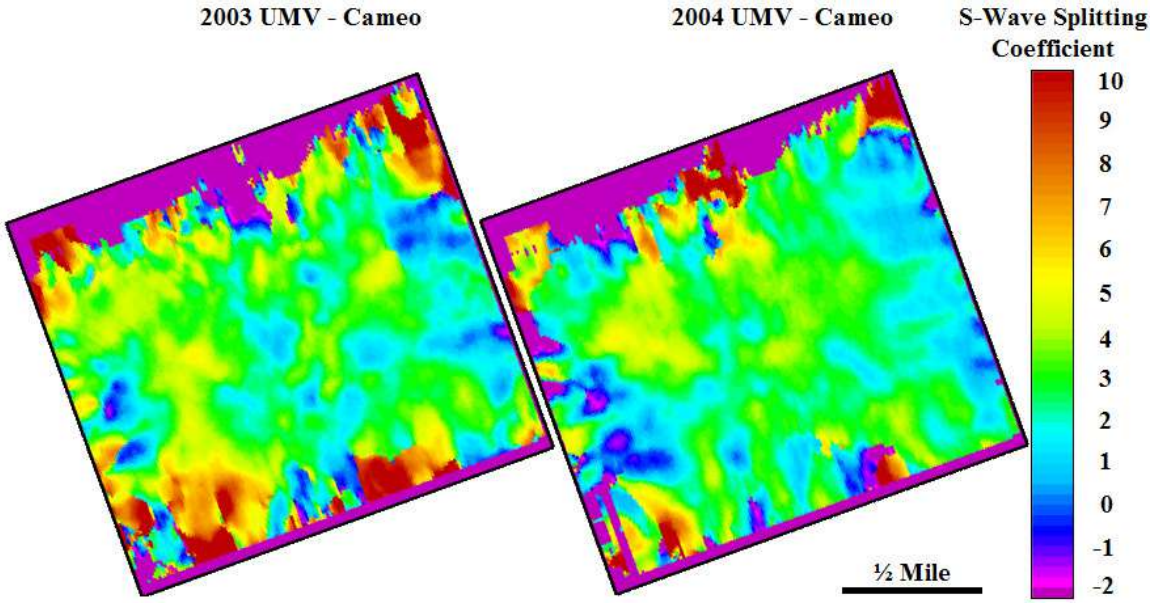

Figure 4.5 - Shear-wave splitting coefficients calculated between the UMV and Cameo horizons for the 2003 and 2004 surveys.

The splitting coefficient plots in Figure 4.5 illustrate the lateral distribution of azimuthal anisotropy within the upper reservoir zone for the 2003 and 2004 seismic snapshots. The plots indicate that there are changes in the shear-wave splitting resulting from production. Differencing the two plots further illustrates the change in splitting coefficients (Figure 4.6). The difference of the plots reveals the presence of both increases and decreases in the splitting coefficient from 2003 to 2004. Negative values indicate a decrease, while positive values indicate an increase in the splitting coefficients. The right plot in Figure 4.6 is the same as the left, but with – 1 % to + 1 % difference masked out. This range is viewed as the background level of change, or noise in the data.

The initial expectation is for a decrease in the s-wave splitting coefficients as a result of production. This hypothesis is made under the assumption that a single fracture

or crack set was inducing the s-wave splitting. As gas is produced and pore pressure is depleted the resulting increase in effective pressure would squeeze the sampled unit of rock. This would result in the closing of the fractures and an increase the stiffness of the rock unit being sampled by the slow s-wave. The result is an increase in the slow s-wave propagation velocity. The fast shear-wave velocity is not expected to change, since the fast polarization would be sampling the same stiff matrix component of the rock. These changes would result in a decrease of the time-shifts between the S11 and S22 arrivals from the 2003 to 2004 surveys.

The splitting coefficients calculated between the UMV and Cameo horizons do exhibit decreased values from 2003 to 2004 (Figure 4.6). Negative difference values are predominantly dispersed through the southwest corner of the survey, and in isolated areas within the central portion of the survey. There are also zones of increased splitting coefficients located in the central portion of the survey. The positive difference values indicate that the subsurface interval of interest has experienced an increased separation of the fast and slow s-wave velocities. The observation of changes in the time-lapse splitting coefficients indicates an ability to monitor reservoir changes through the use of time-lapse shear-wave seismic data.

To aid in analyzing the change in the s-wave splitting coefficients, the difference map was broken up into two regions. These regions were based on the value and distribution of change (Figure 4.6). The first region, denoted as region A, is in the central part of the survey. This region is dominated by small background changes, along with isolated areas of increased splitting values. There are also isolated instances of decreased splitting coefficients, but they have a smaller extent compared to the zones of increase. The second region, denoted as region B, is located in the southwest corner of the survey. This region is dominated by a large zone containing decreased splitting coefficient values. Since the calculation of the shear-wave splitting coefficients is based on a comparison of time thickness values between horizons, comparing the fast and slow

isochrons of the individual surveys is necessary. This provides a greater understanding of the cause of the observed differences.

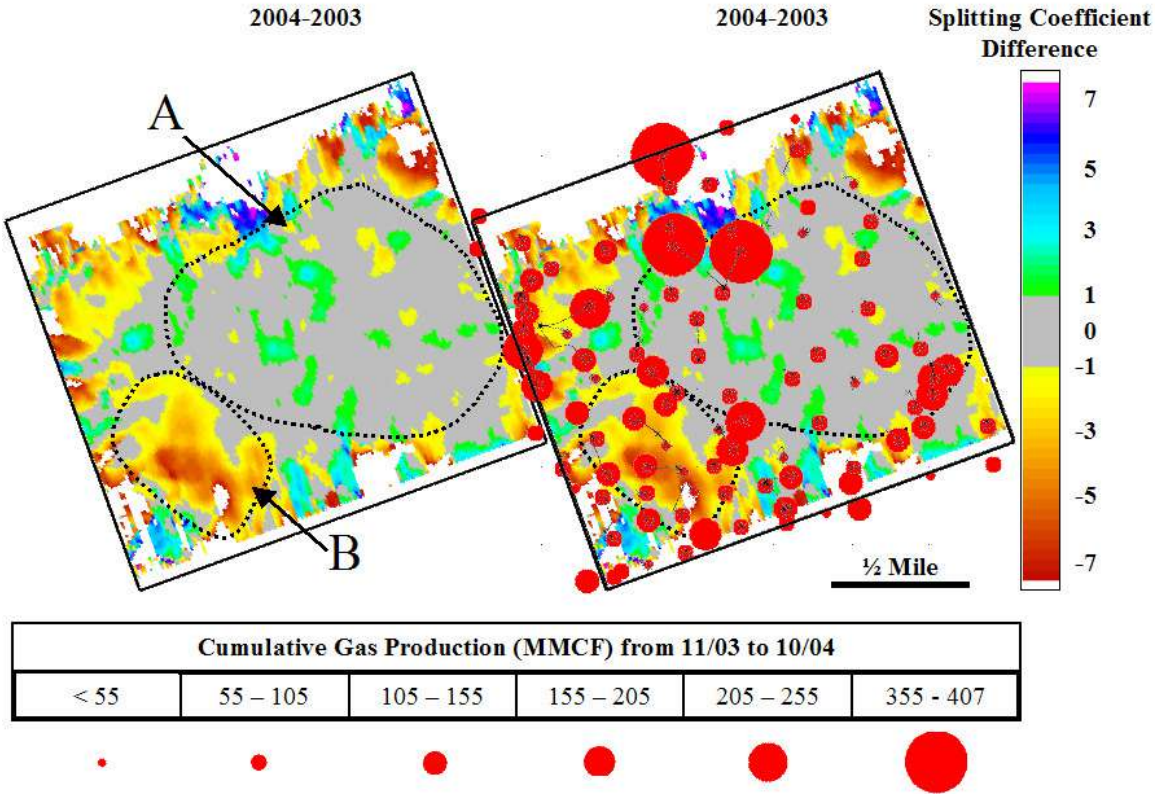

Figure 4.6 - Difference in the 2004 and 2003 shear-wave splitting coefficients calculated between the UMV and Cameo horizons. Negative values indicate a decrease in the coefficient. The right plot also has the cumulative gas production during the time-lapse interval overlain on it.

The first region of focus is the large central area of the survey (Figure 4.6). This region is part of the high fold area of the survey, and contains the most repeatable portion of the data. The main characteristics of interest in this region are the isolated zones of increased splitting coefficient values. Figure 4.7 plots the difference in the interval time between the UMV and Cameo horizons between the 2004 and 2003 surveys. The left plot is the interval difference from the S11 data. Region A does not exhibit a high level

of change in the S11 interval time. This indicates that the change in the splitting coefficients is not dominated by changes in the fast s-wave velocity. The right plot is the interval difference from the S22 data. Region A exhibits zones of strong increase in the S22 traveltime interval from 2003 to 2004. Increases are noted by positive difference values. These areas of increase correspond directly to the increases in s-wave splitting coefficients plotted in Figure 4.6. This indicates that the increases in the splitting coefficients are dominated by decreased S22 velocities.

Under the initial assumption of a single fracture set aligned with the fast s-wave polarization, the observed changes do not correspond to expected changes in the subsurface. The initial hypothesis was that an increase in effective pressure results in a decrease in the fracture density and increases in the slow s-wave velocity. Under the single fracture set assumption, these observations would suggest that if all the previous assumptions concerning the data, processing, and cross-equalization are correct, changes are resulting from an increase in the single fracture network density. While this conclusion was not anticipated, the strength of the data insists on the validity of the observations. These changes indicate that additional complexities are present in the subsurface. One possibility could be the presence of locally variable stresses. These stresses could lead to lateral variations in the shear wave polarizations, and may result in unanticipated changes from production. The stress variations could also play a role in the creation or opening of additional fractures or cracks as the stress in the rock change with production.

Cumulative gas production per well through region A is relatively consistent at a rate of between 55 and 105 MMCF during the interval from the 2003 to 2004 surveys (Figure 4.6). There are a few higher productivity wells in the southeast corner of the region, and two large producers of greater than 400 MMCF on the northern edge of the region. Cumulative production is plotted at the bottom-hole location for each well. Due to the fact that the production values from each well are a commingling of the production from every perforated zone, a complete understanding of zone specific productivity is not

possible. Production was plotted at the bottom-hole location for two reasons. The first reason is that the perforations are completed in the bottom, almost vertical section of the well. The second reason is that multiple wells are drilled off of a single surface pad. This causes the upper portion of the wells to be in close proximity until they deviate and move apart at depth. Since zone specific production is not available, the bottom-hole location is considered to be a good representation of the general location where production is originating.

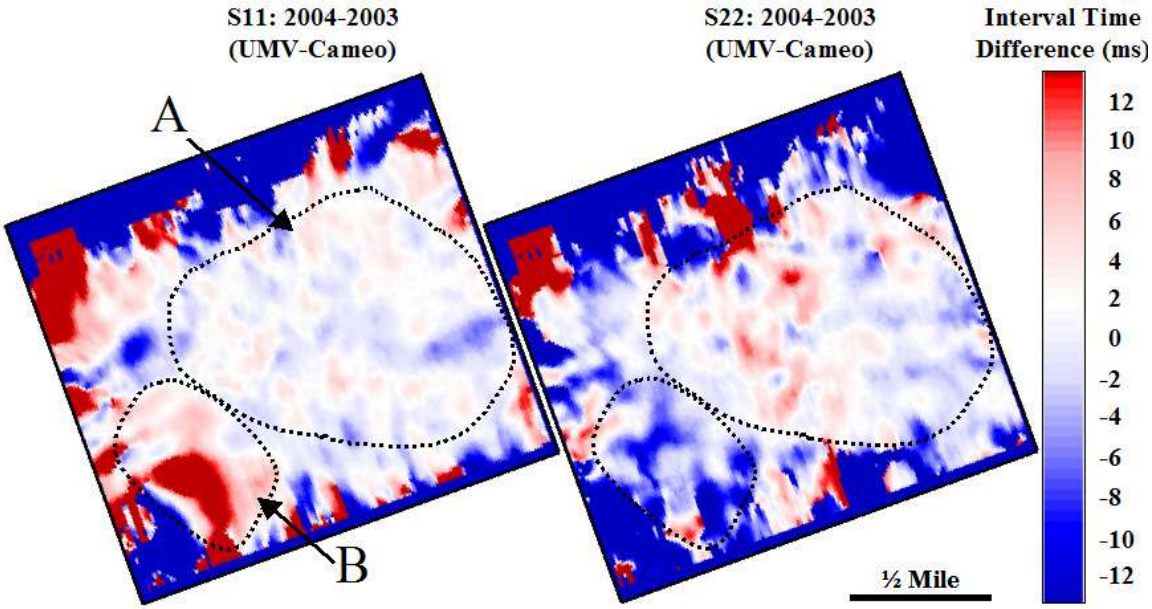

Figure 4.7 - Difference in the interval time between the UMV and Cameo horizons between the 2004 and 2003 surveys for the S11 and S22 volumes.

The two northern high productivity wells will not be taken into consideration due to their position along the edge of the survey associated with the topographic rise of the Roan Cliffs. The southeastern high productivity wells fall in a lower fold region of the data, but appear to have highly repeatable data. These wells are of interest, but do not appear to correspond to any strong changes in the shear-wave splitting coefficients between the UMV and Cameo horizons. The possible explanation for insignificant

change near these wells could be associated with the age of the wells. These three main wells RWF 332-21, RWF 432-21, and RWF 532-21 (Figure 4.8), were completed in May of 2004. This occurred during the interval between the time-lapse surveys. Only having approximately 4 months of production prior to the shooting of the 2004 survey may have limited the amount of observable subsurface changes. This could be caused by three factors. The first factor may be that production was dominated by the deeper perforations below the Cameo horizon. This is a result of higher pore pressure with depth playing a role in holding back production from completed zones in the shallower reservoir interval. The second cause could be associated with the fact that despite high production numbers, the pressure drop in the reservoir was not large enough to cause noticeable changes in the seismic data. A better parameter to correlate with changes in the seismic data would be the amount of reduction in reservoir pressure with production and time. This is suggested because pressure change is assumed to be the major cause of change in the subsurface. The final factor may be that the large production numbers are a result of the localized effect of the hydraulic fracturing in the wells. The early strong production is caused by the localized depletion near the well bore where the hydraulic fracturing had the greatest affect in fracturing the sandstone interval.

Through the rest of region A are localized areas of increased splitting coefficients occurring on the western side, and decreased splitting coefficients occurring on the eastern side. The presence of localized areas with values above the background noise level indicates an ability to use seismic data to monitor changes in the subsurface. While the polarity of these changes cannot be fully explained their presence is encouraging in demonstrating the application of s-wave time-lapse data. It is also interesting that the locations of a number of the wells in the region align with these areas of change. The orientation and trend of localized changes may also indicate an ability to further increase the understanding of reservoir characteristics. The presence of positive changes through the interval suggests additional subsurface characteristics that have not been taken into consideration.

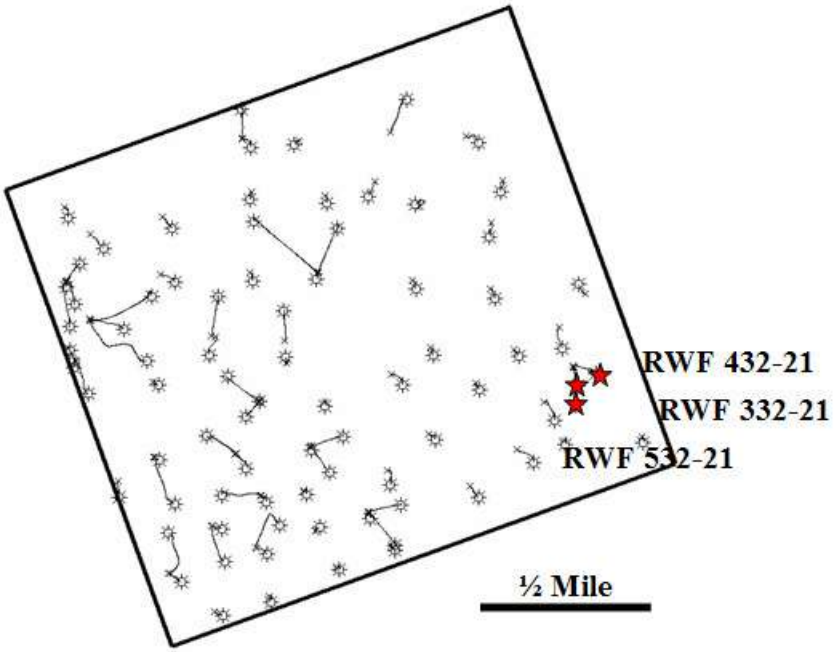

Figure 4.8 - Location of RWF 432-21, RWF 332-21, and RWF 532-21 wells within RCP survey.

The north-northwest trend of positive increases through the central portion of Region A may indicate two things. The first could be the presence of enhanced natural fracturing in zones with multiple or dense fracture networks. Changes to these 'sweet spots' may result in unanticipated changes in the seismic data resulting from increased complexity. While the splitting coefficient change does not follow the initial hypothesis, the localized and consistent nature of the change indicates areas of interest that may be changing as a result of production from nearby wells.

The second cause could be the presence of a fault trend running through the central part of the survey. Faulting through the reservoir is difficult to observe in the seismic data, but may be identifiable through the time-lapse analysis as production alters the subsurface characteristics. The presence of faulting in the field could result in areas of increased or enhanced natural fracturing, or the creation of locally variable stress fields. The enhanced fracture networks and stress fields may be reacting to gas

production and pressure depletion in an unpredicted way that can not be fully understood with this type of analysis.

The localized zones of decreased splitting coefficients do agree with the initial single fracture set assumption. Decreases in S22 traveltimes indicate a velocity increase. This is in agreement with the initial assumption of decreases in a single fracture set density. The agreement of four wells with the areas of change is also a positive indication of change. Due to their limited presence, and the presence of increases in the splitting coefficients, the complexity of the subsurface interval between the UMV and Cameo horizons has been underestimated. The presence of change indicates that the use of time-lapse s-wave data is a useful tool for monitoring production, both through anticipated and unanticipated changes. An increased investigation of the field, through the use of prestack p- and s-wave data and the extensive well log information available will be necessary to further understand and identify the cause of changes in the s-wave data.

The second region of interest is the southwest corner of the survey (Figure 4.6). The main feature of interest in this region is the strong trend of decreased splitting coefficient values between the years. Figure 4.7 reveals two trends that lead to this change. The first trend is a strong increase in the S11 interval travel time. This can be attributed to the slowing of the fast s-wave propagation velocity. Large changes of this type occur in the central part of region B, but also continue outward towards the limits of the region. Interval traveltime increases correspond to what is observed from the time-shifts calculated at the UMV (Figure 4.2) and Cameo levels (Figure 4.3) of the S11 volumes between the 2003 and 2004 surveys. Positive time-shifts at the UMV level and negative time-shifts at the Cameo level indicate a thickening of the interval time between the horizon time-shift due to limiting the maximum time-shift to 10 ms. This was done to prevent cycle skipping when calculating and applying the time-shift. The limitation on the applied time-shifts was an additional factor in using the original volumes to perform the splitting coefficient analysis.

The S22 interval times also exhibit decreased values through region B. This would indicate an increase in the slow s-wave velocity from 2003 to 2004. The decreases correspond to positive time-shifts at the Cameo level between the S22 2003 and 2004 surveys. A shrinking of the interval time between the UMV and Cameo horizons is the cause of these positive time-shifts. These two sets of changes indicate that the fast s-wave velocities are slowing, while the slow s-wave velocities are increasing, resulting in a reduction in traveltime differences between the S11 and S22 volumes. While the presence of decreased splitting coefficients is the anticipated result of pressure depletion and production, the cause of the change differs from the initial expectation.

Compared to the production in region A, region B has dense well spacing with individual well production levels ranging from 155 to 255 MMCF. The high level of production through this region, and the dominant presence of decreased splitting coefficient values, indicates that the time-lapse seismic data is monitoring changes between the UMV and Cameo events. The large consistency in the area of change further indicates that this subsurface interval is experiencing a consistent type of change, and that enhanced reservoir connectivity may be present. Connectivity through this region may be a result of a large fault trending in a northwest direction through region B. This fault is evident in the p-wave data, but not distinct in the s-wave data (Keighley 2006). The presence of this fault would result in the presence of increased natural fracturing in the region. Enhanced fracturing, along with hydraulic fractures created during the completion of the wells would allow for a large interval of the reservoir being in connected. The production of gas from numerous wells would then allow for gas to be produced from a large interval, both laterally and vertically. This would explain the strong continuous distribution of decreased splitting coefficients.

Along with higher production levels through region B compared to A, there is also a more significant presence of younger wells in this region. A younger well is one that was drilled and completed either between the 2003 and 2004 surveys, or within a year or two prior to the shooting of the base survey. The young nature of these wells

provides another reason for more continuous change through this region. The hydraulic fracturing performed in the completion of the wells, results in the creation of a large artificial fracture network, and the large initial boost in production that makes the wells economic (Figure 4.11). The artificial fracturing and strong surge in production would result in the strongest expected episode of subsurface change in the life of the well. This is expected due to the highest levels of production, and the largest expected drop in pore pressure around the well. The increased number of young wells in region B compared to region A and the higher well density add confidence to the observation of the continuous distribution of change. These observations also suggest an optimal timing for the time-lapse surveys. Optimal timing for the observation of production induced changes appears to be within a year or two of the wells initial completion, and suggests an interval of approximately three years between the surveys.

The cause of change through this interval indicates the need for a further investigation of s-wave polarization data. An understanding of lateral variations in the polarizations, both in the individual surveys and between the surveys, may indicate that the use of a single rotation angle for both surveys is inadequate. This may also indicate that the polarization angles may be changing with production, and that variations in the surveys are a result of polarization variations instead of the assumed velocity changes between consistent polarizations. A more complete understanding of the necessary rotation angles would allow for a further separation of differences in the fast and slow shear wave volumes, and would help to quantify the values of change.

Similar to region A the isolation of changes in the splitting coefficients may provide a deeper understanding of subsurface characteristics. The break in change between region A and B may indicate the presence of a fault trend running through the survey. The variation in the polarity of the change and its cause may be the result of complex fracture networks containing multiple fracture sets and stress variations through the region. This could induce unanticipated changes, and an inconsistent reaction to s-wave data and production. A better understanding would be possible with the use of a

larger survey that could provide an understanding of deep seated faults. An issue with monitoring faults with this data is that they splay out and become unidentifiable through the Mesaverde Group (Cumella and Ostby 2003).

4.3.2 Lower Reservoir

The second interval that was investigated falls between the Cameo and 2700 ms horizons (Figure 4.4). This interval represents the coastal and marine depositional environments that contain relatively continuous coal intervals overlying continuous marine sands. The continuity and strength of the 2700 ms horizon limited confident event picking to the southwestern half of the survey. The thick black line in Figure 4.9 bounds the area of confident horizon picking. The southwest corner of the survey contains positive difference values that correspond to the location of several wells with cumulative gas production of between 55 and 255 MMCF during the time-lapse interval. The agreement between well locations and splitting coefficient changes in this region leads to the conclusion that production between the 2003 and 2004 surveys has resulted in subsurface changes that can be monitored with highly repeatable seismic surveys.

Zooming in on the southwest corner of the splitting coefficient difference map illustrates the alignment of high productivity wells with zones of change (Figure 4.10). The bottom edge of Figure 4.10 also contains high levels of negative change that are associated with edge effects in the low fold region of the survey. The central area of positive differences aligns with the location of two top producing wells during the time-lapse interval. Similar to the UMV to Cameo interval, increases in the splitting coefficients are a result of an increase in the S22 traveltime interval from 2003 to 2004. This corresponds to a slow s-wave velocity decrease. The fast s-wave traveltime interval remains relatively constant for this interval.

Table 4.2 provides the cumulative gas production, completion date, and gas productivity ranking during the time-lapse interval for the four wells near this zone. The

RMV 212-20 and RMV 60-20 wells are older, smaller gas producers that are located along the edge of the zone of change. The high productivity RWF 443-20 and RWF 543-20 wells are located within the zone of change.

Several factors must be considered to evaluate change through this interval. The first factor is the close proximity of the wells. The bottom-hole locations for the four wells of interest are approximately 500 feet apart, with three of the wells being drilled from the same surface pad location. The close proximity of the completed intervals would allow for the anticipation of communication between the producing intervals. The second factor that must then be considered are differences in the cumulative production rates. The large differences in the production rates indicate that the newer RWF wells producing intervals have not been depleted by production from the older RMV wells.

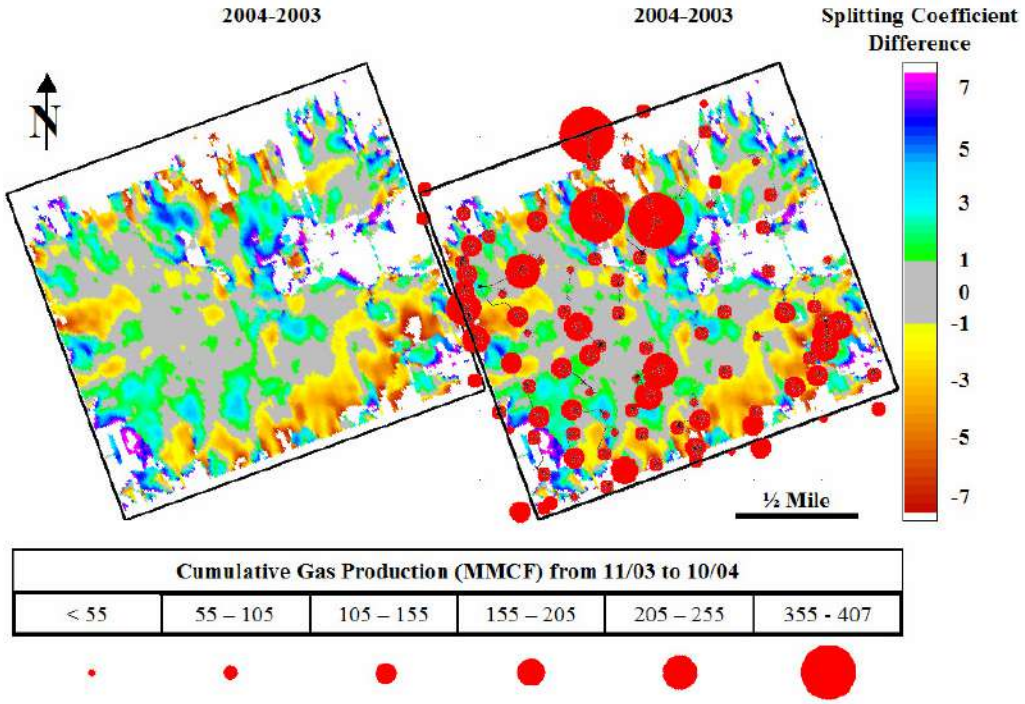

Figure 4.9 - Difference in the 2004 and 2003 shear-wave splitting coefficients calculated between the 2700 ms and Cameo horizons. Negative values indicate a decrease in the coefficient. Right plot also has the time-lapse gas production overlain on it.

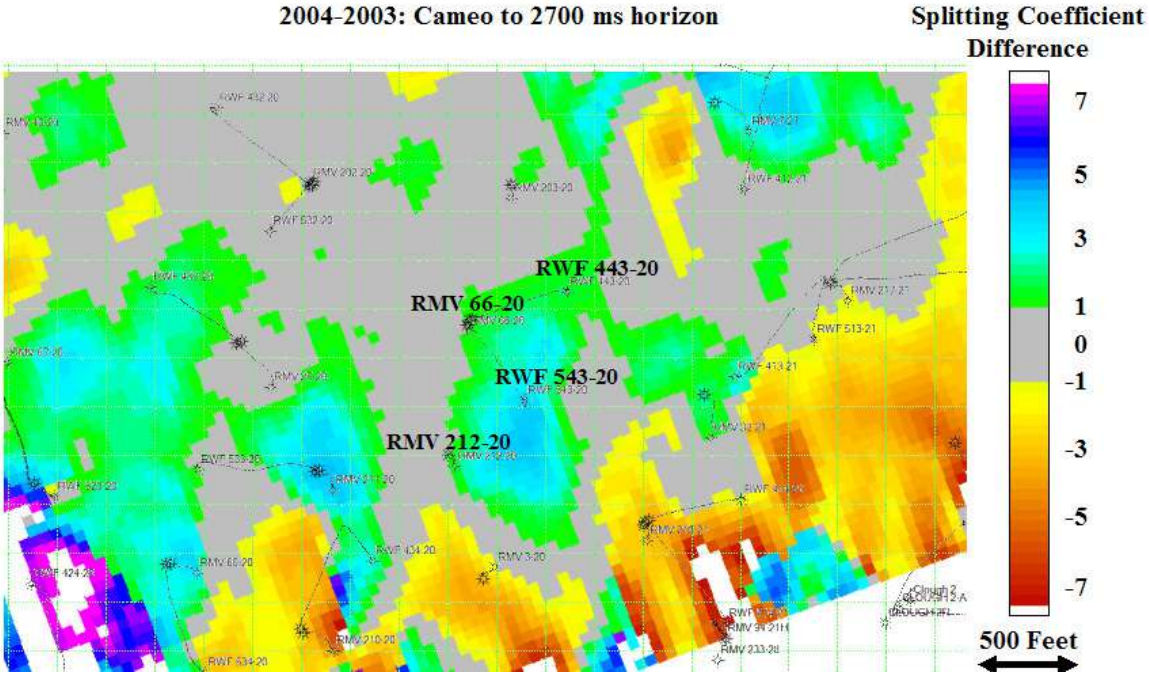

Figure 4.10 - Difference in the 2004 and 2003 shear-wave splitting coefficients calculated between the 2700 ms and Cameo horizons. Zoomed in view of the southwest corner of Figure 4.9.

Table 4.2 – Production and completion dates for wells of interest in the B region.

Well	Cum. Production (MMCF)	Completion Date	Rank
RWF 443-20	244	February 2004	4th
RWF 543-30	198	February 2004	7th
RMV 212-20	65	November 1998	69th
RMV 66-20	52	December 1996	80th

The initial production levels and decline curves are similar for all four wells (Figure 4.11). This similarity at the beginning of the well's lives indicates that in general the wells are being completed in virgin reservoir compartments. Due to the absence of pressure depletion and zone specific production data this assumption cannot be applied to

every completed interval. It does suggest, however, that despite tight well spacing the lateral extent of productive reservoir compartments is limited, and tight well spacing is required to maximize hydrocarbon recovery. If there was strong well communication you would expect an increase in the older well production levels as the new wells come in communication with the older wells producing intervals. This would provide an enhanced drainage area for the old wells. Along with a jump in the older well production you would also expect a lower level of initial production for the new wells as they intersect depleted zones. While production levels would suggest limited communication, the initial production levels are most likely dominated by the enhanced localized permeability caused by the hydraulic fractures. The production data would suggest that the hydraulic fracture networks are not intersecting, but does not necessarily indicate that the reservoir compartments are not in communication.

A recommendation for further understanding of these changes is the monitoring of pressure decline during the life of the well, zone specific pressure testing prior to the completion of the well, and production logging. This type of data would allow for the enhanced understanding of depleted intervals, well communication, and the calibration of changes in the seismic data with interval specific production and depletion.

An additional parameter that must be considered in understanding production and reservoir compartmentalization through this interval is the presence of natural and manmade hydraulic fractures. Previous work by others has provided a broad understanding of natural and induced fracture direction within Rulison Field area. Studies of core collect at the MWX site (Lorenz 2003)indicates that natural fractures are oriented in the WNW (~293 deg) direction (Lorenz 2003). While this site is approximately two miles south of the RCP survey area, it provides the only oriented core information near the field. The MWX findings also agree with work done by (Higgins 2006), who found natural fracture directions between approximately 285 and 293 degrees through the interpretation of image logs collected at Rulison Field. (Vasconcelos and Grechka 2006) also found a dominant WNW (~293 deg) fracture orientation through

work with the 2003 RCP survey at the prestack level. Additional insight was gathered about the creation of natural fracture networks through the collection of microseismic data during the hydraulic fracturing of two wells in Rulison Field (Wolhart, Odegard et al. 2005). The microseismic monitoring gave an average orientation for artificially induced fractures of 283 degrees and 286 degrees respectively for the two wells that were monitored. These data also provided insight into the lateral extent of the hyrdraulic fracturing. The strong agreement between the numerous sources of information suggests a relatively consistent maximum horizontal stress direction and fracture orientation of approximately WNW. Fractures are expected to be oriented parallel to the maximum horizontal stress, and open perpendicular to them, so that fracture orientation and maximum horizontal stress are aligned (Higgins 2006). While this information provides a generalization of the subsurface properties, localized variations cannot be established based on the sparse nature of the data. Strong localized variations in fracture networks and stress fields are expected to play a major part in determining the change in the response of the time-lapse seismic data.

Along with providing additional information on fracture orientation, the microseismic data also provided insight into the lateral extent of the subsurface affected by the hydraulic fracturing. The work by (Wolhart, Odegard et al. 2005), shows that the hydraulic fracture treatments propagate to lengths of approximately 500 to 600 feet in the ESE direction, and approximately 300 to 400 feet in the WNW direction. The width of the affected zones is approximately 300 feet. Plotting a generalized interpretation of these elliptical fracture patterns shows strong agreement with zones of change in the splitting coefficients between the Cameo and 2700 ms horizons (Figure 4.12). The elliptical drainage areas were oriented in the WNW direction with approximate extent of 300 feet to the WNW, and 500 feet to the ESE. The width of the ellipse at the widest point is 300 feet. The ellipses plotted in Figure 4.12 show strong agreement between the expected drainage areas, and changes in the splitting coefficients. The staggered drilling patterns appear to be adequately draining the subsurface, at least perpendicular to the

drainage ellipses. Amalgamation of the zones of strong difference may indicate well communication. This communication does not appear to be caused by the communication of producing zones, but may be resulting from the communication of pressure, and stress changes within the subsurface.

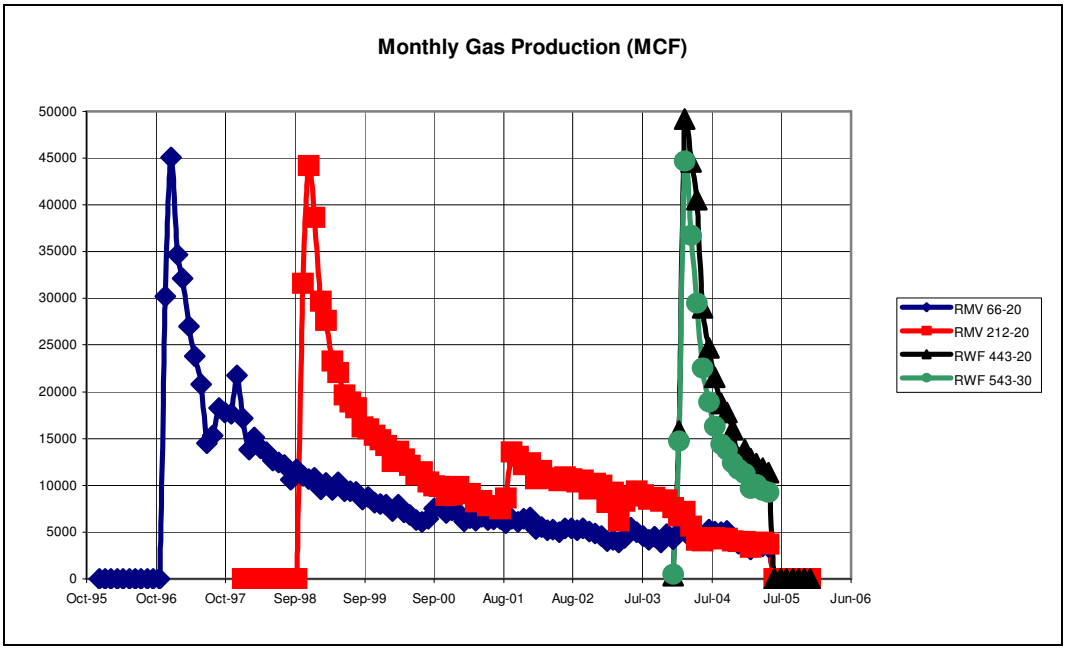

Figure 4.11 - Monthly gas production for the four wells of interest in the southwest corner of the survey.

The correlation between areas of change through this interval, and changes in region B of the UMV to Cameo interval further suggest the presence of subsurface complexities. These complexities, as mentioned earlier, could be the result of a fault trend running through the southwest corner of the survey. This would increase the complexity of localized natural fracturing, and variations in the stress field. Increased complexities may be able to account for unexpected changes in the splitting coefficient.

While the drainage patterns agree with areas of change through the central part of Figure 4.12, there are other areas where the location of wells and splitting coefficient

differences do not agree. The western part of the plot shows extensive positive differences, but only a few wells bounding the area of change. This could be explained by the presence of edge effects causing change, or more optimistically, by increased lateral connectivity in this region. Increased connectivity could result from the presence of additional fracture sets. This would allow for larger drainage patterns and areas of change from only a few productive wells. The northern part of the plot, however, shows wells with little or no change associated with them. Two of these wells were drilled in May of 1997 with individual cumulative production of approximately 70 MMCF during the time-lapse interval. The other two wells were drilled in July of 2004 with cumulative production of between 150 and 180 MMCF. The age and production levels of these wells may limit observable changes in the subsurface. On the one hand the older lower productivity wells may have stabilized so that subsurface changes during the time-lapse interval are negligible. On the other hand, the younger wells may not have had enough time for strong pressure depletion to cause observable changes away from the wellbore. Another issue that may limit the observation of change in some areas is the inability to distinguish individual zones of high production. This could suggest that the northern area has not experienced strong production from this interval, while the central and western areas have experienced strong production through this interval leading to observable differences. This is where pressure and production testing could provide insight into the presence of depleted and high productivity zones, and also provide a chance to calibrate the findings of this research.

The observation of s-wave splitting coefficient change between the 2003 and 2004 surveys for both the UMV to Cameo and Cameo to 2700 ms horizon interval indicates the ability to monitor changes in tight-gas sandstone reservoir with highly repeatable s-wave seismic surveys. While the cause of the change is not completely clear, its presence is a strong indication of drainage patterns and connectivity of the reservoir compartments. The agreement of the drainage ellipses and areas of change for the Cameo to 2700 ms horizon indicate that drilling patterns play a major role in

maximizing the efficiency of hydrocarbon recovery. The correlation with production also indicates that to most effectively observe changes in the s-wave splitting coefficients, the second or third year of production for new wells must be bounded by the time-lapse surveys. The interval between the time-lapse surveys could also be extended to two or three years to increase the observation of larger subsurface change.

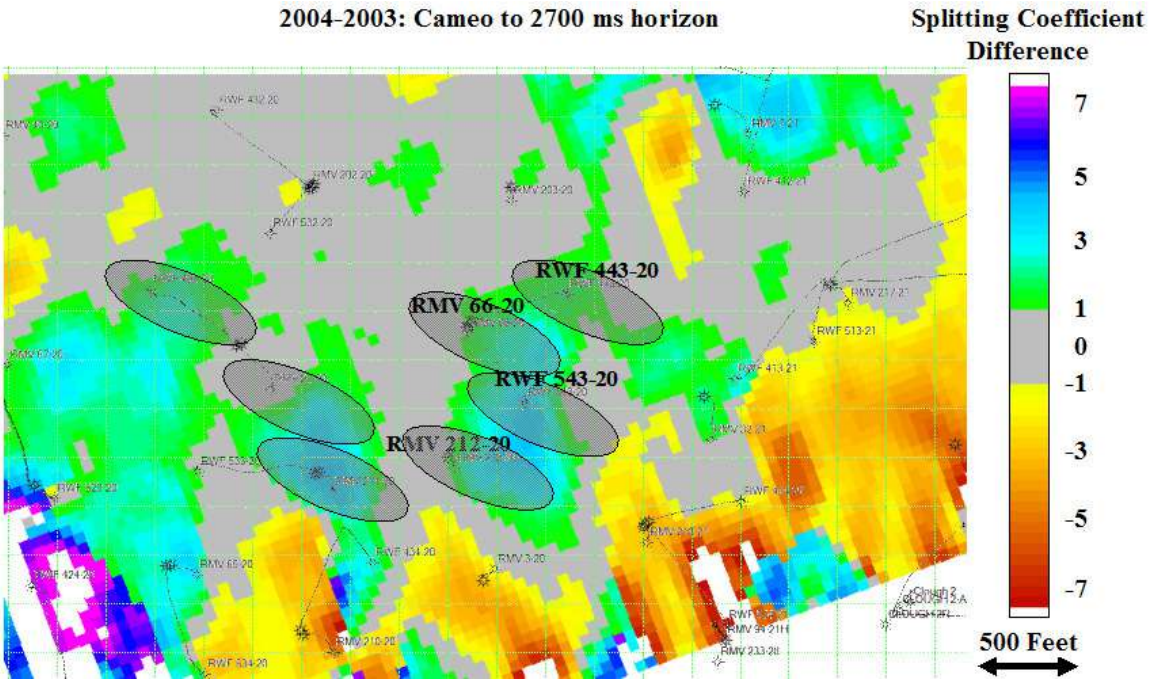

Figure 4.12 - Difference in the 2004 and 2003 shear-wave splitting coefficients calculated between the 2700 ms and Cameo horizons. Zoomed in view of the southwest corner of Figure 4.9. Anticipated drainage ellipses are also displayed.

Chapter 5 Impedance Quick Look

5.1 Introduction

Changes in the s-wave splitting coefficients provide insight into the lateral distribution of production induced reservoir changes during the time-lapse interval. While this information is important for understanding drainage patterns and productive intervals, the calculation of the splitting coefficients over large intervals limits the vertical resolution of the information. Due to the discontinuity of the upper and lower reservoir sections, and the lack of zone specific pressure and production information, only general conclusions can be drawn concerning productivity through the large vertical intervals. This implies that while production induced changes can be observed in this interval a zone specific understanding is impossible. To increase the understanding of time-lapse changes within individual zones such as perforated sand packages, the vertical resolution of the time-lapse signal must be improved. Increased resolution was achieved through the inversion of the seismic reflectivity data to shear impedance. Inverting for impedance values increases the resolution in comparison to the seismic data by enhancing the bandwidth content of the information, and providing layer specific information in comparison to interface reflectivity information (Badachhape 2002). The simplistic inversion process used in this process provided a quick and simple look at the expected impedance information of the volumes.

The inversion of the 2003 and 2004 cross-equalized fast and slow s-wave volumes was performed in Hampson-Russell's Strata 6.5 software package. The process was performed separately for the four data volumes. The bandpass filtered poststack migrated S11 and S22 data volumes were inverted from the 2003 survey, while the cross-equalized S11 and S22 volumes were inverted from the 2004 survey. The cross-equalization

procedure applied to the 2004 volumes included the application of the time-varying time-shift. The cross-equalization and time alignment are necessary so that direct comparisons can be made of impedance values for the same corresponding subsurface interval sampled by the base and monitor surveys.

A 'coloured inversion', CI, technique included in the Strata software package was used to invert the data for impedance values. 'Coloured inversion' was chosen for its simplicity, short implementation time, and strong similarity to more complex inversion schemes (Lancaster and Whitcombe 2000). An additional benefit of this technique is the use of a single convolutional inversion operator. After the calculation of the operator, it is applied as a filter to the data. This is beneficial for a time-lapse study because it provides a consistent conversion between reflectivity data and impedance information. While this is a simple technique, it provides limited understanding that can be provided by more complex and interative inversion techniques. Under the assumption that the time-lapse data has been properly cross-equalized the expectation is that the use of a single operator will limit variations in the impedance values resulting from the conversion process.

The idea behind 'coloured inversion' is the use of an operator 'whose amplitude spectrum maps the mean seismic spectrum to the mean earth AI spectrum, and has a –90 degrees phase shift' (Lancaster and Whitcombe 2000). This implies that a single conversion is calculated and applied to the entire data set. This aspect limits the robustness of the technique compared to other inversion techniques, but is balanced by the simplicity and speed of its application. The information required to create the operator is obtained from the seismic data, and the well log information from the RWF 332-21 well located in the southwest corner of the survey (Figure 5.1).

The conversion process involved two main steps. The first step was the creation of an initial low frequency impedance model. This model was created with the use of the log velocity and density information collected in the RWF 332-21 well. This well was chosen because a cross-dipole sonic log was collected in it. This log provided both fast

and slow s-wave velocities, along with p-wave velocities. Separate initial models were created for the S11 and S22 volumes.

The second step involved the conversion of the seismic data through the use of the inversion operator computed using the Strata software. Two inversion operators were used. The operators were specific to the S11 and S22 data volumes calculated with the use of the 2003 seismic data sets. All four s-wave volumes were converted separately. After the converted volumes were computed the S11 volumes were differenced, and the S22 volumes were differenced between the surveys to monitor time-lapse changes in the shear impedance.

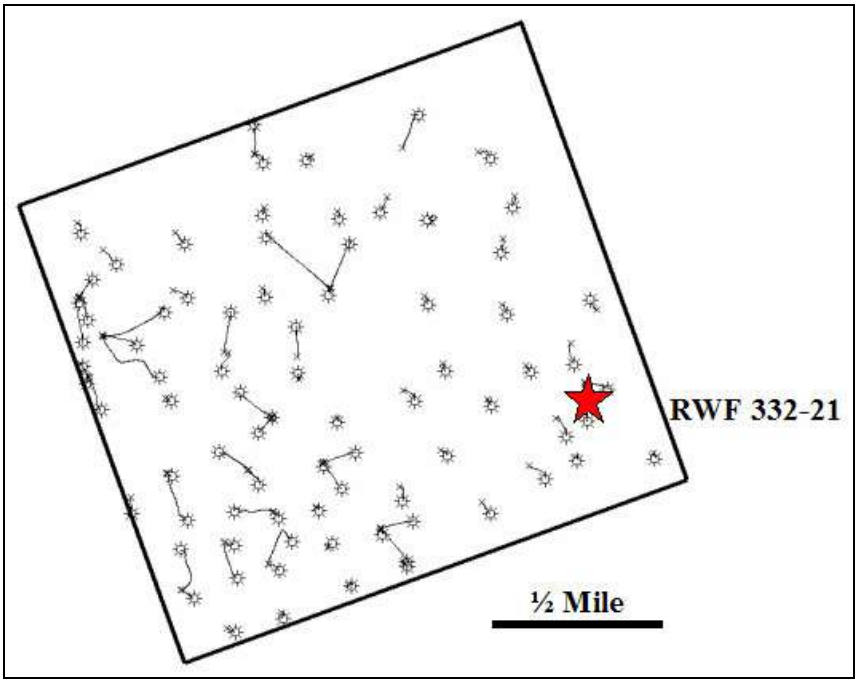

Figure 5.1 - Location of RWF 332-21 well within the RCP survey area.

5.2 Sonic Log Correction

Before computing the initial model, correlation between the seismic data and cross-dipole sonic logs was performed. Correlation is completed through a matching of events between an extracted seismogram from the surveys, and a computed synthetic seismogram from the log information. The extracted seismogram was from the area around the RWF 332-21 well, and is used to represent the 2003 data set. The computed synthetic seismogram was calculated from the density, and shear and compressional sonic logs. Correlation of the synthetic and extracted seismograms is necessary to adjust the sonic logs to provide a better representation of the subsurface velocity profile sampled by the seismic data. This can also account for unknown sonic velocities above the reservoir that were not sampled by the cross-dipole sonic log. The correlation was performed separately for the S11, S22, and p-wave 2003 volumes. The sonic logs used were the fast and slow shear slowness logs that were processed by Halliburton from the raw cross-dipole sonic log and the accompanying P-wave sonic log. The correlation was performed through a matching of corresponding strong events between the extracted and synthetic seismograms. The matched events were aligned through stretching and squeezing of the slowness logs. The adjusted log was then used to recompute the time to depth conversion.

Figure 5.2 shows the correlation between the computed synthetic seismogram and an extracted seismogram from the 2003 S11 data volume. The synthetic seismogram was computed with the bulk density and fast shear (S1) slowness log from the RWF 332-21 well, along with a wavelet that was extracted from the 2003 S11 volume. The adjustment of the sonic log was based on the alignment of the UMV, Cameo, and other strong events below and around the Cameo event. The adjustments to the sonic log resulted in a correlation coefficient between the synthetic and extracted seismograms of approximately 0.61. The correlation coefficient was calculated between 1825 and 2675 ms, which is representative of the reservoir interval. A relatively low correlation coefficient is

expected due to discontinuous low amplitude nature of the UMV to Cameo interval, where the log derived synthetic seismogram may not be highly comparable to the extracted seismogram. The low value can also be attributed to imperfect wavelet calculation, errors in the log values, and velocity differences resulting from the different frequency content of the log and seismic measurements. Since the low energy interval between the UMV and Cameo events does not allow for the strong correlation of the synthetic and extracted events it is assumed that the alignment of the UMV and Cameo events also correctly aligns the events between them.

Figure 5.3 shows the correlation between the computed synthetic seismogram, and the extracted seismogram from the 2003 S22 data volume. The synthetic seismogram for this correlation was computed using the bulk density and slow shear (S2) slowness from the RWF 332-21 well. The wavelet used was extracted from the 2003 S22 data volume. The achieved correlation coefficient between the synthetic and extracted seismogram is approximately 0.58, and was calculated between 1825 and 2675 ms. Similar to the S11 data, the correlation of the seismograms was based on the alignment of the UMV, Cameo, and other strong events below and around the Cameo event. Alignment of the discontinuous interval between the UMV and Cameo events is also assumed to be correct based on the end event alignment. A low value for the correlation coefficient is attributed to the same issues that were mentioned for the S11 correlation.

The p-wave sonic log was also corrected in the same fashion as the shear sonic logs. The computed synthetic seismogram was compared to an extracted seismogram from the 2003 poststack migrated p-wave data volume. The wavelet used to calculate the seismogram was also extracted from the 2003 p-wave volume. The correlation coefficient between the seismograms reached a maximum of 0.6, similar to the values for the S11 and S22 data.

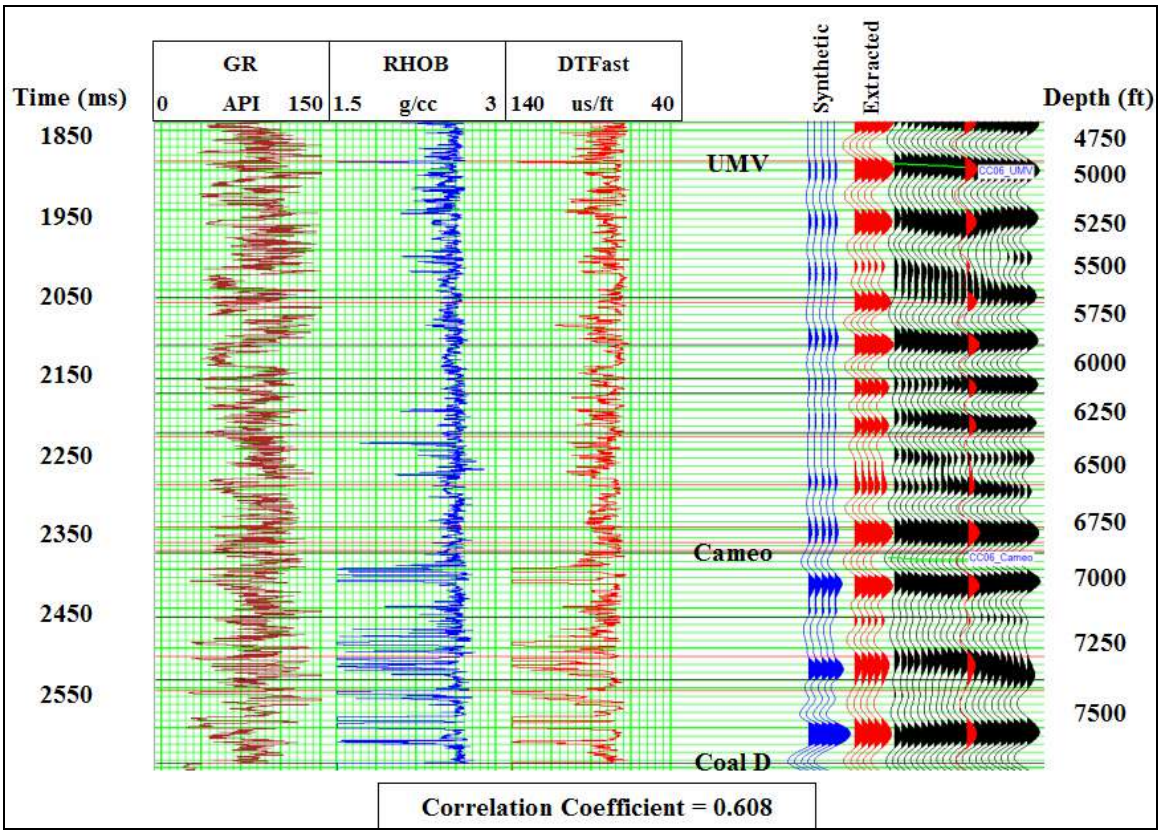

Figure 5.2 - Correlation between the computed synthetic and extracted seismograms from the 2003 S11 data volume after the alignment of corresponding strong events. Gamma ray, bulk density, and S1 slowness are also plotted.

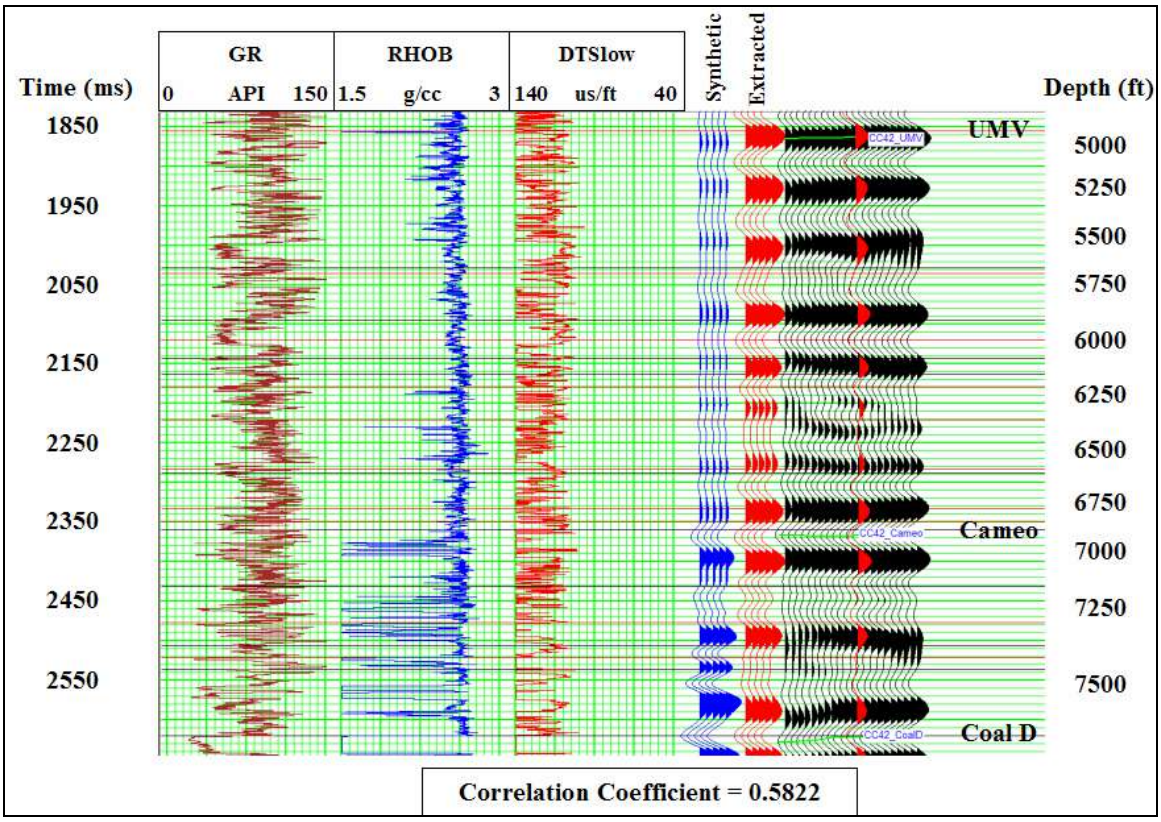

Figure 5.3 - Correlation between the computed synthetic and extracted seismograms from the 2003 S22 data volume after the alignment of corresponding strong events. Gamma ray, bulk density, and S2 slowness are also plotted.

5.3 Quick Look Inversion Process

After correcting the s- and p-wave sonic logs the initial s-impedance model was built. This was a low frequency model that was based off the bulk density and sonic logs. The high pass frequency for the model was chosen to be 10 Hz, with the high cut frequency chosen to be 15 Hz. These are default values used by the Strata software. Separate models were built for both the S11 and S22 data volumes. Each model was used in the inversion of its respective type of 2003 and 2004 seismic data. The output sample rate for the inverted volumes was the same as the seismic data at 2 ms.

The 2003 and 2004 data volumes were inverted using the full spectrum approach available in Strata. This inversion design contains both the low and high frequency information. The inversion operators used were separate for the S11 and S22 inversions. These operators were calculated from the information provided by the RWF 332-21 well, and the 2003 s-wave seismic volumes. The goal of these operators is to map the seismic spectrum of the reflectivity data to the earth's impedance spectrum. Along with spectrum matching the operator also has a –90 degrees phase shift (Lancaster and Whitcombe 2000). Figure 5.4 shows the S11 and S22 inversion operators that were used during the CI process.

After the conversion of the seismic volumes the percent change in impedance was calculated between the years. The percent change was calculated by differencing the 2004 and 2003 volumes and dividing by the 2003 impedance volumes Equation 5.1.

Equation 5.1

$$\frac{(Z_{2004} - Z_{2003})}{Z_{2003}} * 100$$

Z represents the impedance value, or density multiplied by velocity, and the subscript represents values from the 2003 or 2004 surveys. The resulting values illustrate the change in impedance that occurred between the base and monitor surveys. The distribution and location of these changes can indicate areas that have experienced observable production related change.

Before an investigation of the changes was performed, the percent difference impedance volumes were converted to depth. This was done to provide a deeper understanding of the structural nature of the reservoir, and to allow for a direct comparison of changes in the S11 and S22 volumes, along with a stronger tie to well paths, formation tops, and perforation information.

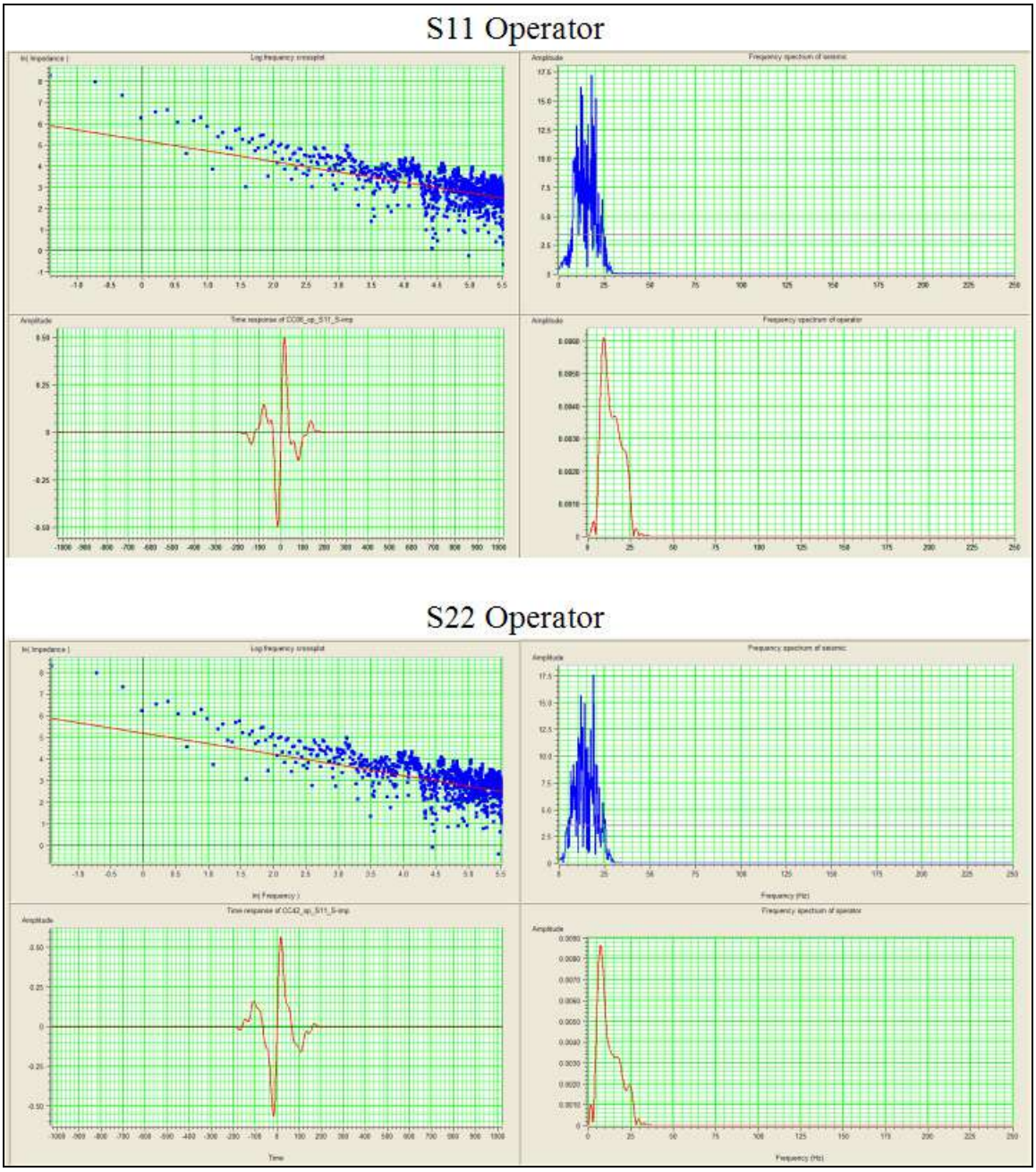

Figure 5.4 - S11 and S22 inversion operators. Bottom left plot in the upper and lower panels is the time response of the operator, and the bottom right plot is the frequency spectrum of the operator.

The time to depth conversion was performed using the velocity model that was calculated during the creation of the initial impedance model. The velocity model was developed through the use of the well log velocity information from the RWF 332-21 well. Additionally the conversion was further constrained by the tying of the picked UMV horizon in time with the UMV surface in depth. The UMV surface in depth was computed using the UMV formation picks from the wells drilled in Rulison Field. In addition to converting the volumes, the UMV and Cameo horizons were also converted to depth. This was done separately for the S11 and S22 horizons picked in the 2003 volumes. It was completed in a similar fashion to the volume conversion using the velocity model created with the initial impedance model.

Figure 5.5 and Figure 5.6 are examples of the percent impedance difference for the S11 and S22 data volumes after being converted to depth. The main feature to notice in these figures is the low level of change in the impedance values. Values from -1.5% to 1.5% are considered the background level of change, and are masked out to improve the observation of larger change values. In both the S11 and S22 sections, the zone surrounding the UMV horizon exhibits minimal change. This is expected due to the fact that no production occurred at this level, and because this interval was used to guide the cross-equalization process. It is also evident that not much change is present around the Cameo horizon. The main difference between the S11 and S22 difference sections is the presence of larger values of change in the S22 data. This is expected with the anticipation that the S22 data is going to be more sensitive to production related changes. Another characteristic of the difference sections is the presence of both positive and negative change occurring in the same zone. These changes are the result of side lobes due to the band limited nature of the inversion process.

The largest levels of change occur in three areas. The first area is the interval above the UMV, especially above a depth of approximately 3,500 feet. This interval, in general, exhibits strong variations in amplitude and seismic character in the original reflectivity data. Due to these large variations the equalization process was unable to

fully eliminate differences in this shallower static section. The main reason for these variations could be the result of higher noise levels in the lower fold interval. The impedance difference values in this region illustrate the preservation of changes through this section after the cross-equalization process.

The second interval exhibiting large changes in both the S11 and S22 data volumes falls between the UMV and Cameo horizons. There can be two main causes for this change. The first cause is related to the application of the time-varying time-shift. Due to the low energy nature of this interval the cross correlation time-shift was unable to calculate reliable time-shifts. By limiting the application of the time-shifts in the last stage of the cross-equalization process to shifts with correlation values of greater than 0.8, small necessary time-shifts may not have been applied. This could result in the observed variations being caused by small time-shifts between the surveys, compared to actual changes in the impedance values. This aspect of change can be evaluated by comparing the calculated time-shifts and correlation values with impedance change values through zones of interest. The second cause for large differences through this interval is related to the production of gas. Evaluating the reliability of these changes will involve a comparison of impedance change, the time-varying time-shifts applied, and the correlation coefficient values associated with those time-shifts.

The third area occurs below the Cameo level. This area includes the more continuous coal layers. This zone is penetrated by several wells, and is believed to be productive from both the completed sand and coal intervals.

The low level of background change is an indication of the data's high repeatability, the value and potential of dedicated time-lapse surveys. It also indicates the strength of the cross-equalization process in minimizing differences in the surveys. Limiting differences between the surveys increases the chances of observing production related changes, and indicates the value of this tool for monitoring production in unconventional tight gas reservoirs.

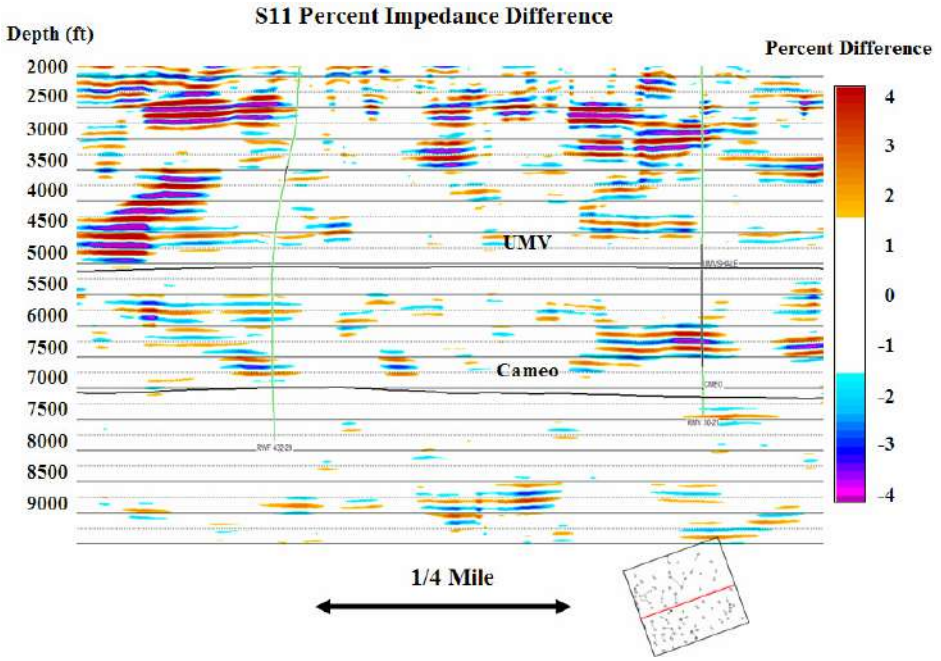

Figure 5.5 - Crossline 76 of the S11 percent impedance difference between the 2003 and 2004 surveys. The section was converted to depth.

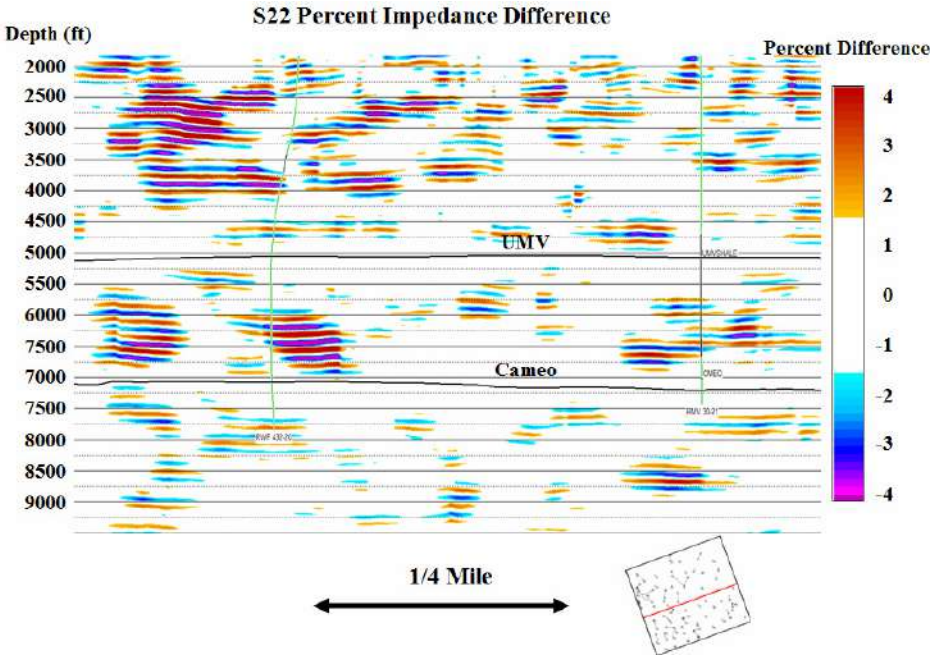

Figure 5.6 - Crossline 76 of the S22 percent impedance difference between the 2003 and 2004 surveys. The section was converted to depth.

5.4 Time-Lapse Changes

Now that areas of impedance change can be observed, the key is to identify areas of strong change, and evaluate their reliability and relation to production. To identify areas of larger change the root-mean-square (RMS) of the percent impedance difference values were calculated between the UMV and Cameo horizons. This provides an indication of the lateral distribution of larger change. The RMS difference values for both the S11 and S22 intervals between the horizons exhibit similar change (Figure 5.7). The southwest corner exhibits zones of increased difference in both data types. The central and eastern region of both surveys, however, exhibit lower levels of difference values. After identifying these two general regions of change a comparison was made with the distribution of the cumulative gas production that occurred between the two surveys (Figure 5.8).

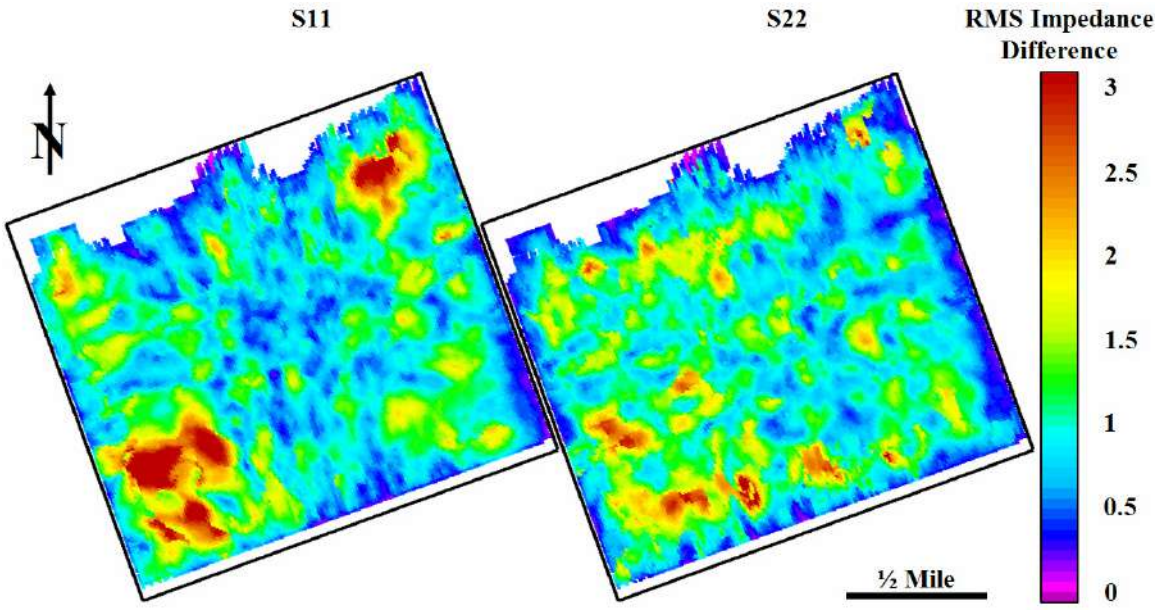

Figure 5.7 - RMS value of the percent impedance difference values between the UMV and Cameo horizons.

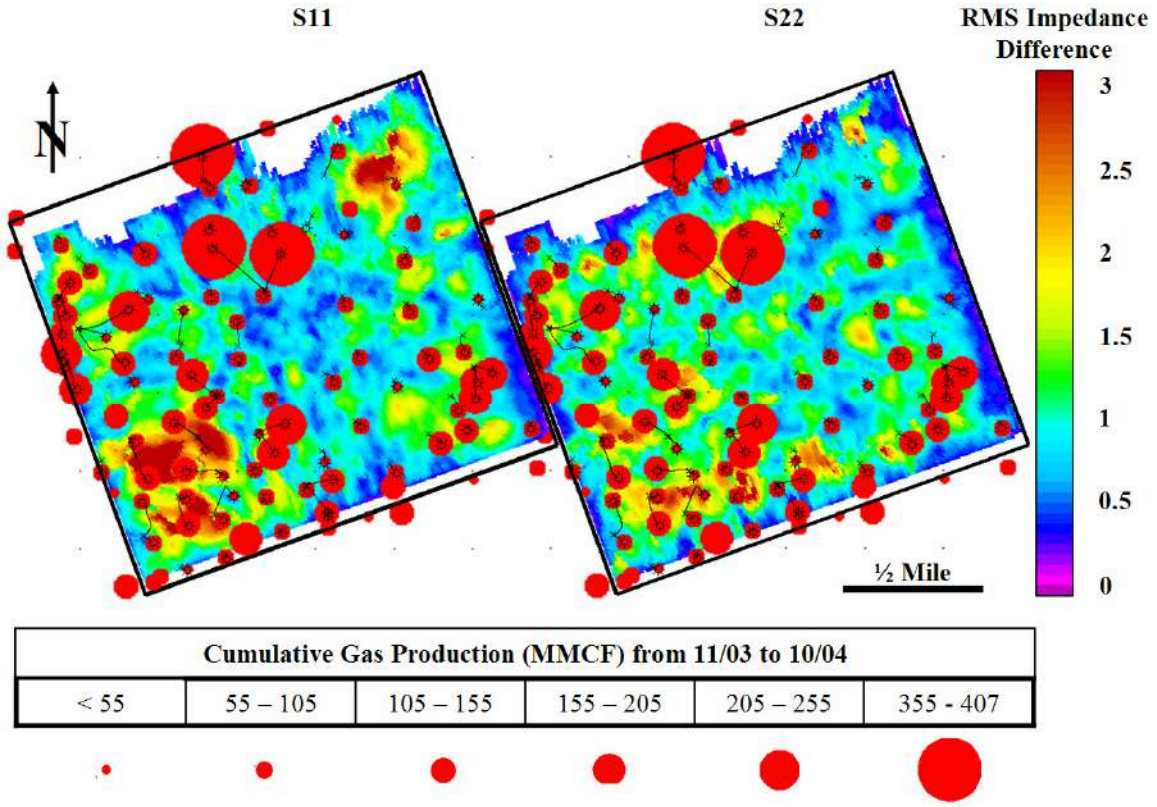

Figure 5.8 - RMS values of the percent impedance difference values between the UMV and Cameo horizons. Overlain is the cumulative gas production for each well between the two surveys.

On the one hand, the distribution of production indicates that the southwest corner of the survey area contains wells with higher cumulative production values. The central region, on the other hand, contains wells that generally have much lower cumulative production numbers. There are five higher productivity wells located in the north central region and the southeast corner, but in general the central area exhibits lower production numbers. This correlation of production and time-lapse difference is similar to the correlation established with changes in the shear-wave splitting coefficients between the surveys. The area of large continuous change values in the southwest corner of the S11 data slice can be attributed to time-shifts between the two surveys that were not completely eliminated during the time-varying time-shift. This was a result of limiting

the maximum time-shift that was permitted. While the calculation of the RMS difference through this interval is an indication of the lateral extent of changes in the impedance values, it is similar to the shear-wave splitting coefficient analysis in that it is only providing an average over the entire interval. Understanding individual zones of change requires looking at vertical sections of the percent impedance difference data volume.

Figure 5.5 and Figure 5.6 illustrate the vertical distribution of change running approximately east-west along crossline 76. Comparing this distribution with the correlation coefficient values calculated during the calculation of the time-varying time-shift shows a strong connection between low correlation values and areas of larger impedance difference (Figure 5.9 and Figure 5.10). This strong correlation is consistent for both the S11 and S22 data, and throughout the data sets. This relationship implies two possible scenarios. The first scenario suggests that changes in the impedance values are a result of the incorrect calculation and application of the time-varying time-shift from the UMV down. This could be the result of the size chosen for the correlation window, and the more discontinuous and low energy nature of this interval.

The second scenario suggests that the changes observed are the result of production induced variations in the seismic data. The correlation between the low correlation values and zones of impedance change could actually be illustrating the same aspect of the data. The presence of low values throughout the data set, and the isolated nature of zones of larger change suggest that the time-varying time-shift was correctly calculated and applied in the final stage of cross-equalization. This indicates that the observed changes in the impedance values and low correlation values are not related to the presence of time-shifts between the surveys, but are actually illustrating the presence of changes in the seismic character within these zones. The strong correlation values and low impedance difference values near the UMV horizon, and at and below the Cameo support this interpretation by indicating strong repeatability and low noise levels at this interval. The consistency at these levels suggests that the data between the UMV and Cameo horizons should also be highly repeatable and contain low noise levels.

Another interesting aspect of the crossline 76 sections is the location of change within the sections. The location of two wells through this section corresponds to the two main zones of large impedance value differences. This is in comparison to relatively little change through the rest of the interval. The zones of change are also consistent between the S11 and S22 data volumes, indicating further consistency in the data.

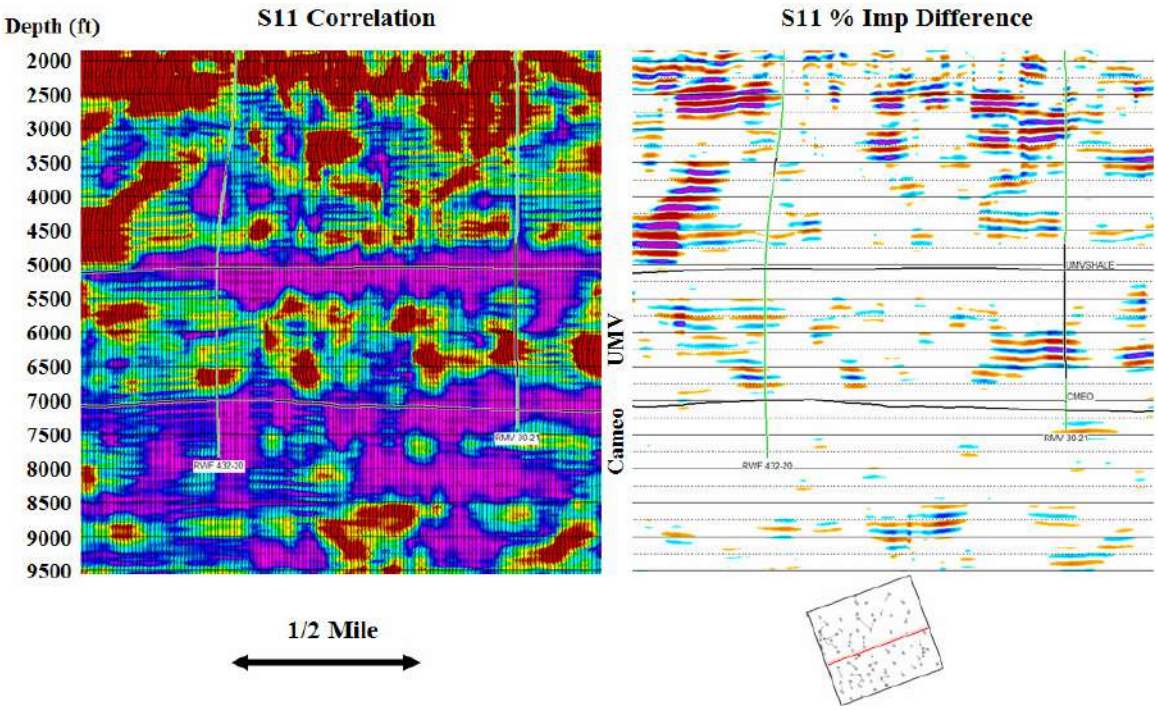

Figure 5.9 - Crossline 76 of the S11 data. Left panel is correlation coefficients calculated during the calculation of the time-varying time-shift. Right panel is the percent impedance difference. Red values are low correlation and purple values are high correlation. The color bar for the impedance difference is the same as in Figure 5.5.

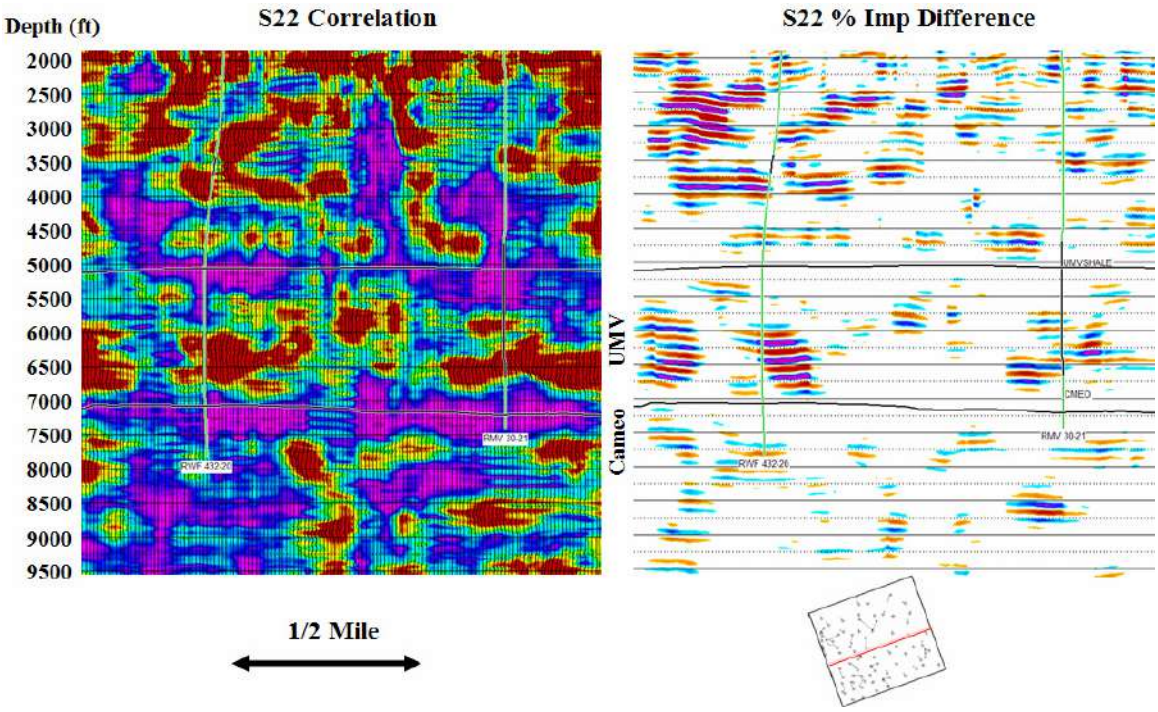

Figure 5.10 - Crossline 76 of the S22 data. Left panel is correlation coefficients calculated during the calculation of the time-varying time-shift. Right panel is the percent impedance difference. Red values are low correlation and purple values are high correlation. The color bar for the impedance difference is the same as in Figure 5.5.

Comparing changes in the impedance values with perforations in well RMV 31-20 illustrates a strong connection between perforated zones and zones of change. The interval from 5,800 to 6,800 feet shows levels of strong difference (Figure 5.11). This zone also contains 10 perforated sandstone packages. The RMV 31-20 well was a middle of the road producer with cumulative production between the surveys of 71.2 MMCF. The well was completed in February of 1999. The consistency of change in both the S11 and S22 data, and the surrounding low levels of change increase the validity of the observations. The strong agreement with the upper perforations is also encouraging.

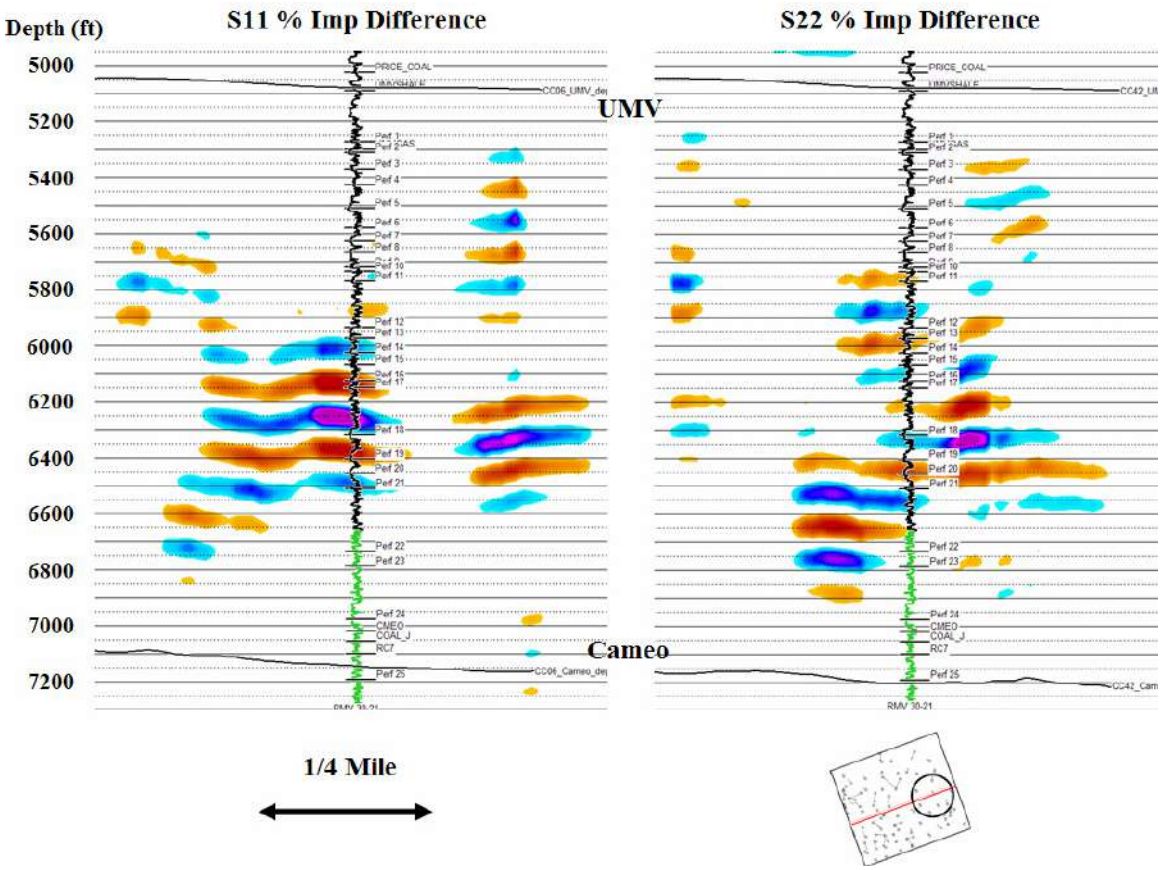

Figure 5.11 - Close-up of S11 and S22 percent impedance change around well RMV 31-20. Gamma ray log and well perforations are also displayed.

The vertical extent of change over approximately 1,000 feet of the subsurface could indicate two things. The first is that there is increased vertical connectivity at this level in the reservoir. This connectivity would result in enhanced communication and a larger zone of drainage and depletion. Calibrating this assumption would require zone specific production and pressure information to understand the productivity and connectivity of the perforated sandstones. Increased connectivity could be the result of enhanced natural fracturing or the stacking of several sandstone packages. It could also be caused by the hydraulic fracturing of the well during the completion stages. This may create a pathway between natural fracture networks, or individual sands. Further understanding of this would require the collection of microseismic data during the

fracturing of the well. The second characteristic that the impedance change may be indicating is that while there may not be strong connectivity between the perforated sandstone packages, the subsurface may be experiencing pressure or stress communication through the interval.

While both the S11 and S22 impedance information show similar change through the upper reservoir interval, the S22 data also shows change within the lower reservoir interval below the Cameo horizon (Figure 5.10). These areas of change also correspond with the presence of well locations. The extent of this change is also indicative of zones with increased connectivity at depth. The presence of change below the extent of the well suggests that there is communication between perforated zones in the well and deeper intervals. This illustrates that there is not only gas production from completed intervals, but also from deeper intervals that may be connected through fault trends or enhanced natural fracturing.

The presence of change in the subsurface is limited to productive intervals between the two surveys. Strong depletion of intervals prior to the base survey would not allow for the monitoring of production related change in these zones. Multiple repeat surveys would be necessary throughout the life of a well to understand the depletion of all the individual productive zones. These additional data, along with zone specific production and pressure data throughout the life of the well would also help to understand individual zones of productivity and depletion during the wells productive life. This leads to the need for real time monitoring of the field to fully characterize and maximize recoverable gas.

There are a few suggestions for improving the inversion process and the understanding of the information provided by it. The first suggestion would be to test and compare other inversion techniques to monitor consistency in the presence of changes. The application of the quick look inversion provided a quick and simple understanding of impedance changes. While this was important, a more thorough inversion process is essential to fully quantify the observed time-lapse impedance

changes. A second suggestion would be refining the correction of the well logs and the time to depth conversion. The final suggestion for understanding changes in the data would be to view and compare time-lapse changes with well information in a three dimensional visualization environment. This would allow for a deeper understanding of the distribution of change throughout the field, and its relationship to the wells.

Chapter 6 Conclusions

6.1 Conclusions

The first use of dedicated shear wave time-lapse seismic surveys has illustrated the potential for monitoring gas production from an unconventional tight gas sandstone reservoir at Rulison Field. The observation of time-lapse changes in both shear-wave splitting coefficients and shear impedance values has allowed for an increased understanding of productive zones and depletion during the time-lapse interval. This type of understanding is essential in creating a thorough characterization of the reservoir, and an ability to maximize recoverable hydrocarbons and recovery efficiency.

The cross-equalization of the 2003 and 2004 seismic surveys provided highly repeatable data that allowed for the monitoring of small time-lapse variations. The strength of the repeatability after this process illustrates the quality of the surveys, the processing, and the cross-equalization procedure. By cross-equalizing the surveys, random variations not related to production were minimized between the surveys. This was necessary to control slight variations that may have been introduced by small differences in survey geometry, acquisition, noise levels, and source characteristics. The cross-equalization of both the fast and slow shear wave data volumes of the surveys is one of the first applications of this type of procedure with this type of data. The quality of the data and the equalization process is an indication of the potential resource that shear wave data provides, and its ability to monitor production from complex and challenging reservoir settings.

The first attribute that was used to monitor changes through the reservoir interval was the variation of shear-wave splitting coefficients between the surveys. The joint use of both the fast and slow shear wave information was able to provide a robust measure of change through the reservoir. Changes in the shear wave data were also enhanced by the

presence of fractures in the reservoir. Time-lapse changes in the splitting coefficients can be broken up into two categories. The categories are based on the polarity of the change.

The upper reservoir section between the UMV and Cameo horizons contains both increases and decreases in the splitting coefficient (Figure 4.6). The central region of the survey is mainly dominated by the presence of increases in the splitting coefficient. Increases in the splitting values do not follow the initial assumption of decreasing the density of a single fracture set with pressure depletion, and illustrate the presence of strong complexities in the reservoir interval. While the change observed through this region is not consistent with the initial assumptions, the localized nature and the low background level of change illustrate an ability to monitor changes resulting from gas production. These changes also exhibit a north-northwest trend that may be indicative of enhanced natural fracturing or localized variations in stress due to the presence of faulting. Another aspect of this region is the low production levels during the time-lapse interval. Low production numbers and minimal amounts of time-lapse change validate the consistency in the data, and the presence of the anomalies.

The southwest corner of the upper reservoir interval also exhibits strong areas of change. This change is observed as a decrease in the splitting coefficient. The lateral consistency of the change is important in validating it presence. The dense well spacing and high production levels during the time-lapse interval illustrate enhanced connectivity in this region. Communication could be in the form of enhanced natural and artificial fracture networks that are connecting wells, or a more regionally consistent change in pressure and stress fields due to the large number of producing wells. The extent of the change would indicate that the dense well spacing is working to, on average, effectively drain the reservoir. The presence of a fault running through this region also indicates the structural component of the reservoir that provides enhanced productivity and time-lapse change resulting from an increased fracture presence.

The lower reservoir interval between the Cameo and the 2700 ms horizon also exhibits areas of changes (Figure 4.12). Change through this interval is dominated by the

presence of increases in the splitting coefficient. There are also decreases present, but they are located near the edge of the surveys where edge effects limited confident picking of the 2700 ms horizon. These areas of change correspond to the location of wells in the area. The size and orientation of the anomalies also corresponds to the expected orientation and general size of the drainage ellipses calculated from microseismic information (Wolhart, Odegard et al. 2005). The alignment of the well location and expected drainage patterns indicates that through this interval the shear wave data is able to monitor production related changes through time-lapse variations in the splitting coefficients. This also indicates the potential for accessing bypassed pay zones below the Cameo horizon. Areas of limited change would be indicative of these zones. One concern with this assumption is the fact that the time-lapse surveys only monitored a year of production. This would not allow for the monitoring of depletion that may have occurred prior to the initial survey. Multiple surveys during the life of the wells would increase the ability to monitor the areas of depletion, and allow for a more confident identification of depleted intervals.

The second type of analysis that was used to monitor time-lapse changes was a comparison of shear impedance values from the base to monitor surveys. Differences were monitored in both the S11 and S22 data types. Slightly larger changes were observed in the S22 data, but the location and distribution of change was consistent between both the S11 and S22 data types (Figure 5.5 and Figure 5.6). This analysis provided a higher resolution understanding of changes through the reservoir interval. Low values of change at the UMV and Cameo levels illustrate high repeatability between the surveys. Change between the UMV and Cameo levels at crossline 76 of the survey correspond to perforated zones in the upper reservoir interval (Figure 5.11). These large changes compared to the relatively low background changes through the rest of the interval are a good indication of production monitoring. The extent of the anomalies also indicates significant connectivity through this interval. Connectivity could come in the form of enhanced fracture networks, or the communication of pressure and stress fields

through the interval. Similar to the observation of change in the splitting coefficient, this tool can provide information on bypassed pay. As mentioned previously the limited time-frame between surveys would not be able to monitor previously depleted zones. This may result in previously depleted zones exhibiting little or no change that could be interpreted as bypassed pay. A way to mitigate this situation is the collection of multiple surveys over the life of the wells, along with the collection of pressure and production information in the wells.

Below the Cameo horizon the presence of change is stronger in the S22 impedance data (Figure 5.6). These areas of change occur near and below the bottom of the well. The observation of change below the well locations indicates the sourcing of gas from deeper in the section. This is attributed to the presence of enhanced fracturing that could be the result of faulting through the interval. It also suggests that well should be tested deeper into the marine sands and shales of Iles Formation.

The observed changes in both the shear-wave splitting coefficients and the impedance values, illustrates the need for shear-wave time-lapse analysis. These changes have an enhanced presence over those observed in the time-lapse p-wave study performed on the same data set. The more extensive distribution of change in the s-waves data over the same time interval, illustrates the robust nature of s-waves in this reservoir setting. The fact that shear waves are strongly sensitive to variations in fracture density and stress fields is an important reason for their use in this setting. The limited change observed in the p-wave time-lapse study illustrates that traditional seismic surveys are not adequate for observing production related changes in this reservoir setting. The economic benefit of avoiding drilling into and completing depleted reservoir intervals is quickly evident.

The main conclusion of this work is that the application of dedicated time-lapse shear wave seismic surveys is a valid approach for monitoring production in a tight gas sandstone reservoir. The highly repeatable nature of the dedicated surveys and the strength of the cross-equalization process allow for the robust monitoring of gas

production and pressure depletion. This illustrates the potential and importance of both shear wave data and time-lapse studies in this reservoir setting.

6.2 Recommendations

Recommendations for additional analysis of this type include the collection of additional data to calibrate the findings of this works, and the use of additional tools to analyze the data. Zone specific pressure and production information would provide additional insight into the reservoir characteristics. This type of information collected both at the beginning and throughout a wells life would help to establish the location of highly productive intervals and depleted zones. This would allow for the calibration of changes in the seismic data with known areas and periods of depletions and productivity. The collection of additional surveys would also allow for an understanding of change throughout the wells life, and could provide a link between pressure and production information and time-lapse anomalies. Microseismic surveys throughout the field could also help to establish subsurface variations and the extent of hydraulic fracturing.

Monitoring different aspects of the shear wave data could also provide insight into time-lapse changes. This should include a prestack analysis of the data, along with both a lateral and vertical analysis of changes in the polarization angles. Monitoring polarization variations both within the individual surveys and in a time-lapse sense could provide a deeper understanding of the complexity of change and its cause. Different cross-equalization and inversion techniques should also be tested to further verify the observed changes. An extensive three dimensional visualization approach to locating the extent of the changes is also necessary to fully understand the distribution of change within the reservoir. An in depth analysis of the deep seated fault systems and its upward presence through the reservoir interval could also provide insight into localized variations in fracture density and stress fields.

A final tool that is necessary to fully understand observed time-lapse changes is the modeling of the reservoir rocks response to the removal of gas and pressure depletion. This should include the integration of both well log information and lab tests of core samples.

REFERENCES CITED

Alford, R. M. (1986). Shear data in the presence of azimuthal anisotopry. Presented at the 56th Annual SEG Meeting. Houston.

Angerer, E., S. Crampin, et al. (2000). "Changes in Shear-wave Anisotropy in Time-lapse Data: a Case Study." EAGE 2000 Expanded Abstract.

Badachhape, A. R. (2002). Acoustic Impedance Inversion Results Used to Detect Shallow Gas Hazards and Geopressured Zones. Geopressure: Conceptual Advances, Applications, and Future Challenges, SEG/EAGE Summer Research Workshop.

Benson, R. D. and T. L. Davis (2000). "Time-Lapse Seismic Monitoring and Dynamic Reservoir Characterization, Central Vauum Unit, Lea County, New Mexico." SPE Reservoir Evaluation and Engineering **3**(1): 9.

Boyd-Gorst, J., P. Fail, et al. (2001). "4-D time lapse reservoir monitoring of Nelson Field, Central North Sea: Successful use of an integrated rock physics model to predict and track reservoir production." The Leading Edge **20**: 14.

Burke, L. (2005). Reservoir Characterization Project Spring 2005 Sponsor Meeting. Colorado School of Mines.

Calvert, R. (2005). Insight and Methods for 4D Reservoir Monitoring and Characterization, Society of Exploration Geophysicists.

Cole, R. D. and S. P. Cumella (2005). "Sand-Body Architecture in the Lower Wiliiams Fork Formation (Upper Cretaceous), Coal Canyon, Colorado, with Comparison to the Piceance Basin Subsurface." The Mountain Geologist **42**(3): 23.

Colorado Interstate Gas. (2006). "Piceance Basin Expansion Project." Retrieved 7/10/2006, 2006, from www.cigco.com/piceance.asp.

Colorado Oil and Gas Conservation Commission. (2006). "COGIS - Production Data Inquiry, Rulison Field (2003, 2004, 2005)." Retrieved 7/10/2006, 2006, from http://oil-gas.state.co.us.

Crampin, S. (1981). "A review of wave motion in anisotropic and cracked elastic media." Wave Motion **3**: 27.

Crampin, S. and Y. Gau (2005). "Comment on "Systematic Analysis of Shear-Wave Splitting in the Aftershock Zone of the 1999 Chi-Chi, Taiwan, Earthquake: Shallow Crustal Anisotropy and Lack of Precursory Changes, by Yungfeng Liu, Ta-Liang Teng, and Yehuda Ben-Zion"." Bulletin of the Seismological Society of America **95**(1): 7.

Cumella, S. P. and D. B. Ostby (2003). Geology of Basin-Center Gas Accumulation, Piceance Basin, Colorado. Piceance Basin 2003 Guidebook. T. M. O. Kristime M. Peterson, Donna S. Anderson. Denver, The Rocky Mountain Association of Geologists**:** 57.

Davis, T. L., M. J. Terrell, et al. (2003). "Multicomponent seismic characterization and monitoring of the $C0_2$ flood at Weyburn Field, Saskatchewan." The Leading Edge: 11.

Eberhart-Phillips, D., D.-H. Han, et al. (1989). "Empirical relationships among seismic velocity, effective pressure, porosity, and clay content in sandstone." Geophysics **54**(1): 8.

Eiken, O., I. Brevik, et al. (2000). "Seismic monitoring of CO_2 injected into a marine acquifer." SEG 2000 Expanded Abstract.

Gouveia, W. P., D. H. Johnston, et al. (2004). "Jotun 4D: Characterization of fluid contact movement from time-lapse seismic and production logging tool data." The Leading Edge: 7.

Greaves, R. J. and T. J. Fulp (1987). "Three-dimensional seismic monitoring of an enhanced oil recovery process." Geophysics **52**(9): 13.

Hampson-Russell (2006). PRO4D Menu.

Hampson-Russell (2006). Shaping Filter

Hampson-Russell Software Services (2006). PRO4D 2.2.

Higgins, S. (2006). Geomechanical modeling as a reservoir characterizing tool at Rulison field, Piceance Basin, Colorado. Geophysics. Golden, Colorado School of Mines. **M.S.**

Hoffman, R., X. Xu, et al. (2005). "Effective Pressure or what is the effect of pressure?" The Leading Edge: 4.

Input/Output (2005). System Four Brochure. Stafford, TX, Input/Output.

Jansen, K. J. (2005). Seismic investigation of wrench faulting and fracturing at Rulison Field, Colorado. Geophysics. Golden, Colorado School of Mines. **Master of Science**.

Johnson, R. C. (1989). "Geologic history and hydrocarbon potential of Late Cretaceous-Age, low permeability reservoirs, Piceance Basin, western Colorado." USGS Bulletin **1787-E**.

Johnston, D. H. (2006). RCP Equalization. M. Rumon. Golden.

Keighley, D. (2006). P-wave time-lapse seismic data interpretation at Rulison field, Piceance Basin, Colorado. Geophysics. Golden, Colorado School of Mines. **M.S.**

Kragh, E. and P. Christie (2002). "Seismic repeatability, normalized rms, and predictability." The Leading Edge(July): 7.

Krohn, C. E. (1984). "Geophone ground coupling." Geophysics **49**: 9.

Kusuma, M. (2005). Analysis of time-lapse P-wave seismic data from Rulison Field, Colorado. Geophysics. Golden, Colorado School of Mines. **M.S.**

Kuuskra, V. A. and J. Ammer (2004). "Tight Gas Sands Development - How to Dramatically Improve Recovery Efficiency." GasTIPS **10**(1): 5.

Lancaster, S. and D. Whitcombe (2000). "Fast-track 'coloured' inversion." SEG 2000 Expanded Abstract.

Law, B. E. and J. B. Curtis (2002). "Introduction to unconventional petroleum systems." AAPG Bulletin **86**: 2.

Lorenz, J. C. (2003). Fracture Systems in the Piceance Basin: Overview and Comparison with Fractures in the San Juan and Green River Basins. Piceance Basin 2003 Guidebook. T. M. O. Kristime M. Peterson, Donna S. Anderson. Denver, Rocky Mountain Association of Geologists**:** 20.

Lumley, D. E. (2001). "Time-lapse seismic reservoir monitoring." Geophysics **66**: 3.

Lynn, H. and L. A. Thomsen (1986). Reflection Shear-Wave Data along the Principal Axes of Azimuthal Anisotropy. 1986 SEG Expanded Abstract. Houston.

MacBeth, C., J. Stammeijer, et al. (2006). "Seismic monitoring of pressure depletion evaluated for a United Kingdom continental-shelf gas reservoir." Geophysical Prospecting **54**: 18.

Mattocks, B. (2004). Rulison 3D-VSP Polarization Analysis. Reservoir Characterization Project Fall 2004 Sponsor Meeting, Colorado School of Mines.

Meunier, J., F. Huguet, et al. (2000). Expanded Abstract: Reservoir Monitoring using Permanent Sources and Vertical Receiver Antennae. 2000 Society of Exploration Geophysics Annual Meeting, Society of Exploration Geophysicists.

NaturalGas.org. (2004). "Resources." U.S. Natural Gas Resource Estimates Retrieved 7/10/2006, 2006, from www.naturalgas.org/overview/resources.asp.

Nelson, P. H. (2003). A Review of the Multiwell Experiment, Williams Fork and Iles Formations, Garfield County, Colorado. Petroleum Systems and Geologic Assessment of Oil and Gas in the Uinta-Piceance Province, Utah and Colorado. USGS Uinta-Piceance Assessment Team. Denver, USGS**:** 23.

Rickett, J. E. and D. E. Lumley (2001). "Cross-equalization data processing for time-lapse seismic reservoir monitoring: A case study from the Gulf of Mexico." Geophysics **66**(4): 10.

Rojas, E. (2005). Elastic rock properties of tight gas sandstones for reservoir characterization at Rulison Field, Colorado. Geophysics. Golden, Colorado School of Mines. **M.S.**

Ross, C. P. and M. S. Altan (1997). "Time-lapse seismic monitoring: Some shortcomings in nonuniform processing." The Leading Edge **16**: 6.

Ross, C. P., G. G. Cunningham, et al. (1996). "Inside the cross-equalization black box." The Leading Edge **15**: 7.

Sheriff, R. E. and L. P. Geldart (1995). Exploration Seismology, Cambridge University Press.

Talley, D. J., T. L. Davis, et al. (1998). "Dynamic reservoir characterization of Vacuum Field." The Leading Edge **17**(10): 6.

Thomsen, L. (2002). Understanding seismic anisotropy in exploration and exploitation, Society of Exploration Geophysicists.

Thomsen, L., I. Tsvankin, et al. (1999). "Coarse-layer stripping of vertically variable azimuthal anisotropy from shear-wave data." Geophysics **64**: 12.

Topper, R., K. L. Spray, et al. (2003). "Ground Water Atlas of Colorado." Retrieved 7/10/2006, 2006, from http://geosurvey.state.co.us/wateratlas/chapter6_2page1.asp.

Vasconcelos, I. and V. Grechka (2006). Seismic characterization of multiple fracture sets from multicomponent, multiazimuthal, 3D data: Rulison Field, CO. Center for Wave Phenomena Annual Meeting, Center for Wave Phenomena, Colorado School of Mines.

Winarsky, R. (2006). RCP Seismic Processing Questions. M. Rumon. Golden.

Wolhart, S. L., C. E. Odegard, et al. (2005). "Microseismic Fracture Mapping Optimizes Development of Low-Permeability Sands of the Williams Fork Formation in the Piceance Basin." SPE International: 13.